Journal of Hazardous Materials

Ice and aqueous photochemistry of high-ring chlorinated polycyclic aromatic hydrocarbons: A systematic assessment of persistence and risk in cold regions

--Manuscript Draft--

Manuscript Number:	HAZMAT-D-26-01092R1
Article Type:	Research Paper
Keywords:	Chlorinated PAHs; Ice & aqueous photochemistry; Photodegradation kinetics; Transformation mechanisms; Toxicity evolution
Corresponding Author:	Peng Zhang, Ph.D. Shaanxi University of Science and Technology CHINA
First Author:	Linke Ge
Order of Authors:	Linke Ge
	Rongyan Xu
	Jack Garnett
	Peng Zhang, Ph.D.
	Dongxiao Bai
	Siyuan Wang

April 29, 2026

Ref. No: HAZMAT-D-26-01092

Title: Ice and aqueous photochemistry of high-ring chlorinated polycyclic aromatic hydrocarbons: A systematic assessment of persistence and risk in cold regions

Dear Editor,

Many thanks for the editor's and reviewers' insightful and constructive comments on our manuscript, as well as highlighting areas that need more information or improvement. We have carefully studied all the comments and suggestions raised by the editor and reviewers. As a result, we have now undertaken major revisions to the manuscript as requested.

Importantly, to enhance the quality of the manuscript, we have supplemented some new data [Fig. 3 (electron paramagnetic resonance (EPR) spectra and contribution ratios ($R_{\cdot OH}$), Figs. S6-S8 (density functional theory (DFT) calculations), Table S6 (the pH change values of reaction solutions) and Table S13 (Environmental photolytic half-lives ($t_{1/2,E}$) for the parent PAHs and hydroxylated (OH-) PAHs)], added the relevant discussion and clarified the reaction mechanisms (Lines 203-208, 248-252, 317-325, 346-349, 370-381 and 397-399). Furthermore, we have added the term 'high-ring' to the title, and emphasized the novelty and significance of this study in the introduction and conclusion. In addition, according to the reviewers' suggestion, we revised the graphical abstract, Figs 1-2, 6 (the original Fig. 5) and S9 (the original Fig. S6). Please refer to our detailed responses to the editor's and reviewers' comments. The manuscript has also been polished overall following the journal guidelines. All the changes have been marked and highlighted with heavy-blue words in the revised MS and Supplementary Material. A clean copy of the revised manuscript is also attached. We now hope that the manuscript is suitable for publication in *Journal of Hazardous Materials*.

Thank you for your consideration!

Yours sincerely,

Dr. Peng Zhang

E-mail address: zhangpeng4477@sust.edu.cn.

Environmental Implication (maximum limit:100 words)

Chlorinated PAHs are widely detected in aquatic systems, urging novel insights into their glacial and aqueous environmental fate, especially for high-ring Cl-PAHs (≥ 3 rings). In this study, not only photolysis kinetics, pathways and photo-induced toxicity of three high-ring Cl-PAHs varied between the reaction media (ice/water), but the main dissolved substances displayed more significant promotion or inhibition effects in ice than in water. These findings elucidate the nuanced similarities and divergences between ice and aqueous photochemistry, thereby enabling more accurate evaluation of the environmental fate and risks posed by PAH analogues and derivatives in seasonally ice-covered regions.

Graphical Abstract

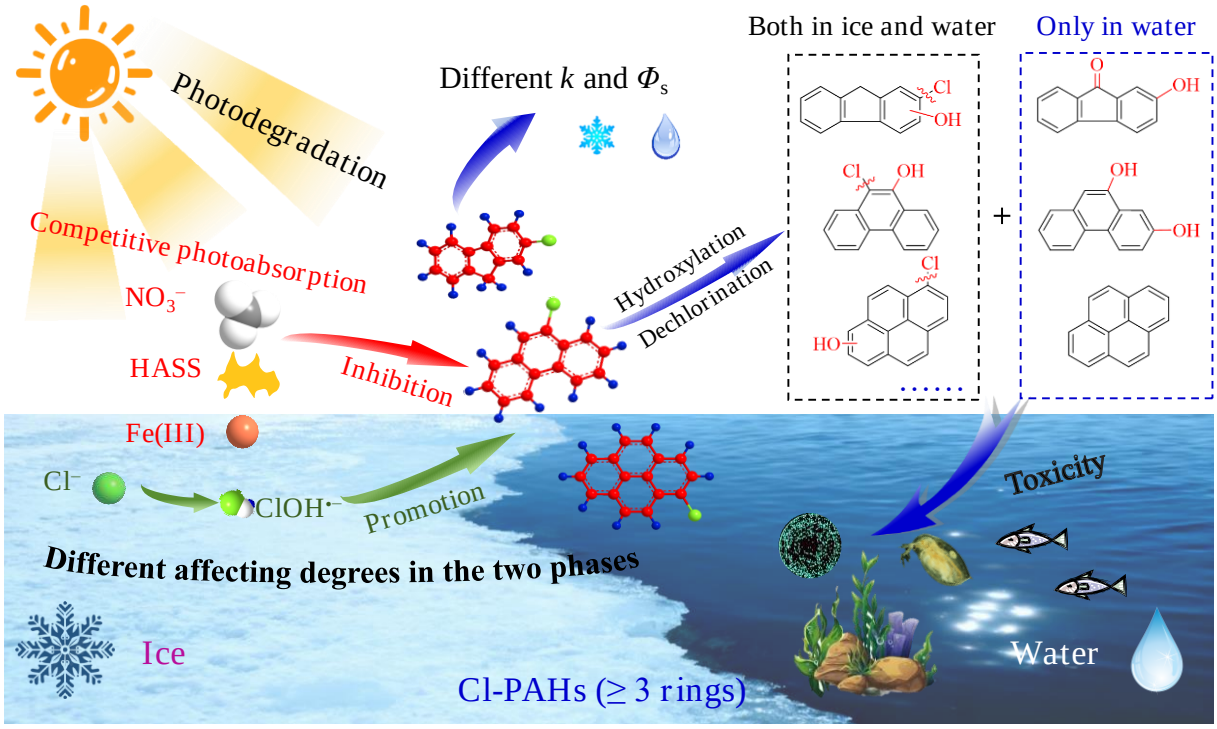

Highlights

- The study fills a gap in ice/aqueous photochemistry of high-ring Cl-PAHs (≥ 3 rings)
- Photolysis kinetics depended on the reaction media (ice/water) and chemical structures
- Apart from dechlorination and hydroxylation, several pathways varied between two phases
- Main dissolved substances displayed more notable promotion or inhibition effects in ice
- Toxicity evolution mechanism was clarified with *Vibrio fischeri* and ECOSAR assessment

Responses to Editor's and Reviewers' Comments

Ref. No.: HAZMAT-D-26-01092

Title: Ice and aqueous photochemistry of high-ring chlorinated polycyclic aromatic hydrocarbons: A systematic assessment of persistence and risk in cold regions

☞ **Response to Editor's Decision Notification:**

I hope this email finds you well. The review of your manuscript, Ice and aqueous photochemistry of chlorinated polycyclic aromatic hydrocarbons: A systematic assessment of persistence and risk in cold regions, submitted to *Journal of Hazardous Materials* has been completed. Reviewer 3 has raised concerns regarding the novelty of the work, noting that similar differences in contaminant photodegradation between water and ice have been reported in previous studies. I share this concern and recommend that the authors more clearly articulate the significant contribution of this work beyond the existing literature. Clarifying what new mechanistic insight, methodology, or environmental relevance this study provides will be important for the manuscript to be considered suitable for publication in the *Journal of Hazardous Materials*.

Response: We would like to express our sincere gratitude for your professional review of the manuscript. We have carefully studied the reviewer comments on the manuscript. The comments are constructive, which have greatly helped us improve the quality of this manuscript. In the revised manuscript, we have carefully considered and fully addressed all the comments point by point. We have supplemented some new data [Fig. 3 (electron paramagnetic resonance (EPR) spectra and contribution ratios ($R_{\cdot OH}$), Figs. S6-S8 (density functional theory (DFT) calculations), Table S6 (the pH change values of reaction solutions) and Table S13 (Environmental photolytic half-lives ($t_{1/2,E}$) for the parent PAHs and hydroxylated (OH-) PAHs)], added the relevant discussion and clarified the reaction mechanisms (Lines 203-208, 248-252, 317-325, 346-349, 370-381 and 397-399). Furthermore, we have added the term "high-ring" to the title, and emphasized the novelty and significance of this study in the introduction and conclusion. In addition, according to the reviewers' suggestion, we revised the graphical abstract, Figs 1-2, 6 (the original Fig. 5) and S9 (the original Fig. S6). Please see the changes marked in the revised manuscript and the revised supplementary material.

☞ **Response to Editor's Comments:**

In addition to reviewer's comment, I have included some of my own comments which need to

be addressed prior to resubmission.

Line 210: Please include standard deviation of measurement for the pseudo-first-order degradation rate constant to show that the differences observed between ice and water are statistically significant, particularly for 2-ClFL and 9-ClPHE.

Response: We appreciate the editor for the insightful comment. In fact, the standard deviation of measurement for the pseudo-first-order degradation rate constant (k) is available in the supplementary material (Table S7). For instance, the k values of 2-ClFL, 9-ClPHE and 1-ClPY were $(12.50 \pm 0.21) \times 10^{-3}$ min^{-1}, $(3.60 \pm 0.14) \times 10^{-3}$ min^{-1} and $(9.45 \pm 0.80) \times 10^{-3}$ min^{-1} in ice, respectively. While in the aqueous phase they were $(14.61 \pm 2.82) \times 10^{-3}$ min^{-1}, $(2.15 \pm 0.05) \times 10^{-3}$ min^{-1} and $(1.55 \pm 0.13) \times 10^{-3}$ min^{-1}, respectively. These data indicated that, with the exception of 2-ClFL ($p > 0.05$), the photodegradation of 9-ClPHE ($p < 0.01$) and 1-ClPY ($p < 0.01$) exhibited significant differences between ice and water. Moreover, the standard deviation of the fold is provided in the Lines 224-226. Please see the revised contents in the manuscript and supplementary material (Table S7).

The revised section in the manuscript is as follows:

Lines 224-226: Analysis of data (Table S7) also showed a much greater increase in degradation rates between ice and water conditions for 1-ClPY (6.10 ± 0.01 fold, $p < 0.01$) than 9-ClPHE (1.67 ± 0.03 fold, $p < 0.01$) and 2-ClFL (1.17 ± 0.21 fold).

Please specify the pH during experiments clearly in the manuscript.

Response: Thanks for your careful reviewing. To illustrate the changes of pH values in the reaction solution during the experiment, we carefully repeated the photolytic experiments and measured the pH values of the reaction solutions at each sampling time point using a precision pH meter (PB-10, Sartorius Scientific Instruments Co., Ltd., Beijing, China). As shown in Table S6, the results indicated that the pH values measured during the reaction fluctuated within 0.3 unit. Based on a one-way analysis of variance (SPSS version 31.0), it was found that pH variations within the experimental replicates for the identical Cl-PAHs were minimal ($p > 0.05$). Therefore, we can confirm that the photochemical differences between ice and water are not caused by pH changes. Please see Lines 187-188 in the revised manuscript and supplementary material.

The revised section in the manuscript is as follows:

Lines 187-188: Slight pH fluctuations (less than 0.3 units, $p > 0.05$) were recorded in the

individual photolytic experiments (Table S6).

The revised section in the supplementary material is as follows:

Page 12: **Table S6.**

Table S6. The solution pH values measured during the individual photolytic experiments of Cl-PAHs.

Media	Cl-PAHs	Initial pH at t_0	pH changes from t_0 to t_5 (t_0, t_1, t_2, t_3, t_4, t_5)*	Significance level
In ice	2-ClFL	6.41	6.41, 6.37, 6.32, 6.17, 6.12	$p > 0.05$
		6.42	6.42, 6.40, 6.34, 6.19, 6.14	
		6.44	6.44, 6.37, 6.38, 6.20, 6.15	
	9-ClPHE	6.62	6.62, 6.56, 6.50, 6.43, 6.35	$p > 0.05$
		6.63	6.63, 6.54, 6.49, 6.42, 6.34	
		6.59	6.59, 6.51, 6.47, 6.41, 6.33	
	1-ClPY	6.27	6.27, 6.25, 6.23, 6.18, 6.13	$p > 0.05$
		6.26	6.26, 6.26, 6.22, 6.18, 6.13	
		6.29	6.29, 6.27, 6.24, 6.19, 6.14	
In water	2-ClFL	6.48	6.48, 6.37, 6.28, 6.24, 6.22	$p > 0.05$
		6.50	6.50, 6.38, 6.28, 6.25, 6.24	
		6.45	6.45, 6.36, 6.27, 6.23, 6.19	
	9-ClPHE	6.63	6.63, 6.58, 6.53, 6.47, 6.41	$p > 0.05$
		6.65	6.65, 6.61, 6.52, 6.51, 6.42	
		6.61	6.61, 6.56, 6.58, 6.46, 6.39	
	1-ClPY	6.35	6.35, 6.30, 6.30, 6.27, 6.20	$p > 0.05$
		6.38	6.38, 6.35, 6.30, 6.26, 6.21	
		6.37	6.37, 6.36, 6.29, 6.25, 6.21	

Notes: * For apparent photolytic experiments, t_0, t_1, t_2, t_3, t_4 and t_5 are corresponding to the sampling times in Fig. 1 of the manuscript, i.e., 0 min, 30 min, 60 min, 90 min and 120 min for all the three Cl-PAHs in ice; 0 min, 15 min, 30 min, 60 min and 120 min for 2-ClFL in water; 0 min, 120 min, 240 min, 360 min and 480 min for 1-ClPY and 9-ClPHE in water.

Line 286-288: The scavenging of OH radicals by chloride ions is only important under acidic conditions. Hence, this explanation is valid only if the pH during experiments is in the acidic range (i.e. < 4). A more reasonable explanation would be direct photoactivation of chloride ions to generate chlorine based radicals. How did the authors reject the possibility that direct photoactivation of chloride ions is not important.

Response: Thanks for your question. Under simulated sunlight ($\lambda > 290$ nm), chloride ions (Cl^-) exhibit no significant absorption (Fig. S9). Moreover, in the neutral aqueous system, the following two reactions occur only to a negligible extent:

$$Cl^- + h\nu \rightarrow Cl\cdot + Cl_2^{\cdot -} \text{ (direct photoactivation of } Cl^-)$$

$$\cdot OH + Cl^- \rightarrow Cl\cdot + Cl_2^{\cdot -} \text{ (scavenging of hydroxyl radicals (}\cdot OH) \text{ by } Cl^-)$$

Therefore, we have provided reasonable explanations. Please see Lines 317-325 in the revised manuscript and Fig. S9 (the original Fig. S6) in the revised supplementary material.

The revised section in the manuscript is as follows:

Lines 317-325: The enhanced rate of photolysis of 9-ClPHE in the presence of Cl^- can be ascribed to the formation of more reactive chlorine species (e.g., $ClOH^{\cdot -}$) via scavenging $\cdot OH$ by Cl^- in neutral solution (El Omar et al. 2012), understood as follows:

$$9\text{-ClPHE} + h\nu \longrightarrow 9\text{-ClPHE}^* \quad (1)$$

$$9\text{-ClPHE}^* \xrightarrow{+H_2O} \cdot OH \text{ (proved by EPR spectra in Fig. 3)} \quad (2)$$

$$\cdot OH + Cl^- \underset{k_2}{\overset{k_1}{\rightleftharpoons}} ClOH^{\cdot -} \quad (k_1 = 4.3 \times 10^9\ M^{-1}s^{-1},\ k_2 = 6.1 \times 10^9\ M^{-1}s^{-1}) \quad (3)$$

At high concentrations of Cl^-, generation of reactive $ClOH^{\cdot -}$ species is likely to reach a point whereby further promotion effects are weakened through the transformation of $ClOH^{\cdot -}$ into $Cl\cdot$ and $Cl_2^{\cdot -}$ (El Omar et al. 2012). Meanwhile, changes in the microstructure of ice under high salinity conditions also influence the photodegradation rate of coexisting organic solutes (Chen et al. 2019, Mason et al. 2022).

The revised section in the supplementary material is as follows:

Page 33: **Fig. S9.**

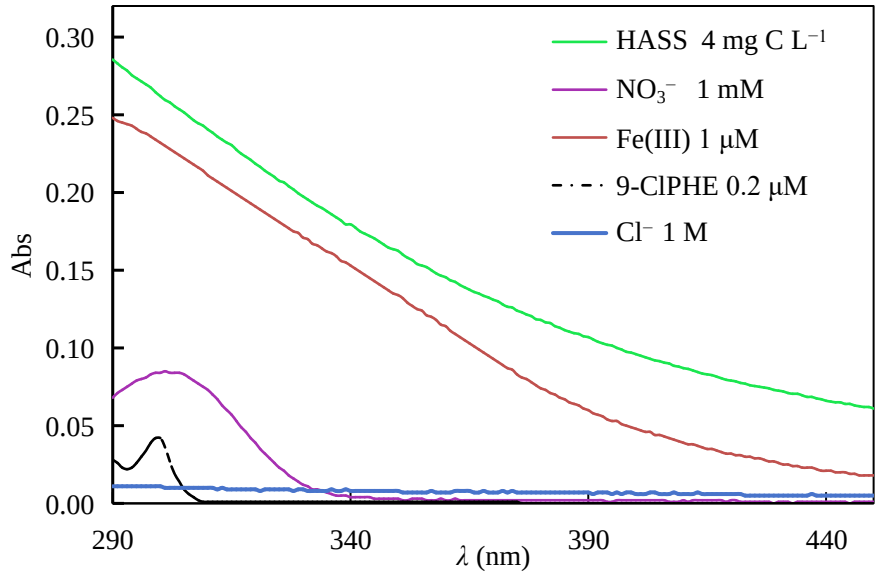

Fig. S9. The UV-Vis absorption spectra of Cl^-, humic acid sodium salt (HASS), NO_3^-, Fe(III) and 9-ClPHE

☞ **Response to Reviewer #1 Comments:**

This manuscript presents a comprehensive investigation into the photochemical behavior of three high-ring chlorinated polycyclic aromatic hydrocarbons (Cl-PAHs) in ice and aqueous matrices. The study systematically examines photodegradation kinetics, transformation pathways, the effects of dissolved constituents, and toxicity evolution. The topic is highly relevant to *Journal of Hazardous Materials*, particularly given the growing concern about emerging contaminants in cold regions. The experimental design is thoughtful, the data are extensive, and the findings contribute valuable insights to an understudied area. However, several significant issues need to be addressed before the manuscript can be considered for publication.

Response: We appreciate the reviewer for the positive comments and insightful suggestions. They are very helpful and constructive. We have supplemented some new data [Figs. S6-S8 (DFT calculations) and Table S13 (Environmental photolytic half-lives ($t_{1/2,E}$))], as well as provided more discussions corresponding to the concentration selection of individual factors (Lines 162-164), the limitations of product structure speculation (Lines 248-252), the reaction mechanism for Cl^- and ·OH (Lines 317-325), and more explanations on environmental half-lives (Lines 370-381) and toxicities (Lines 397-399). Furthermore, Figs. 2, 6 (the original Fig. 5) and S9 have also been optimized. Please see the changes marked in the revised manuscript and the revised supplementary material.

1. The identification of transformation products relies exclusively on HPLC-MS/MS data without confirmation using authentic standards (Section 3.3, Figure 2, Table S8). While this approach is common in exploratory studies, several proposed structures—particularly those differentiating between ice and aqueous phases (e.g., P196 for 2-ClFL only in water; P202 for 1-ClPY only in water)—are tentative at best. The manuscript does not adequately discuss the limitations of structure assignment based solely on mass spectral fragmentation, especially for distinguishing positional isomers of hydroxylated products. Furthermore, the mechanistic explanation for why certain pathways occur only in one phase is underdeveloped. For example, why does 9-ClPHE undergo only hydroxylation to P228 in ice but further transform to P210 in water? Is this due to differences in ROS availability, diffusion constraints in the ice matrix, or enrichment effects?

Response: Thanks for your careful observation. To address the limitations of product identification using HPLC-MS/MS, we further employed density functional theory (DFT)

calculations to predict the structural sites that were susceptible to free radical attack, thereby facilitating the differentiation of positional isomers of hydroxylated products. We also further examined the total ion current spectra and searched for signals of the products formed by 9-ClPHE in ice. However, no evidence for the formation of P210 in ice was observed. It is likely that this product was not formed, or its yield was too low to be detected. In previous studies, 4-Cl-1-OHN and 4-NO_2-1-OHN are more prone to generating multi-hydroxylated products in ice (Ge et al. 2025), whereas hydroxyfluorene tends to carry out multi-hydroxylated reactions in water (Ge et al. 2023). For Cl-PAHs, most of them generated multi-hydroxylated products both in ice and in water, although 9-ClPHE did not form multi-hydroxylated products, which was an exception. Based on these findings, we cannot simply attribute the further transformation of P228 into P210 in water to factors such as differences in ROS availability, diffusion constraints in the ice matrix, or enrichment effects. Notably, multi-hydroxylated products that are more likely to form may depend on these compound structures. Please see the revised contents in the manuscript and supplementary material.

The revised section in the manuscript is as follows:

Lines 173-176: In addition, the electrostatic potential (ESP), the highest occupied molecular orbital (HOMO), the lowest unoccupied molecular orbital (LUMO) and Fukui indices of the three Cl-PAHs were calculated by density functional theory (DFT).

Lines 248-252: Furthermore, the DFT calculations (Figs. S6-S8) indicated the most possible reaction sites of each compound susceptible to radical attack (e.g., ·OH). By integrating the HPLC-MS/MS data, the chemical structures of key products are tentatively proposed, along with the phototransformation pathways of the three Cl-PAHs both in ice and in water (Fig. 2).

Lines 265-274: The prevalence of hydroxylation reaction can be ascribed to the generation of ·OH radicals from the photo-sensitization of the parent compounds in the two phases. As shown in Fig. 3, EPR spectra showed four sets of peaks with 1:2:2:1 under irradiation, corresponding to the characteristic of the DMPO-·OH, which verified the generation of ·OH from photo-sensitization of Cl-PAHs. Combined with radical quenching experiments (Text S1), the participation of ·OH in the apparent photolysis was confirmed, and the contribution ratios ($R_{\cdot OH}$) of self-sensitized photo-oxidation via ·OH to the apparent photolysis were illustrated in Fig. 3. The ·OH was speculated during the photolysis of several PAHs and SPAHs (Ge et al. 2025, Sarmiento et al. 2023). However, the formation and participation of ·OH were proved in

the present study.

Lines 278-285: **Fig. 2.**

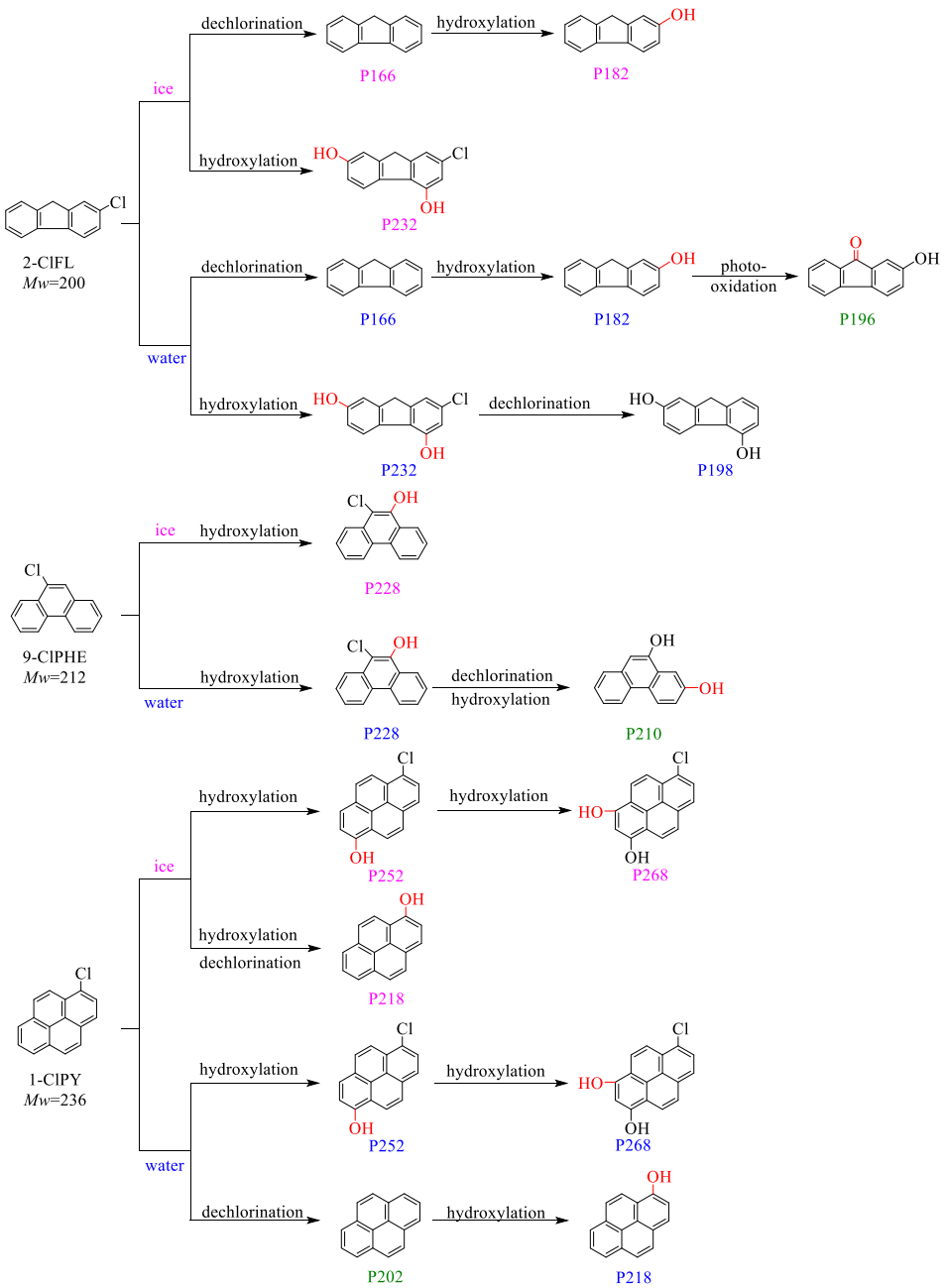

Fig. 2. Photolytic products and transformation pathways associated with the three Cl-PAHs. The photogenerated intermediates are designated as P_{Mw}, where *Mw* denotes molecular weights calculated from the most abundant isotopes. P_{Mw} is marked with different colors to distinguish the products generated in different phases. Among them, 'magenta' indicates products formed in ice, 'blue' indicates products in water, and 'green' represents products that were only formed in the aqueous phase.

Lines 287-289: **Fig. 3.**

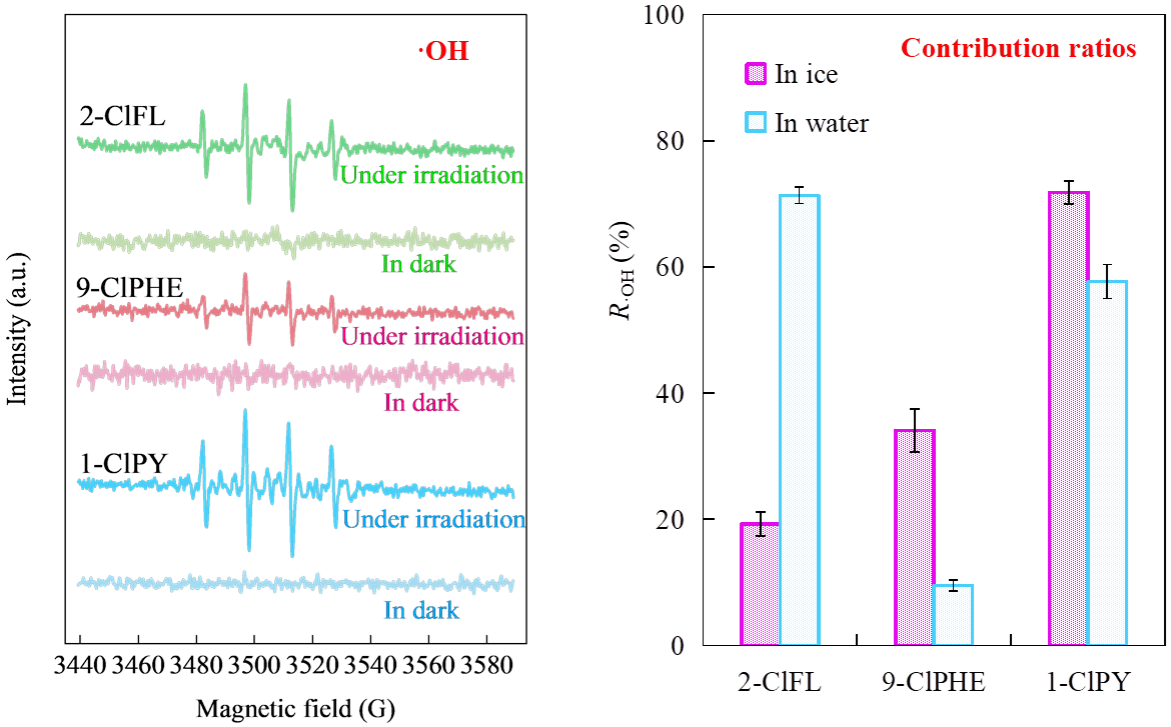

Fig. 3. The electron paramagnetic resonance (EPR) spectra (left) and the contribution ratios ($R_{\cdot OH}$) of self-sensitized photo-oxidation via ·OH to the apparent photolysis (right) for the three Cl-PAHs.

The revised section in the supplementary material is as follows:

Pages 30-32: **Figs. S6-S8.**

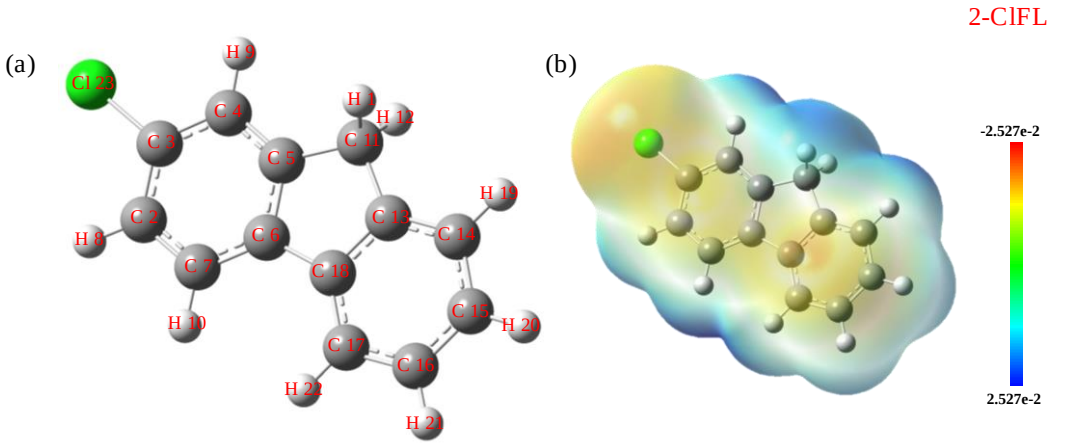

(e)

Atom	Site	q(N)	q(N+1)	q(N–1)	f^-	f^+	f^0
H	1	0.0469	0.0237	0.0697	0.0227	0.0233	0.0230
C	2	-0.0480	-0.0859	-0.0017	0.0464	0.0379	0.0421
C	3	0.0227	-0.0485	0.0882	0.0656	0.0711	0.0683
C	4	-0.0500	-0.1059	-0.0148	0.0353	0.0559	0.0456
C	5	0.0053	-0.0228	0.0456	0.0403	0.0281	0.0342
C	6	-0.0076	-0.0578	0.0429	0.0505	0.0502	0.0503
C	7	-0.0371	-0.1020	0.0096	0.0467	0.0650	0.0558
H	8	0.0492	0.0203	0.0784	0.0292	0.0289	0.0291
H	9	0.0487	0.0164	0.0751	0.0264	0.0323	0.0294
H	10	0.0474	0.0152	0.0745	0.0271	0.0322	0.0297
C	11	-0.0415	-0.0548	-0.0251	0.0165	0.0133	0.0149
H	12	0.0469	0.0237	0.0697	0.0227	0.0233	0.0230
C	13	0.0003	-0.0283	0.0435	0.0431	0.0286	0.0359
C	14	-0.0455	-0.0975	-0.0090	0.0365	0.0520	0.0443
C	15	-0.0429	-0.1255	0.0434	0.0863	0.0826	0.0845
C	16	-0.0432	-0.0828	0.0047	0.0479	0.0396	0.0438
C	17	-0.0431	-0.1037	0.0028	0.0459	0.0606	0.0532
C	18	-0.0087	-0.0512	0.0380	0.0467	0.0424	0.0446
H	19	0.0435	0.0113	0.0717	0.0282	0.0322	0.0302
H	20	0.0438	0.0027	0.0813	0.0375	0.0411	0.0393
H	21	0.0440	0.0137	0.0751	0.0311	0.0303	0.0307
H	22	0.0432	0.0127	0.0696	0.0264	0.0305	0.0285
Cl	23	-0.0738	-0.1726	0.0669	0.1408	0.0987	0.1198

Fig. S6. The chemical structure (a), the electrostatic potential (ESP) (b), the highest occupied molecular orbital (HOMO) (c), the lowest unoccupied molecular orbital (LUMO) (d), and Fukui indices (f^-, f^+ and f^0) distribution (e) of 2-ClFL.

9-ClPHE

(a) (b)

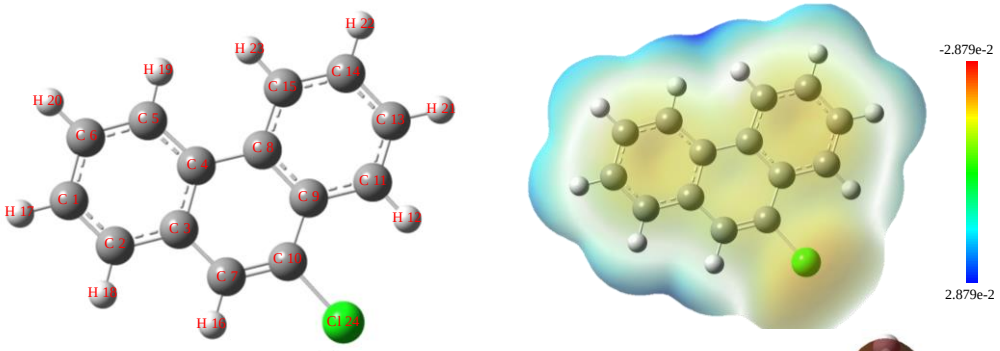

(c) (d)

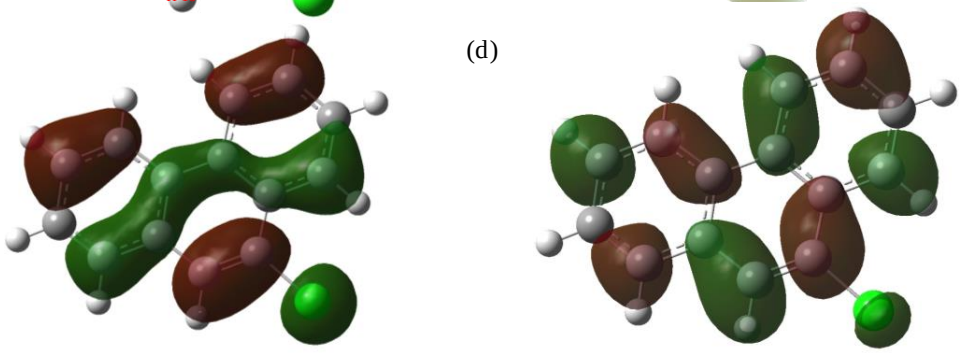

(e)

Atom	Site	q(N)	q(N+1)	q(N–1)	f^-	f^+	f^0
C	1	-0.0404	-0.0789	-0.0032	0.0371	0.0385	0.0378
C	2	-0.0390	-0.0877	0.0150	0.0540	0.0487	0.0514
C	3	0.0000	-0.0233	0.0279	0.0278	0.0234	0.0256
C	4	0.0009	-0.0234	0.0280	0.0270	0.0243	0.0257
C	5	-0.0396	-0.0772	-0.0006	0.0390	0.0376	0.0383
C	6	-0.0405	-0.1107	0.0342	0.0748	0.0701	0.0724
C	7	-0.0480	-0.1294	0.0257	0.0737	0.0814	0.0776
C	8	0.0045	-0.0178	0.0209	0.0164	0.0222	0.0193
C	9	-0.0068	-0.0282	0.0076	0.0145	0.0214	0.0179
C	10	0.0231	-0.0465	0.0881	0.0650	0.0696	0.0673
C	11	-0.0429	-0.0963	0.0105	0.0534	0.0534	0.0534
H	12	0.0363	0.0096	0.0602	0.0240	0.0267	0.0253
C	13	-0.0384	-0.0771	-0.0010	0.0374	0.0386	0.0380
C	14	-0.0387	-0.1090	0.0257	0.0645	0.0703	0.0674
C	15	-0.0397	-0.0816	0.0031	0.0428	0.0419	0.0424
H	16	0.0486	0.0117	0.0800	0.0314	0.0369	0.0342
H	17	0.0466	0.0176	0.0750	0.0284	0.0290	0.0287
H	18	0.0448	0.0171	0.0724	0.0276	0.0277	0.0276
H	19	0.0425	0.0209	0.0645	0.022	0.0216	0.0218
H	20	0.0456	0.0094	0.0798	0.0342	0.0362	0.0352
H	21	0.0474	0.0183	0.0749	0.0275	0.0291	0.0283
H	22	0.0464	0.0099	0.0782	0.0319	0.0364	0.0342
H	23	0.0428	0.0202	0.0643	0.0215	0.0226	0.0220
Cl	24	-0.0550	-0.1473	0.0691	0.1241	0.0923	0.1082

Fig. S7. The chemical structure (a), the electrostatic potential (ESP) (b), the highest occupied molecular orbital (HOMO) (c), the lowest unoccupied molecular orbital (LUMO) (d), and Fukui indices (f^-, f^+ and f^0) distribution (e) of 9-ClPHE.

(a) (b) 1-ClPY

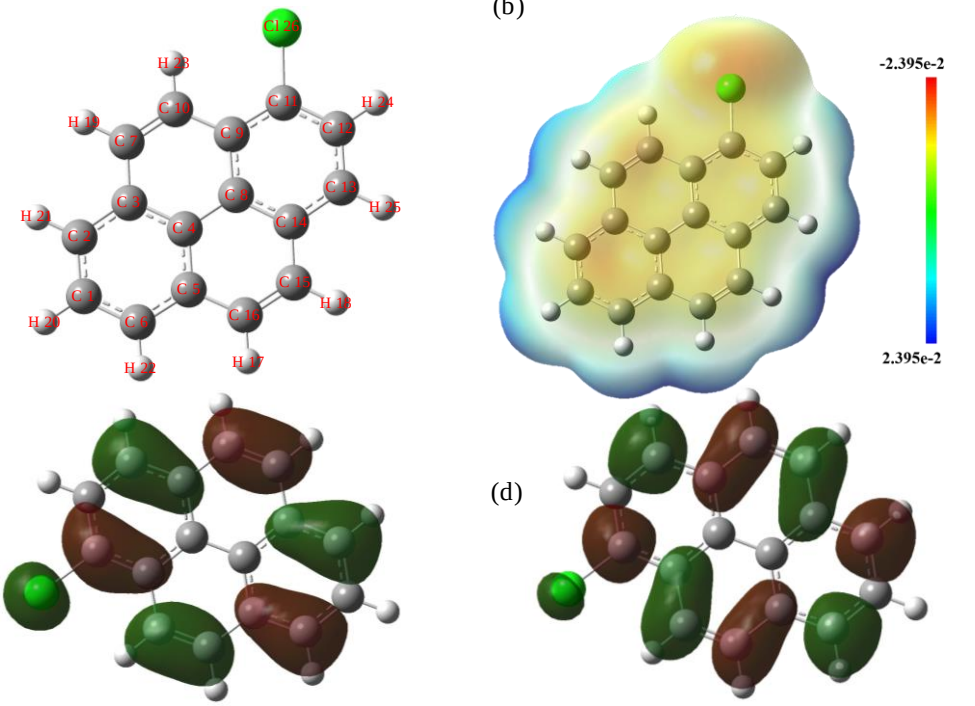

(c) (d)

(e)

Atom	Site	q(N)	q(N+1)	q(N–1)	f^-	f^+	f^0
C	1	-0.0415	-0.0778	-0.0070	0.0345	0.0363	0.0354
C	2	-0.0400	-0.1061	0.0288	0.0688	0.0661	0.0674
C	3	-0.0011	-0.0259	0.0247	0.0258	0.0248	0.0253
C	4	0.0027	-0.0046	0.0101	0.0073	0.0073	0.0073
C	5	-0.0009	-0.0257	0.0230	0.0239	0.0248	0.0244
C	6	-0.0404	-0.1071	0.0294	0.0698	0.0667	0.0683
C	7	-0.0360	-0.0908	0.0145	0.0505	0.0548	0.0527
C	8	0.0055	-0.0020	0.0127	0.0072	0.0075	0.0074
C	9	-0.0073	-0.0335	0.0164	0.0237	0.0263	0.0250
C	10	-0.0443	-0.0957	0.0064	0.0506	0.0515	0.0510
C	11	0.0227	-0.0333	0.0791	0.0564	0.056	0.0562
C	12	-0.0482	-0.0812	-0.0175	0.0307	0.0330	0.0319
C	13	-0.0380	-0.1047	0.0277	0.0657	0.0667	0.0662
C	14	-0.0022	-0.0294	0.0245	0.0266	0.0272	0.0269
C	15	-0.0403	-0.0912	0.0112	0.0515	0.0509	0.0512
C	16	-0.0396	-0.0928	0.0144	0.0540	0.0531	0.0536
H	17	0.0453	0.0158	0.0730	0.0277	0.0295	0.0286
H	18	0.0453	0.0163	0.0725	0.0272	0.0290	0.0281
H	19	0.0463	0.0166	0.0731	0.0268	0.0297	0.0283
H	20	0.0461	0.0179	0.0733	0.0272	0.0282	0.0277
H	21	0.0441	0.0119	0.0746	0.0305	0.0322	0.0313
H	22	0.0437	0.0113	0.0744	0.0307	0.0325	0.0316
H	23	0.0381	0.0117	0.0623	0.0242	0.0265	0.0253
H	24	0.0497	0.0237	0.0746	0.0248	0.0260	0.0254
H	25	0.0470	0.0148	0.0769	0.0299	0.0323	0.0311
Cl	26	-0.0565	-0.1376	0.0473	0.1038	0.0812	0.0925

Fig. S8. The chemical structure (a), the electrostatic potential (ESP) (b), the highest occupied molecular orbital (HOMO) (c), the lowest unoccupied molecular orbital (LUMO) (d), and Fukui indices (f^-, f^+ and f^0) distribution (e) of 1-ClPY.

2. Throughout the abstract, results, and conclusion, the authors state that Cl-PAHs exhibit "greater environmental persistence" than their parent PAHs. However, the data in Table 1 show a wide range of environmental half-lives—from 0.54 days (1-ClPY in Arctic ice/snow) to 89 days (9-ClPHE in Xi'an winter water). The claim of greater persistence is not universally supported; 1-ClPY degrades remarkably fast in Arctic ice. The authors should avoid broad generalizations that could mislead readers about the environmental behavior of all Cl-PAH congeners. Moreover, the comparison with parent PAHs (referenced as Ram et al., 2009) is presented without acknowledging that parent PAHs also exhibit wide variability in photolytic half-lives depending on structure and conditions.

Response: Thank you for your insightful comments. To avoid misleading readers about all Cl-PAH congeners exhibit "greater environmental persistence" than their parent compounds, we have revised the relevant contents to avoid overgeneralization. This can be explained by the values of $t_{1/2,E}$ summarized for fluorene (FL), phenanthrene (PHE), pyrene (PY) and their hydroxylated/chlorinated PAHs in Table S13 (Ge et al. 2016a, Ram et al. 2009). For example, the $t_{1/2,E}$ values for 2-ClFL ranged from 17.17 days (Arctic; 78.91°N, 11.93°E; Ice/Snow) to 77.37 days (Antarctic; 62.21°S, 58.96°W; Water), higher than those for 2-OHFL from 0.012 days (Arctic; 78.91°N, 11.93°E; Ice/Snow) to 0.027 days (Antarctic; 62.21°S, 58.96°W; Snow), and for FL from 0.79 days (Summit, Greenland; 72.58°N, 38.49°W; Snow) to 7.88 days (Alert, Nunavut; 82.5°N, 62.3°W; Snow). Similarly, the $t_{1/2,E}$ values for 9-ClPHE ranged from 15.35 days (Arctic; 78.91°N, 11.93°E; Ice/Snow) to 68.56 days (Antarctic; 62.21°S, 58.96°W; Water), which were greater than those for 9-OHPHE from 0.0042 days (Arctic; 78.91°N, 11.93°E; Ice/Snow) to 0.0079 days (Antarctic; 62.21°S, 58.96°W; Snow), and for PHE from 0.25 days (Neumayer, Antarctic; 70.7°S, 8.3°W; Snow) to 2.75 days (Alert, Nunavut; 82.5°N, 62.3°W; Snow). The $t_{1/2,E}$ values for 1-ClPY were from 0.54 days (Arctic; 78.91°N, 11.93°E; Ice/Snow) to 8.99 days (Antarctic; 62.21°S, 58.96°W; Water), larger than those for 1-OHPY from 0.0033 days (Arctic; 78.91°N, 11.93°E; Ice/Snow) to 0.0050 days (Antarctic; 62.21°S, 58.96°W; Snow), and for PY from 0.042 days (Neumayer, Antarctic; 70.7°S，8.3°W; Snow) to 0.42 days (Alert, Nunavut; 82.5°N, 62.3°W; Snow). Therefore, all the three Cl-PAHs were more persistent in photochemistry than their respective parent PAHs and OH-PAHs (Table S13). The revised contents can be found in the manuscript and supplementary material.

The revised section in the manuscript is as follows:

Lines 26-27: Environmentally relevant photolytic half-lives ($t_{1/2,E}$) extrapolated from laboratory data for the three Cl-PAHs ranged from several hours to tens of days in selected cold regions.

Lines 370-381: Compared to the parent PAHs and OH-PAHs (Table S13), Cl-PAHs generally displayed much longer $t_{1/2,E}$. For instance, the $t_{1/2,E}$ values for 2-ClFL ranged from 17.17 days (Arctic; 78.91°N, 11.93°E; Ice/Snow) to 77.37 days (Antarctic; 62.21°S, 58.96°W; Water), which were larger than those for 2-OHFL from 0.012 days (Arctic; 78.91°N, 11.93°E; Ice/Snow) to 0.027 days (Antarctic; 62.21°S, 58.96°W; Snow), and for fluorene (FL) from 0.79 days (Summit, Greenland; 72.58°N, 38.49°W; Snow) to 7.88 days (Alert, Nunavut; 82.5°N, 62.3°W; Snow) (Table S13 and associated refs.). The other two Cl-PAHs were also more persistent than their respective parent PAHs and OH-PAHs. Notably, all parent PAHs and their derivatives exhibit wide variability in the photolytic $t_{1/2,E}$ values, depending on their molecular structures and environmental conditions. Given the greater persistence of Cl-PAHs, the pollutants are likely to persist longer and pose higher ecological risk in cold regions.

The revised section in the supplementary material is as follows:

Page 19: **Table S13.**

Table S13. Environmental photolytic half-lives ($t_{1/2,E}$) of the apparent photodegradation for the parent PAHs, hydroxylated (OH-) PAHs and Cl-PAHs in surface ice/snow and water.

	$t_{1/2,E}$ (day)								
	Antarctic [a]		Arctic [b]		Summit, Greenland [c]	Alert, Nunavut [d]	Neumayer, Antarctic [e]	South Pole [f]	Reference
	Ice/Snow	Water	Ice/Snow	Water	Snow	Snow	Snow	Snow	
FL					0.79	7.88	0.88	1.58	
PHE					0.29	2.75	0.25	0.50	(Ram et al. 2009)
PY					0.042	0.42	0.042	0.083	
2-OHFL	0.027		0.012						
9-OHPHE	0.0079		0.0042						(Ge et al. 2016a)
1-OHPY	0.0050		0.0033						
2-ClFL	64.14	77.37	17.17	20.71					
9-ClPHE	24.93	68.56	15.35	42.22					This study
1-ClPY	0.90	8.99	0.54	5.41					

Notes: fluorene = FL; phenanthrene = PHE; pyrene = PY; the site latitudes, longitudes and seasons: [a] 62.21°S, 58.96°W, summer; [b] 78.91°N, 11.93°E, summer; [c] 72.58°N, 38.49°W, summer; [d] 82.5°N, 62.3°W, summer; [e] 70.7°S，8.3°W, summer; [f] 90°S, summer.

3. The manuscript reports an important discrepancy: ECOSAR predicts that most individual transformation products have comparable or lower toxicity than parent compounds, yet the Vibrio fischeri bioassay shows substantial photo-enhanced toxicity that fluctuates during irradiation (Section 3.4, Figure 5). This is a valuable finding, but the discussion of its implications is superficial.

Response: We appreciate the reviewer for the positive comments. As for the photo-enhanced toxicity, we have provided further discussion. Please see Lines 397-399 in the revised manuscript. Moreover, to further highlight the toxicity evolution of Cl-PAHs during the apparent photolysis, we have supplemented the significance analysis for the differences presented in Fig. 6 (the original Fig. 5) in the revised manuscript.

The revised section in the manuscript is as follows:

Lines 397-399: This might be attributed to the formation of hydroxylated products, which would more easily pass through the lipid cell membrane of *Vibrio fischeri* and exert a stronger inhibition effect (An et al. 2021, Ge et al. 2025, Zhao et al. 2024).

Lines 405-411: **Fig. 6.**

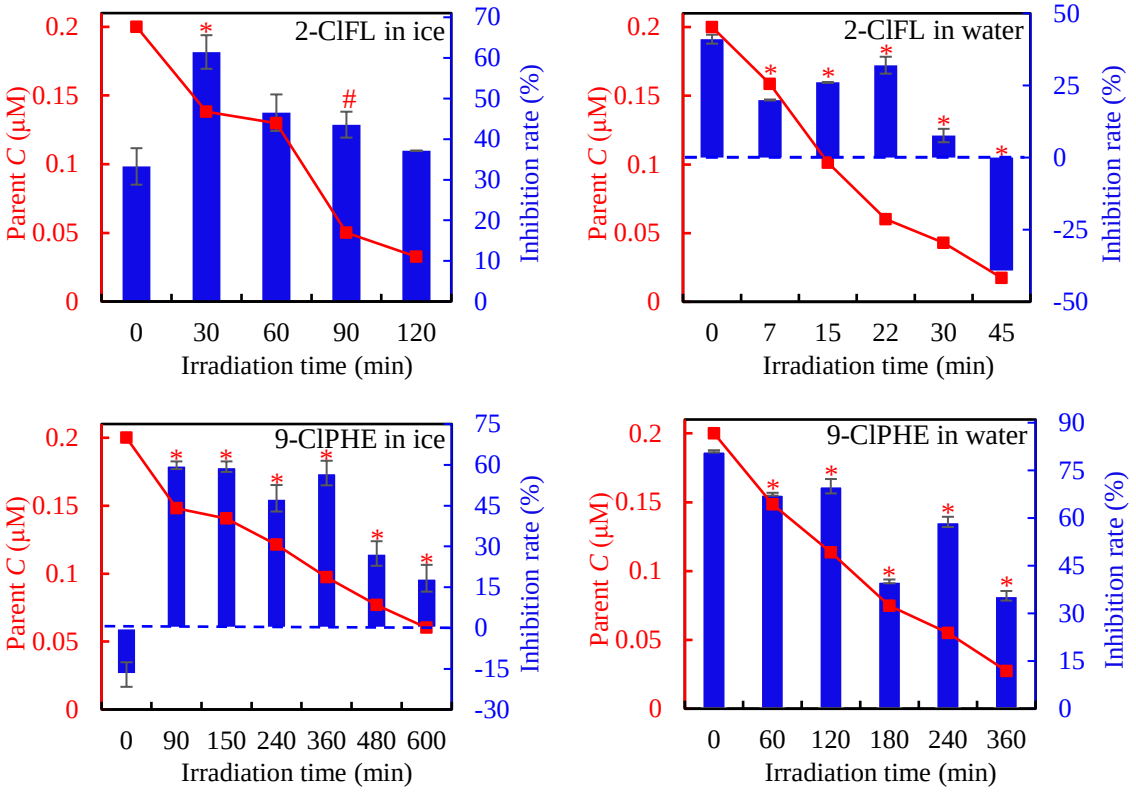

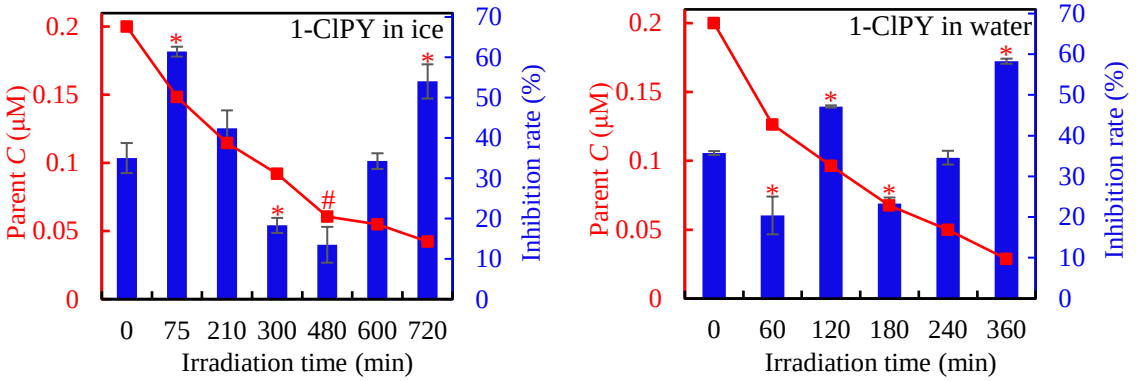

Fig. 6. The evolution of parent concentrations (*C*, ■) of the three Cl-PAHs, as well as the changes of luminescence inhibition rates (*I*%, ■) to *Vibrio fischeri* with the irradiation time in ice and in water. * and # indicate significant differences at $p < 0.01$ and 0.05, respectively, between the corresponding *I*% value at *t* and the initial value at t_0.

4. The rationale for selecting the concentration ranges (Table S4) is not explained. Are these environmentally relevant ranges? If so, please cite sources.

Response: Thanks a lot for your suggestion, and this has been adopted. The concentrations of the four factors in the central composite experiments were selected based on their environmentally relevant concentrations. For instance, Cl^- are widely distributed in nature water. Specifically, the Cl^- content in seawater can be as high as 19000 mg L^{-1} (0.54 M), while its concentration in general surface water and ground water is less than 50 mg L^{-1} (0.001 M) (Wu et al. 2021). Spatially, the global surface-water NO_3^- concentrations are predominantly distributed at 0-10 mg L^{-1} (0-0.16 mM). In some areas impacted by human activities, NO_3^- concentrations are generally higher, mainly falling within the range of 10-30 mg L^{-1} (0.16 mM-0.48 mM), with concentrations in localized hotspots even exceeding 30 mg L^{-1} (0.48 mM) (Wang et al. 2023). The environmental concentrations of Fe(III) are approximately 0.01 mM, dissolved organic matter is ubiquitous in actual water at concentrations of 1-10 mg C L^{-1} (Chen et al. 2025, Yang et al. 2022). Therefore, this concentration ranges selected in the study are environmentally relevant. Please see Lines 162-164 in the revised manuscript.

The revised section in the manuscript is as follows:

Lines 162-164: The concentrations of target factors were selected based on their environmentally relevant ranges (Ge et al. 2016b, Wang et al. 2023, Yang et al. 2022).

5. Figure 4 shows non-monotonic responses (e.g., Cl^- effect peaks at intermediate concentrations). The explanation (lines 292-295) invokes scavenging of Cl^- by *OH, but the

mechanism of promotion at lower concentrations and inhibition at higher concentrations needs more rigorous treatment. Is this truly a scavenging effect, or could it reflect changes in ice microstructure at high salinity?

Response: Thanks for your question. Under simulated sunlight ($\lambda > 290$ nm), chloride ions (Cl^-) exhibit no significant absorption (Fig. S9). Moreover, in the aqueous neutral system, the following two reactions occur only to a negligible extent:

$$Cl^- + h\nu \rightarrow Cl\cdot + Cl_2^{\cdot -} \text{ (direct photoactivation of } Cl^-)$$

$$\cdot OH + Cl^- \rightarrow Cl\cdot + Cl_2^{\cdot -} \text{ (scavenging of hydroxyl radicals (}\cdot OH) \text{ by } Cl^-)$$

Therefore, as for the mechanism of promotion at lower Cl^- concentrations and inhibition at higher Cl^- concentrations, we have provided reasonable explanations. Please see Lines 317-325 in the revised manuscript and Fig. S9 (the original Fig. S6) in the revised supplementary material.

The revised section in the manuscript is as follows:

Lines 317-325: The enhanced rate of photolysis of 9-ClPHE in the presence of Cl^- can be ascribed to the formation of more reactive chlorine species (e.g., $ClOH^{\cdot -}$) via scavenging $\cdot OH$ by Cl^- in neutral solution (El Omar et al. 2012), understood as follows:

$$9\text{-ClPHE} + h\nu \longrightarrow 9\text{-ClPHE}^* \quad (1)$$

$$9\text{-ClPHE}^* \xrightarrow{+H_2O} \cdot OH \text{ (proved by EPR spectra in Fig. 3)} \quad (2)$$

$$\cdot OH + Cl^- \underset{k_2}{\overset{k_1}{\rightleftharpoons}} ClOH^{\cdot -} \quad (k_1 = 4.3 \times 10^9\ M^{-1}s^{-1},\ k_2 = 6.1 \times 10^9\ M^{-1}s^{-1}) \quad (3)$$

At high concentrations of Cl^-, generation of reactive $ClOH^{\cdot -}$ species is likely to reach a point whereby further promotion effects are weakened through the transformation of $ClOH^{\cdot -}$ into $Cl\cdot$ and $Cl_2^{\cdot -}$ (El Omar et al. 2012). Meanwhile, changes in the microstructure of ice under high salinity conditions also influence the photodegradation rate of coexisting organic solutes (Chen et al. 2019, Mason et al. 2022).

The revised section in the supplementary material is as follows:

Page 33: **Fig. S9**.

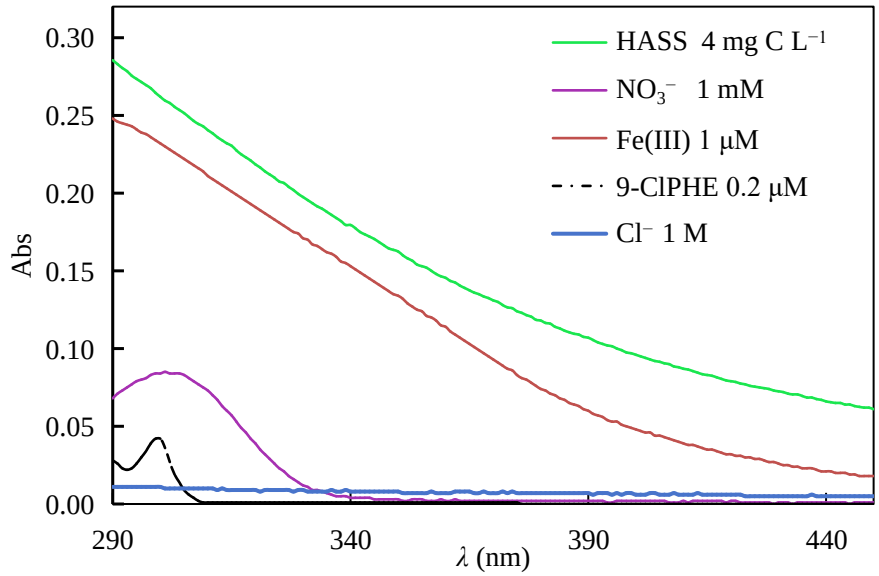

Fig. S9. The UV-Vis absorption spectra of Cl^-, humic acid sodium salt (HASS), NO_3^-, Fe(III) and 9-ClPHE

☞ **Response to Reviewer #2 Comments:**

Reviewer #2: The authors systematically investigated the ice and aqueous photochemistry of three high-cycle chlorinated PAHs (≥ 3 rings), which provides a deep look into the ice and aqueous photochemistry of high-cycle Cl-PAHs. The topic of this work is novel and helpful for evaluating the environmental fate and risk of such pollutants in cold regions. This manuscript is well written and organized, which fits well within the JHM's scope. I recommend its publication of this manuscript after addressing the following specific comments:

Response: Thanks for the positive comments and recommendation. To further improve the quality of the manuscript, we adopted your suggestion, highlighted the novelty and significance of this study (Lines 10-12, 125-129, 430-432), as well as added the "high-ring" in the title. We also have supplemented some related data or explanations on the results [Lines 147-148 (the intensities of simulated sunlight), 346-349 (further comparative discussions) and 397-399 (toxicity)]. Figs. 1-2, 6 (the original Fig. 5), S9 (the original Fig. S6) and the graphical abstract have been optimized. Furthermore, we have revised the format and grammar in the manuscript. Please see the changes marked in the revised manuscript and the revised supplementary material.

1. Introduction. To date, there has been no comparative research on the ice and aqueous photodegradation of high-cycle (≥ 3 rings) Cl-PAHs. These findings in the manuscript are quite

crucial to clarify and evaluate the environmental photochemical persistence and risks posed by the PAH derivatives in seasonally ice-covered regions. Thus, the novelty and significance of the work should be highlighted in the introduction section.

Response: Thanks for the recommendation. We agree with the reviewer that there is still a lack of comparative studies on the ice and aqueous photodegradation of high-ring Cl-PAHs (≥ 3 rings). These results are of great importance for evaluating the environmental photochemical persistence, fate and potential risks of PAH derivatives in seasonally ice-covered regions. Accordingly, we have further highlighted the novelty and environmental significance of this study in the revised introduction section, emphasizing the research gaps and the importance of the present study.

The revised section in the manuscript is as follows:

Lines 10-12: Chlorinated polycyclic aromatic hydrocarbons (Cl-PAHs) are toxic contaminants that are widely detected in cold aquatic environments, highlighting a need to understand their aqueous and glacial fate.

Lines 125-129: This study provides new insights into the distinct phototransformation mechanisms of high-ring Cl-PAHs in ice and aqueous systems, which are currently under-represented in the literature and yet enable more accurate evaluation of the environmental persistence and risks posed by similar PAH analogues in seasonally ice-covered regions.

Lines 430-432: The results provide a useful framework to better assess the environmental persistence and risks of chlorinated PAHs, analogues and other derivatives in cold regions.

The revised section in the graphical abstract is as follows:

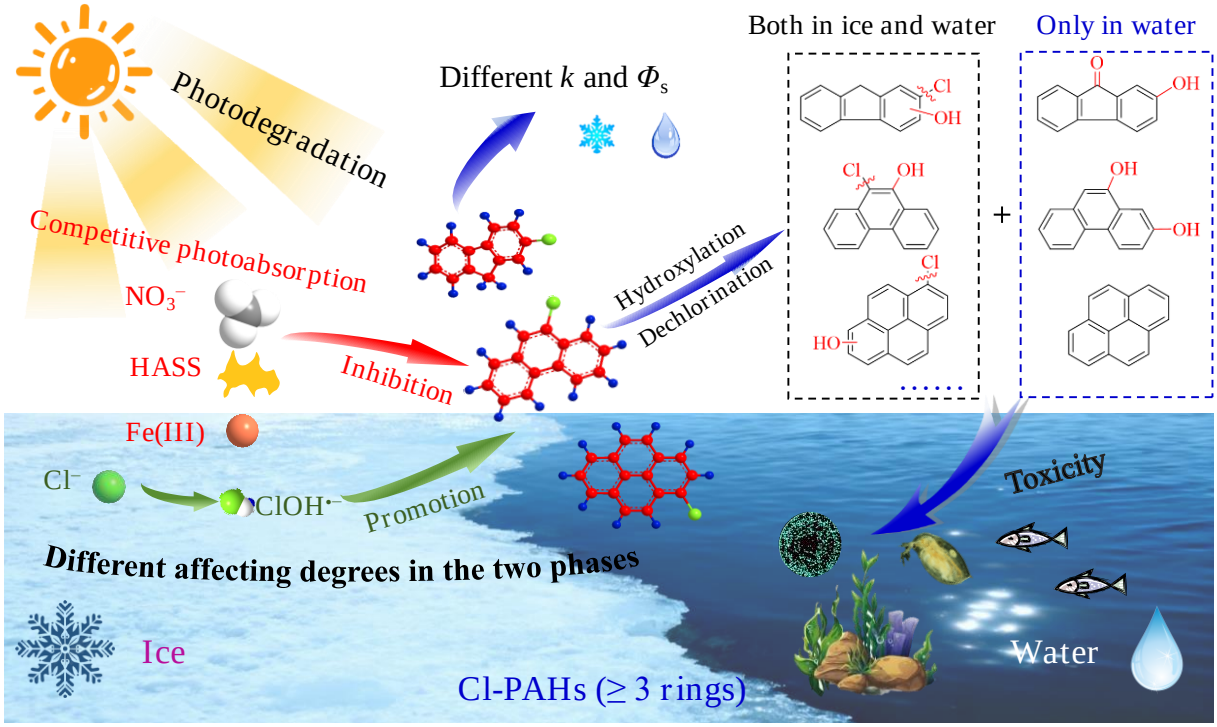

2. This study repeatedly emphasizes the importance of "high-cycle Cl-PAHs" and "≥ 3 rings" in its highlights, abstract, and main text. Indeed, the photo-transformation mechanism of high-cycle Cl-PAHs in ice and water is still a knowledge gap. Therefore, it is recommended that the title include qualifiers such as "high-cycle" or "≥ 3 rings" are added to the title. It will help to clearly highlight the important findings of this study on the high-cycle Cl-PAHs.

Response: Thanks a lot for your constructive suggestion. The suggestion has been adopted. To further highlight the novelty of the "high-cycle Cl-PAHs", we have added "high-ring" to the title. Please see the modified title in the revised manuscript and supplementary material.

The revised section in the manuscript is as follows:

Lines 1-2: Ice and aqueous photochemistry of high-ring chlorinated polycyclic aromatic hydrocarbons: A systematic assessment of persistence and risk in cold regions

The revised section in the supplementary material is as follows:

Page 1 Lines 1-2: Ice and aqueous photochemistry of high-ring chlorinated polycyclic aromatic hydrocarbons: A systematic assessment of persistence and risk in cold regions

3. Materials and methods. The authors attempted to extrapolate the laboratory data to real cold regions. However, light intensity is a crucial parameter in photodegradation. It varies under natural conditions with factors such as water depth and color. When conducting photolytic experiments in the laboratory, did the light intensity differ at different locations within the solution? Did the authors measure it? If so, how was it measured? Please provide detailed explanations.

Response: Thanks for your careful reviewing. We used a UV-A radiometer to measure the intensities of simulated sunlight before and after the test tubes, and took the average values. At wavelengths of 420 nm and 365 nm, the average light intensities at the center of the reaction solution were 8.03 mW cm^{-2} and 8.09 mW cm^{-2}, respectively. Please see Lines 147-148 in the revised manuscript.

The revised section in the manuscript is as follows:

Lines 147-148: The light intensities at the reaction sites were measured with a UV-A radiometer at 420 nm (8.03 mW cm^{-2}) and 365 nm (8.09 mW cm^{-2}), respectively.

4. Materials and methods. Discrepancy of the mass spectrometer model: The model was displayed as "Agilent 1260-6470 BLC-MS^2" in the main text, but it was written as "Agilent triple quadrupole 6470 MS system" in the supplementary material. Please clarify the model and keep it consistent.

Response: Thanks for this useful comment. To ensure consistency in terminology throughout the text, we have standardized the descriptions of instrument models in both the main text and supplementary material to "Agilent 6470B triple quadrupole LC/MS system" after carefully verifying the official model information for Agilent LC-MS/MS instruments. Please see the revised contents in the revised manuscript and supplementary material.

The revised section in the manuscript is as follows:

Lines 168-170: An Agilent 6470B triple quadrupole LC/MS system coupled with an electro spray ionization source operating in negative mode was used to identify key degradation products.

The revised section in the supplementary material is as follows:

Lines 121-122: After the pretreatment steps, samples were analyzed using the Agilent 1260 HPLC combined with the Agilent 6470B triple quadrupole LC/MS system.

5. Sections 3.1 and 3.2. The data in the Fig. 1 may lead readers to mistakenly assume they represent rate constants (k). the labeling of different colors (P_{Mw}) in Fig. 2 is not explained in the figure title.

Response: We appreciate the reviewer for the valuable suggestion. We have revised the description of Fig. 1 in Sections 3.1 and 3.2 to prevent readers from misinterpreting the data as rate constants (k). Meanwhile, we have added an explanation of the color label (P_{Mw}) in the title of Fig. 2 to improve the clarity of the figure. Please see the revised contents in the manuscript.

The revised section in the manuscript is as follows:

Lines 214-216: **Fig. 1.**

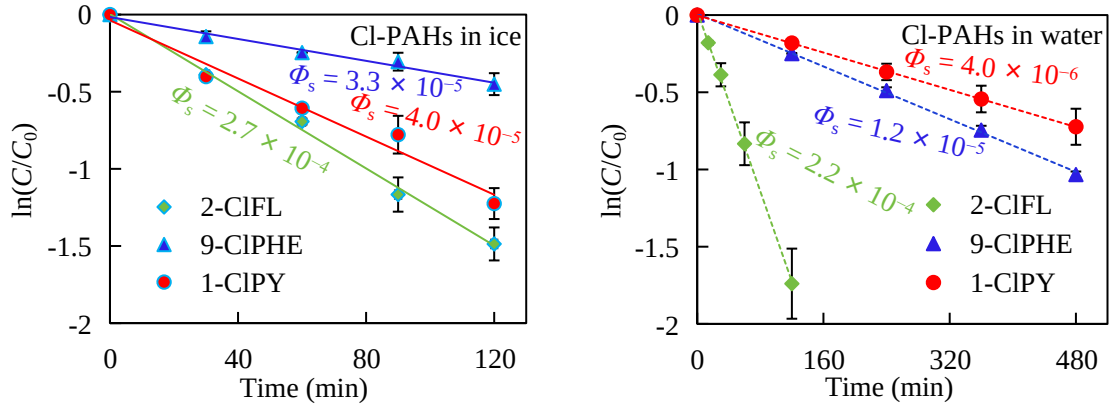

Fig. 1. Simulated solar photolytic kinetics of the three chlorinated PAHs (Cl-PAHs, 2-chlorofluorene (2-ClFL), 9-chlorophenanthrene (9-ClPHE) and 1-chloropyrene (1-ClPY)) in ice and in water.

Lines 278-285: **Fig. 2.**

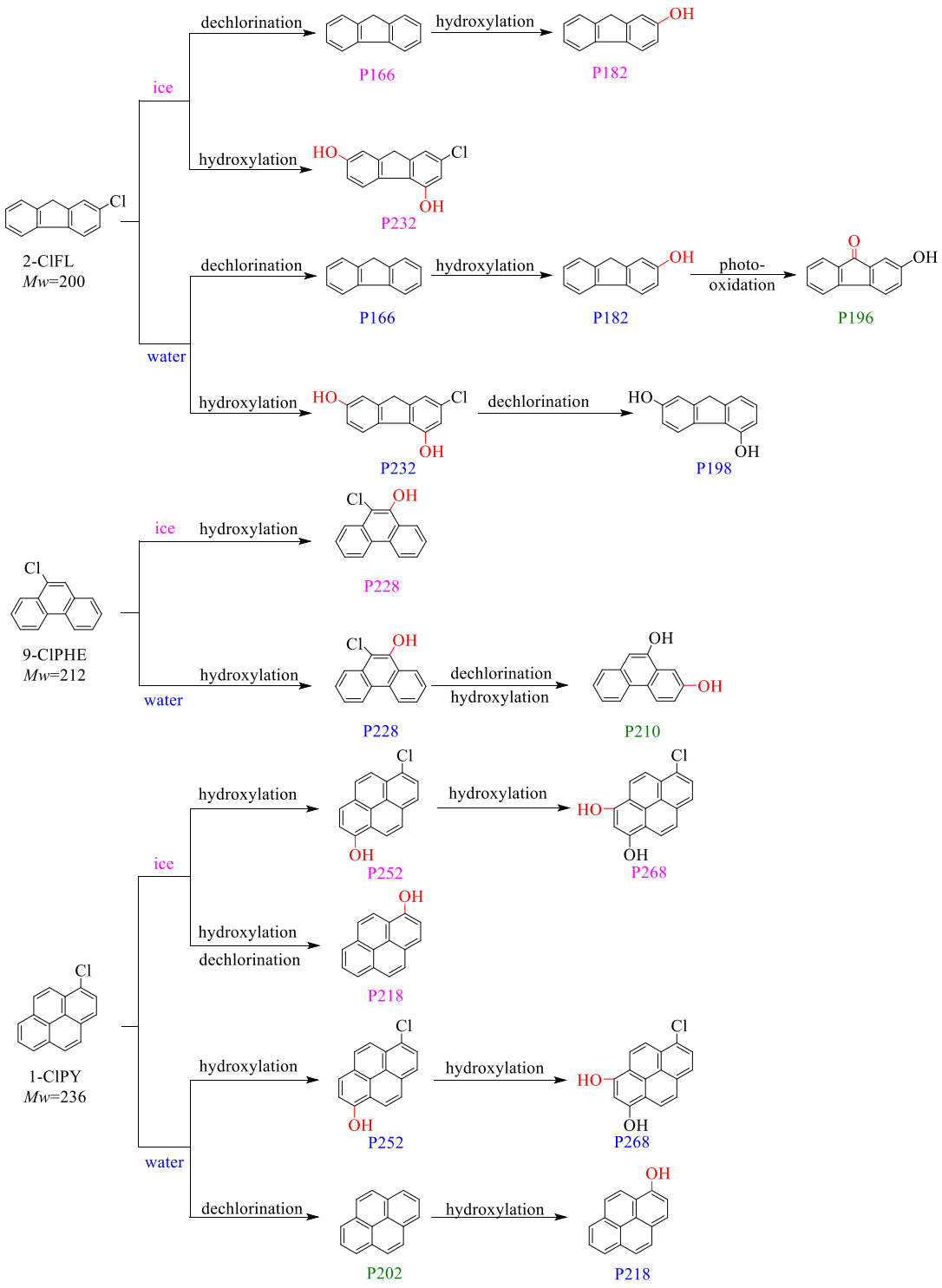

Fig. 2. Photolytic products and transformation pathways associated with the three Cl-PAHs. The photogenerated intermediates are designated as P_{Mw}, where *Mw* denotes molecular weights calculated from the most abundant isotopes. P_{Mw} is marked with different colors to distinguish the products generated in different phases. Among them, 'magenta' indicates products formed in ice, 'blue' indicates products in water, and 'green' represents products that were only formed in the aqueous phase.

6. Section 3.4. To further illustrate the Cl-PAHs toxicity evolution during the apparent photolysis, the authors should perform a significance analysis of the differences in Fig.5.

Response: Thanks for your insightful comment. To further highlight the toxicity evolution of Cl-PAHs during the apparent photolysis, we have supplemented the significance analysis for the differences presented in Fig. 6 (the original Fig. 5) in the revised manuscript. The corresponding statistical results have been added to the figure and elaborated in the revised manuscript. Moreover, we further discuss the reasons for the stronger toxicity of the *Vibrio fischeri* during the photolysis experiment. Please see Lines 397-399 in the revised manuscript.

The revised section in the manuscript is as follows:

Lines 397-399: This might be attributed to the formation of hydroxylated products, which would more easily pass through the lipid cell membrane of *Vibrio fischeri* and exert a stronger inhibition effect (An et al. 2021, Ge et al. 2025, Zhao et al. 2024).

Lines 405-411: **Fig. 6.**

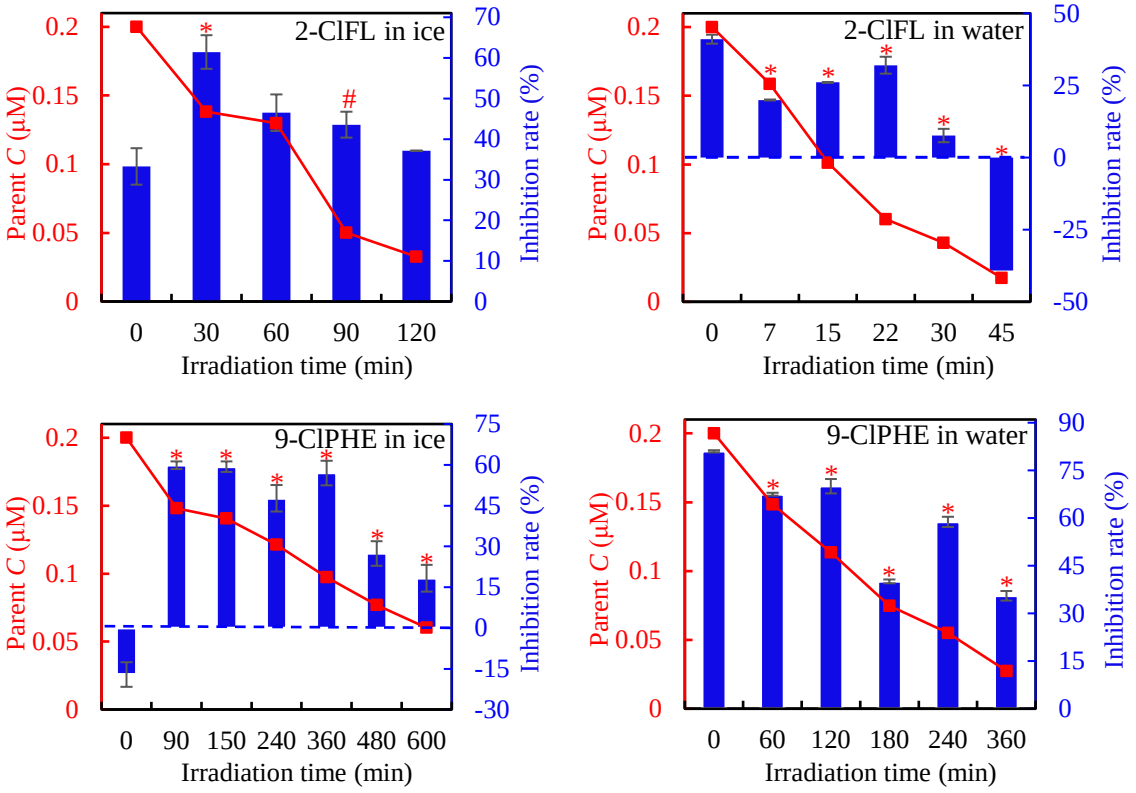

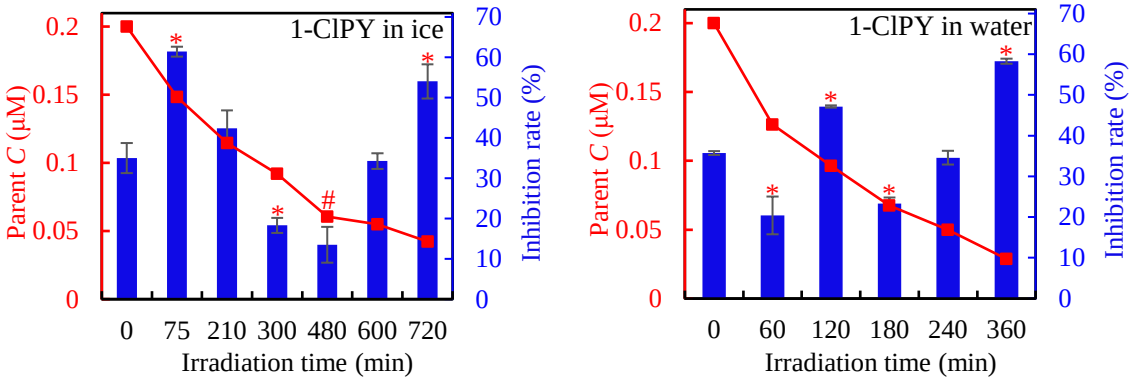

Fig. 6. The evolution of parent concentrations (C, ■) of the three Cl-PAHs, as well as the changes of luminescence inhibition rates (I%, ■) to *Vibrio fischeri* with the irradiation time in ice and in water. * and # indicate significant differences at $p < 0.01$ and 0.05, respectively, between the corresponding I% value at t and the initial value at t_0.

7. Referring to other classes of pollutants such as antibiotics (Water Research, 2025, 286, 124277), the ice photodegradation behavior was influenced with the chemical structure (hydrophilicity) and dissolved organic matter (DOM). As for Cl-PAHs, please compare the ice photochemistry with that of other pollutants (e.g., antibiotics), and discuss the structure-related mechanisms on the key similarities and differences between the ice and aqueous photochemistry.

Response: We sincerely appreciate your helpful comment. In the present study, DOM inhibited Cl-PAH photolysis under simulated sunlight due to comparable spectral absorption. In comparison, DOM exhibited differential inhibition or promotion effects on the photodegradation of antibiotics depending on their hydrophobicity and hydrophilicity (Cui et al. 2025). These observations further demonstrate that the photodegradation is highly dependent on the chemical structure and optical properties of the target compounds. This discussion has been added to the revised manuscript. Please see in Lines 335-338 in the revised manuscript.

The revised section in the manuscript is as follows:

Lines 346-349: In comparison, DOM exerted distinct inhibition or promotion effects on photodegradation depending on the hydrophobicity and hydrophilicity of antibiotics (Cui et al. 2025a). Together, these results confirm that photodegradation is highly dependent on the chemical structure and optical properties of these coexisting dissolved substances.

8. There are many minor errors. Such as, '2,3-dichlornaphthalene underwent photochemical degradation under UV/simulated sunlight which followed first-order kinetics,' (lines 74-75), 'a

series of artificial solutions were prepared' (line 152), 'differences in photochemical degradation rates which indicated that photolysis is also likely to be chemical specific.' (lines 202-203), 'This topic that is underrepresented but important for their environmental persistence and risk assessment in cold regions.' (lines 371-372), 'Cl-PAHs have also frequently detected in tap water' and 'described earlier which highlighted'.

Response: Thanks for your careful observation. We have carefully checked the format and grammars in the revised manuscript. Please see the revised contents in the revised manuscript.

The revised section in the manuscript is as follows:

Lines 27-29: Although ECOSAR predictions indicated that many individual transformation products had comparable or lower toxicity

Lines 63-64: Cl-PAHs have also been frequently detected in tap water (Liu et al. 2021, Tillner et al. 2013).

Lines 68-69: play a key elimination mechanism of many organic pollutants in surface waters

Line 70: The photochemical behavior of certain Cl-PAHs has been examined

Lines 73-76: In aqueous solutions, monochlorinated naphthalenes and 2,3-dichlornaphthalene underwent photochemical degradation under UV/simulated sunlight, which followed first-order kinetics, with the degradation pathways involving hydroxylation, dechlorination and other reactions.

Lines 218-219: differences in photochemical degradation rates, which indicated that photolysis is also likely to be chemical specific.

Lines 330-332: Increased inhibition of photolysis in ice can be rationalized using the same physical mechanisms described earlier, which highlighted enrichment of dissolved solutes at ice grain interfaces.

Line 342: it was apparent in this study that their net affect led to inhibition.

Lines 342-343: This observation can be ascribed to the absorption of a similar light spectrum by 9-ClPHE and dissolved species

Lines 414-415: This topic is underrepresented but important for their environmental persistence and risk assessment in cold regions.

☞ **Response to Reviewer #3 Comments:**

Reviewer #3: This manuscript investigates the ice and aqueous photochemistry of high-cyclic chlorinated PAHs (Cl-PAHs), with an emphasis on photolysis kinetics, transformation pathways,

the effects of water constituents, and toxicity evolution. The work is carefully executed from a technical perspective. However, the study does not reach the level of novelty and depth required for publication in *Journal of Hazardous Materials*.

Response: We sincerely appreciate the valuable and constructive comments from the reviewer. To further improve the quality of the manuscript, we adopted your suggestions, supplemented radical quenching experiments and electron paramagnetic resonance (EPR) spectroscopy to confirm the existence and involvement of ·OH in the apparent photolysis of the three Cl-PAHs [Lines 265-274, Fig. 3 (EPR spectra and the contribution ratios $R_{\cdot OH}$)]. Moreover, we have supplemented some new data [Figs. S6-S8 (DFT calculations), Table S6 (the pH change values of reaction solutions), and Table S13 (Environmental photolytic half-lives ($t_{1/2,E}$) for the parent PAHs and hydroxylated (OH-) PAHs)], added explanations on the results (Lines 203-208, 248-252, 317-325, 346-349, 370-381 and 397-399), and optimized the Figs 1-2, 6 (the original Fig. 5) and S9 (the original Fig. S6). We have further emphasized the novelty and significance of this work in the revised manuscript and added the "high-ring" in the title. Please see the changes marked in the revised manuscript and the revised supplementary material.

Major concerns

1.One of the core findings of this study is that the photodegradation rate in ice is significantly higher than in water, which the authors primarily attribute to physical enrichment processes during freezing. However, this phenomenon and its underlying physical mechanisms have already been widely reported and thoroughly validated in previous studies concerning other PAHs and their derivatives. Applying this known framework to a new set of Cl-PAH analogs constitutes incremental research. The manuscript produces results that closely mirror previous findings, thus offering no new theoretical insights into environmental photochemistry.

Response: We thank the reviewer for the critical and thoughtful assessment. To our best knowledge, this is the first study to comprehensively investigate the ice and aqueous phase photochemistry of high-ring Cl-PAH congeners (≥ 3 rings), and to link their transformation pathways with resulting changes in toxicity in cold aquatic systems. To further improve the quality of the manuscript, we adopted your suggestions, and supplemented new data (Figs. 3, S6-S8, Table S6 and Table S13).

As for the comment, firstly we further elucidated the reason for the differences in photodegradation of ice and water. Please see Lines 203-208 in the revised manuscript. Furthermore, we have strengthened and highlighted the novelty and environmental significance of this study in the revised introduction section, emphasizing the environmental significance of

this study and its specific contribution. Cl-PAHs are a class of high-toxicity, persistent halogenated pollutants with significant environmental relevance. The similarities and key differences between the ice and aqueous photochemistry of high-cycle Cl-PAHs (≥ 3 rings) have rarely been investigated, particularly under environmentally relevant conditions. Therefore, this research provides new experimental evidence regarding the photochemical fate of high-ring Cl-PAHs in the cryosphere, which is crucial for assessing their environmental persistence and ecological risks in seasonally ice-covered region. Please see the revised contents in the revised manuscript.

The revised section in the manuscript is as follows:

Lines 125-129: This study provides new insights into the distinct phototransformation mechanisms of high-ring Cl-PAHs in ice and aqueous systems, which enables more accurate evaluation of the environmental persistence, fate and risks posed by similar PAH analogues in seasonally ice-covered regions.

Lines 203-208: During water freezing into ice, pollutant molecules are preferentially partitioned into liquid-like regions (LLRs), accompanied by both concentration-enhancement and ice-cage effects (Ge et al. 2023). The dual effects may respectively enhance solute concentrations at the grain boundaries of ice crystals and create micro-fields around them via solvent molecules. The synergistic mechanisms ultimately modulate the photolytic kinetics of the solute compounds through interfacial microenvironment.

Lines 430-432: The results provide a useful framework to better assess the environmental persistence and risks of chlorinated PAHs, analogues and other derivatives in cold regions.

2.This study concludes that photo-induced hydroxylation and dechlorination are the dominant primary reactions for these Cl-PAHs. When discussing the hydroxylation mechanism, the authors attribute it to the involvement of reactive oxygen species (e.g., ·OH) generated via substrate sensitization. However, this mechanistic pathway is inferred solely from the mass spectra of the final degradation products. The manuscript lacks direct experimental evidence (such as radical quenching experiments or EPR spectroscopy) to confirm their involvement.

Response: We sincerely appreciate the reviewer's insightful and constructive comments. To address the critical concern for the lack of direct experimental evidence for the proposed hydroxylation mechanism, we have supplemented electron paramagnetic resonance (EPR)

spectroscopy and ·OH radical quenching experiment to confirm the generation and participation of ·OH in the apparent photolysis of the three Cl-PAHs. The results can be seen in Fig. 3. Moreover, the sites where Cl-PAHs are prone to attack by free radicals (such as ·OH) are determined through density functional theory (DFT) calculations (Figs. S6-S8), and the product structures were further optimized (Fig. 2). Please see the revised contents in the revised manuscript and supplementary material.

The revised section in the manuscript is as follows:

Lines 153-155: To test whether hydroxyl radicals (·OH) participated in the apparent photolysis, quenching radical experiments were performed using isopropanol as the quencher of ·OH (Text S1).

Lines 170-172: The generated ·OH was identified by electron paramagnetic resonance (EPR) spectra with 5,5'-dimethyl-1-pirroline-N-oxide (DMPO) as a spin-trap reagent. Relevant details are provided in Text S4.

Lines 265-274: The prevalence of hydroxylation reaction can be ascribed to the generation of ·OH radicals from the photo-sensitization of the parent compounds in the two phases. As shown in Fig. 3, EPR spectra showed four sets of peaks with 1:2:2:1 under irradiation, corresponding to the characteristic of the DMPO-·OH, which verified the generation of ·OH from photo-sensitization of Cl-PAHs. Combined with radical quenching experiments (Text S4), the involvement of ·OH in the apparent photolysis was confirmed, and the contribution ratios ($R_{\cdot OH}$) of self-sensitized photo-oxidation via ·OH to the apparent photolysis were illustrated in Fig. 3. The ·OH was speculated during the photolysis of several PAHs and SPAHs (Ge et al. 2025, Sarmiento et al. 2023). However, the formation and participation of ·OH were proved in the present study.

Lines 278-285: **Fig. 2.**

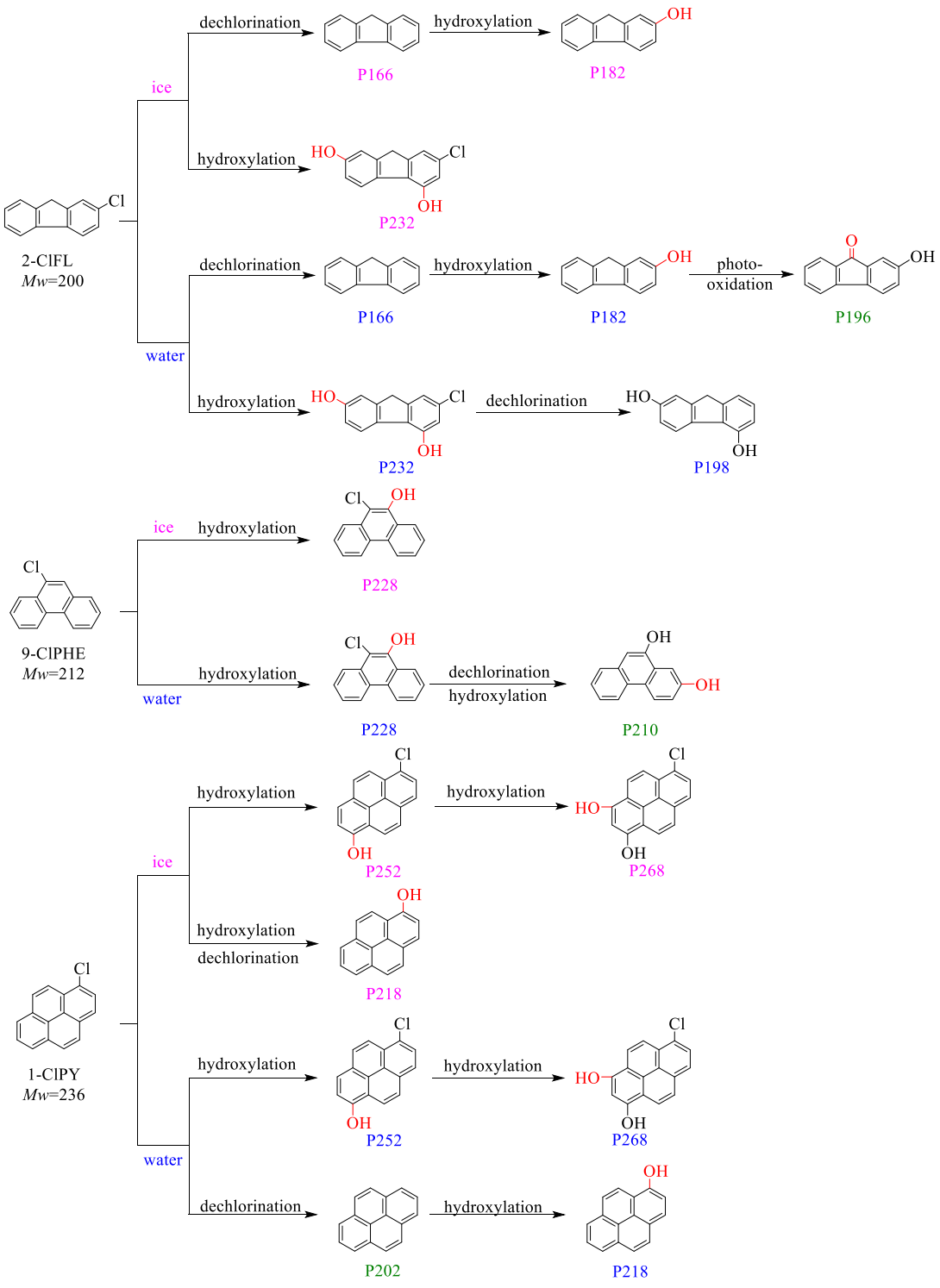

Fig. 2. Photolytic products and transformation pathways associated with the three Cl-PAHs. The photogenerated intermediates are designated as P_{Mw}, where *Mw* denotes molecular weights calculated from the most abundant isotopes. P_{Mw} is marked with different colors to distinguish the products generated in different phases. Among them, 'magenta' indicates products formed in ice, 'blue' indicates products in water, and 'green' represents products that were only formed in the aqueous phase.

Lines 287-289: **Fig. 3.**

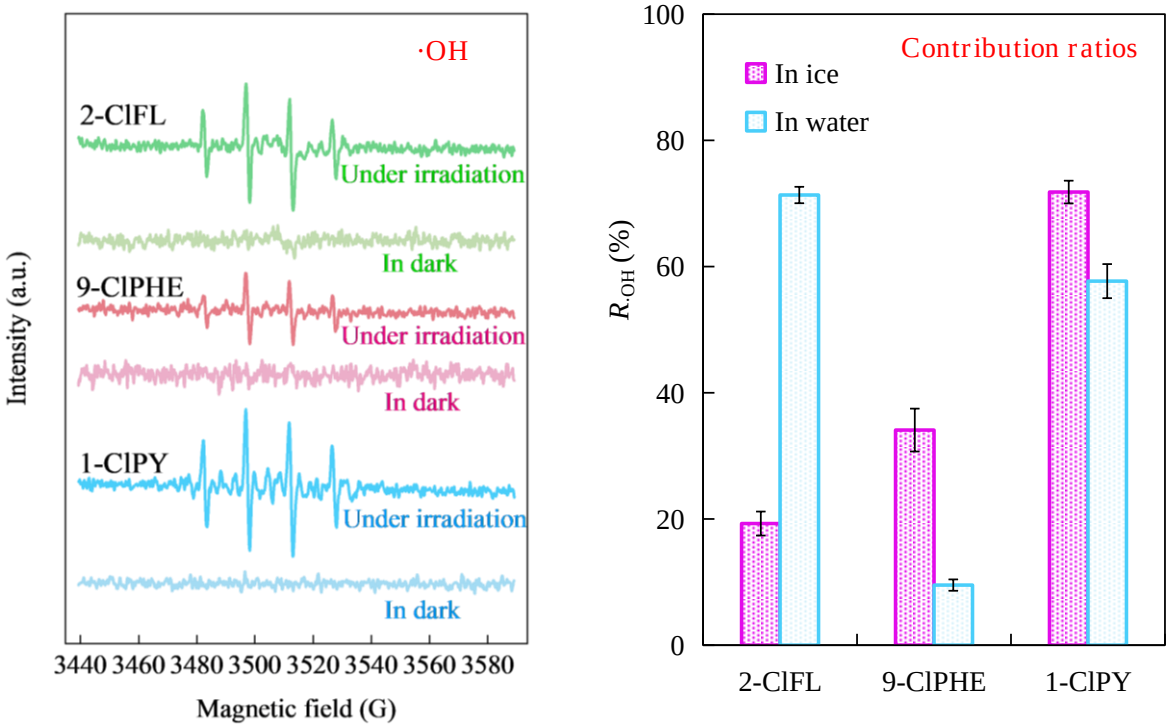

Fig. 3. The electron paramagnetic resonance (EPR) spectra (left) and the contribution ratios ($R_{\cdot OH}$) of self-sensitized photo-oxidation via ·OH to the apparent photolysis (right) of the three Cl-PAHs.

The revised section in the supplementary material is as follows:

Pages 30-32: **Figs. S6-S8**.

2-ClFL

(a) (b)

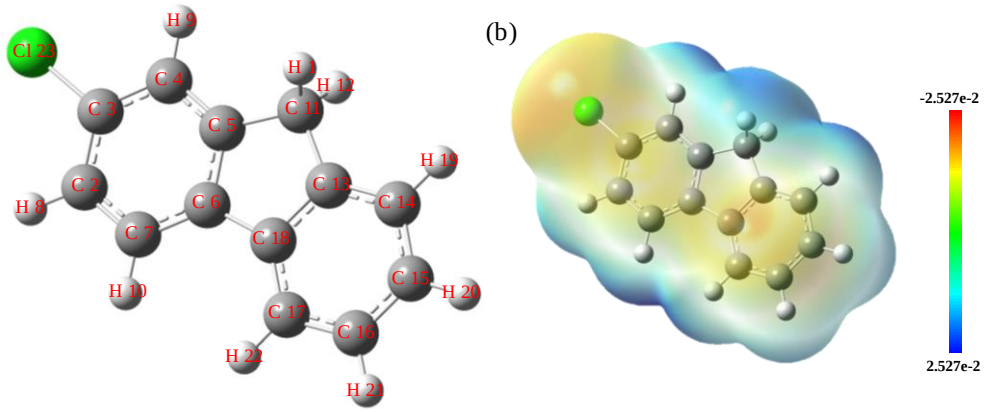

(c) (d)

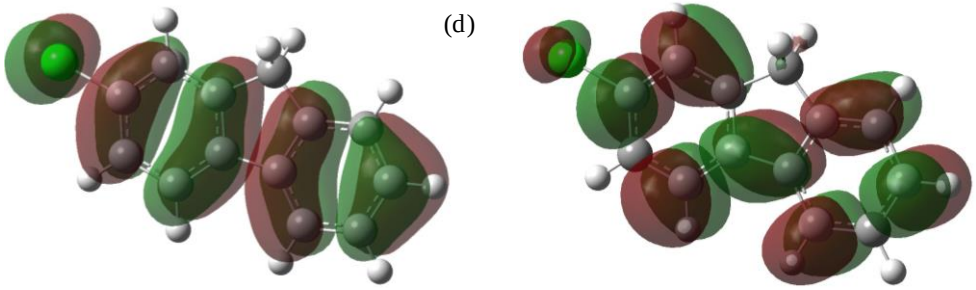

(e)

Atom	Site	q(N)	q(N+1)	q(N–1)	f^-	f^+	f^0
H	1	0.0469	0.0237	0.0697	0.0227	0.0233	0.0230
C	2	-0.0480	-0.0859	-0.0017	0.0464	0.0379	0.0421
C	3	0.0227	-0.0485	0.0882	0.0656	0.0711	0.0683
C	4	-0.0500	-0.1059	-0.0148	0.0353	0.0559	0.0456
C	5	0.0053	-0.0228	0.0456	0.0403	0.0281	0.0342
C	6	-0.0076	-0.0578	0.0429	0.0505	0.0502	0.0503
C	7	-0.0371	-0.1020	0.0096	0.0467	0.0650	0.0558
H	8	0.0492	0.0203	0.0784	0.0292	0.0289	0.0291
H	9	0.0487	0.0164	0.0751	0.0264	0.0323	0.0294
H	10	0.0474	0.0152	0.0745	0.0271	0.0322	0.0297
C	11	-0.0415	-0.0548	-0.0251	0.0165	0.0133	0.0149
H	12	0.0469	0.0237	0.0697	0.0227	0.0233	0.0230
C	13	0.0003	-0.0283	0.0435	0.0431	0.0286	0.0359
C	14	-0.0455	-0.0975	-0.0090	0.0365	0.0520	0.0443
C	15	-0.0429	-0.1255	0.0434	0.0863	0.0826	0.0845
C	16	-0.0432	-0.0828	0.0047	0.0479	0.0396	0.0438
C	17	-0.0431	-0.1037	0.0028	0.0459	0.0606	0.0532
C	18	-0.0087	-0.0512	0.0380	0.0467	0.0424	0.0446
H	19	0.0435	0.0113	0.0717	0.0282	0.0322	0.0302
H	20	0.0438	0.0027	0.0813	0.0375	0.0411	0.0393
H	21	0.0440	0.0137	0.0751	0.0311	0.0303	0.0307
H	22	0.0432	0.0127	0.0696	0.0264	0.0305	0.0285
Cl	23	-0.0738	-0.1726	0.0669	0.1408	0.0987	0.1198

Fig. S6. The chemical structure (a), the electrostatic potential (ESP) (b), the highest occupied molecular orbital (HOMO) (c), the lowest unoccupied molecular orbital (LUMO) (d), and Fukui indices(f^-, f^+ and f^0) distribution (e) of 2-ClFL.

9-ClPHE

(a)

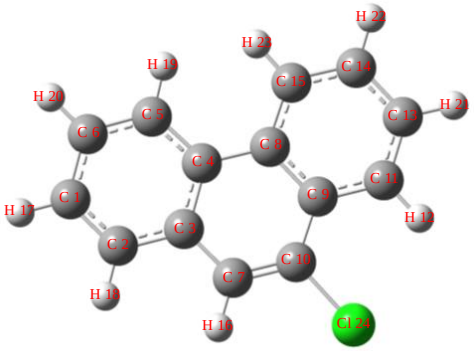

(b)

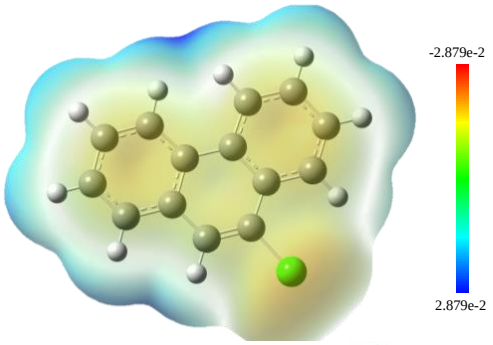

(c)

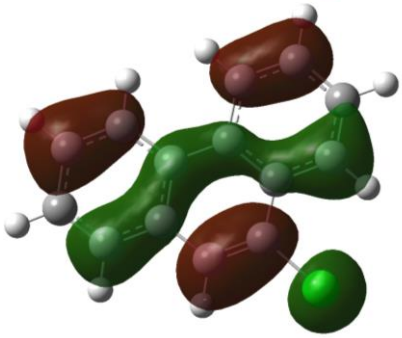

(d)

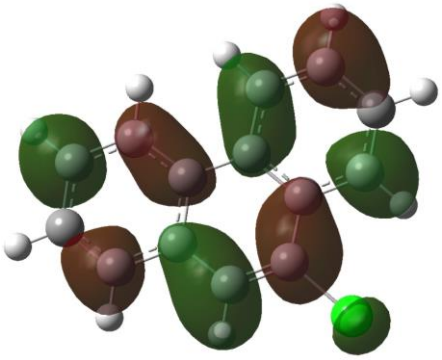

(e)

Atom	Site	q(N)	q(N+1)	q(N–1)	f^-	f^+	f^0
C	1	-0.0404	-0.0789	-0.0032	0.0371	0.0385	0.0378
C	2	-0.0390	-0.0877	0.0150	0.0540	0.0487	0.0514
C	3	0.0000	-0.0233	0.0279	0.0278	0.0234	0.0256
C	4	0.0009	-0.0234	0.0280	0.0270	0.0243	0.0257
C	5	-0.0396	-0.0772	-0.0006	0.0390	0.0376	0.0383
C	6	-0.0405	-0.1107	0.0342	0.0748	0.0701	0.0724
C	7	-0.0480	-0.1294	0.0257	0.0737	0.0814	0.0776
C	8	0.0045	-0.0178	0.0209	0.0164	0.0222	0.0193
C	9	-0.0068	-0.0282	0.0076	0.0145	0.0214	0.0179
C	10	0.0231	-0.0465	0.0881	0.0650	0.0696	0.0673
C	11	-0.0429	-0.0963	0.0105	0.0534	0.0534	0.0534
H	12	0.0363	0.0096	0.0602	0.0240	0.0267	0.0253
C	13	-0.0384	-0.0771	-0.0010	0.0374	0.0386	0.0380
C	14	-0.0387	-0.1090	0.0257	0.0645	0.0703	0.0674
C	15	-0.0397	-0.0816	0.0031	0.0428	0.0419	0.0424
H	16	0.0486	0.0117	0.0800	0.0314	0.0369	0.0342
H	17	0.0466	0.0176	0.0750	0.0284	0.0290	0.0287
H	18	0.0448	0.0171	0.0724	0.0276	0.0277	0.0276
H	19	0.0425	0.0209	0.0645	0.022	0.0216	0.0218
H	20	0.0456	0.0094	0.0798	0.0342	0.0362	0.0352
H	21	0.0474	0.0183	0.0749	0.0275	0.0291	0.0283
H	22	0.0464	0.0099	0.0782	0.0319	0.0364	0.0342
H	23	0.0428	0.0202	0.0643	0.0215	0.0226	0.0220
Cl	24	-0.0550	-0.1473	0.0691	0.1241	0.0923	0.1082

Fig. S7. The chemical structure (a), the electrostatic potential (ESP) (b), the highest occupied molecular orbital (HOMO) (c), the lowest unoccupied molecular orbital (LUMO) (d), and Fukui indices (f^-, f^+ and f^0) distribution (e) of 9-ClPHE.

(a) (b)

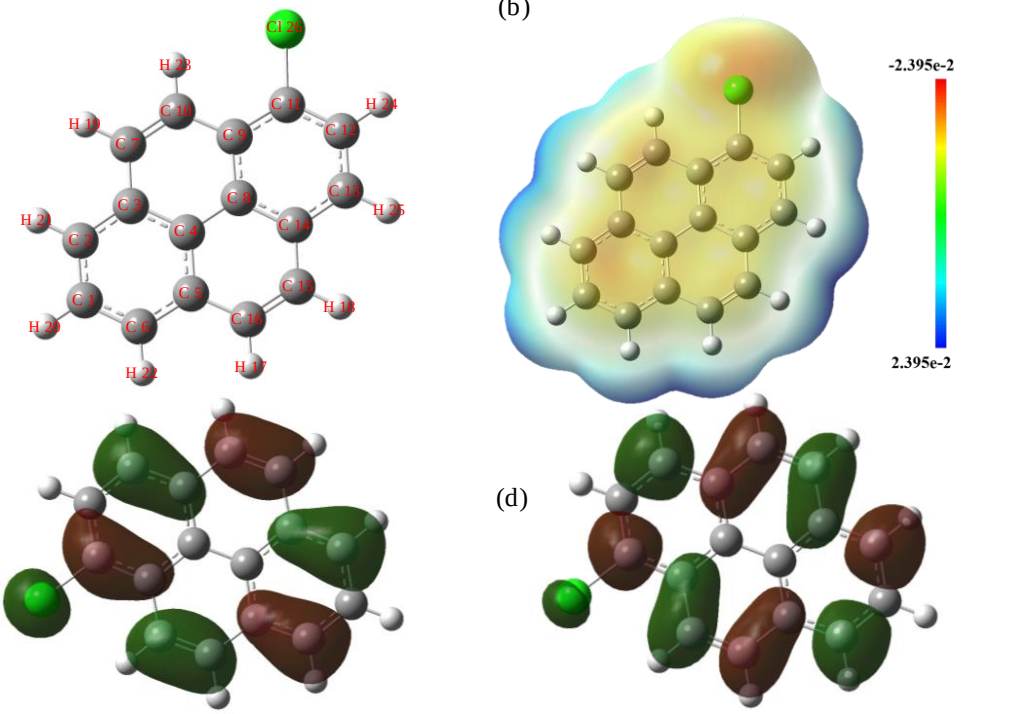

(c) (d)

(e)

Atom	Site	q(N)	q(N+1)	q(N–1)	f^-	f^+	f^0
C	1	-0.0415	-0.0778	-0.0070	0.0345	0.0363	0.0354
C	2	-0.0400	-0.1061	0.0288	0.0688	0.0661	0.0674
C	3	-0.0011	-0.0259	0.0247	0.0258	0.0248	0.0253
C	4	0.0027	-0.0046	0.0101	0.0073	0.0073	0.0073
C	5	-0.0009	-0.0257	0.0230	0.0239	0.0248	0.0244
C	6	-0.0404	-0.1071	0.0294	0.0698	0.0667	0.0683
C	7	-0.0360	-0.0908	0.0145	0.0505	0.0548	0.0527
C	8	0.0055	-0.0020	0.0127	0.0072	0.0075	0.0074
C	9	-0.0073	-0.0335	0.0164	0.0237	0.0263	0.0250
C	10	-0.0443	-0.0957	0.0064	0.0506	0.0515	0.0510
C	11	0.0227	-0.0333	0.0791	0.0564	0.056	0.0562
C	12	-0.0482	-0.0812	-0.0175	0.0307	0.0330	0.0319
C	13	-0.0380	-0.1047	0.0277	0.0657	0.0667	0.0662
C	14	-0.0022	-0.0294	0.0245	0.0266	0.0272	0.0269
C	15	-0.0403	-0.0912	0.0112	0.0515	0.0509	0.0512
C	16	-0.0396	-0.0928	0.0144	0.0540	0.0531	0.0536
H	17	0.0453	0.0158	0.0730	0.0277	0.0295	0.0286
H	18	0.0453	0.0163	0.0725	0.0272	0.0290	0.0281
H	19	0.0463	0.0166	0.0731	0.0268	0.0297	0.0283
H	20	0.0461	0.0179	0.0733	0.0272	0.0282	0.0277
H	21	0.0441	0.0119	0.0746	0.0305	0.0322	0.0313
H	22	0.0437	0.0113	0.0744	0.0307	0.0325	0.0316
H	23	0.0381	0.0117	0.0623	0.0242	0.0265	0.0253
H	24	0.0497	0.0237	0.0746	0.0248	0.0260	0.0254
H	25	0.0470	0.0148	0.0769	0.0299	0.0323	0.0311
Cl	26	-0.0565	-0.1376	0.0473	0.1038	0.0812	0.0925

Fig. S8. The chemical structure (a), the electrostatic potential (ESP) (b), the highest occupied molecular orbital (HOMO) (c), the lowest unoccupied molecular orbital (LUMO) (d), and Fukui indices (f^-, f^+ and f^0) distribution (e) of 1-ClPY.

References

An, Z., Han, D., Sun, J., Mei, Q., Wei, B., Li, M., Qiu, Z., Bo, X., Wang, X., Xie, J., Zhan, J., He, M., 2021. Full insights into the roles of pH on hydroxylation of aromatic acids/bases and toxicity evaluation. Water Res 190, 116689. https://doi.org/10.1016/j.watres.2020.116689.

Chen, C., Chen, L., Yao, Y., Artigas, F., Huang, Q., Zhang, W., 2019. Organotin release from polyvinyl chloride microplastics and concurrent photodegradation in water: Impacts from salinity, dissolved organic matter, and light exposure. Environ Sci Technol 53(18), 10741-10752. https://pubs.acs.org/doi/10.1021/acs.est.9b03428.

Chen, J.N., Chen, L.j., Wu, L.L., Yan, C.Y., Sun, N.X., Peng, G.L., Yang, S.G., He, H., Qi, C.D., 2025. Activation of metabisulfite by dissolved Fe(III) at environmentally relevant concentrations for organic contaminants degradation. Int J Mol Sci 26(3), 953. https://doi.org/10.3390/ijms26030953.

Cui, J.S., Chen, Y., Cheng, F.Y., Yang, H., Qu, J., Zhang, Y.-n., Peijnenburg, W.J.G.M., 2025. Hydrophilicity-dependent photodegradation of antibiotics in ice: Freeze-concentration effects and dissolved organic matter interactions drive divergent kinetics, pathways and toxicity. Water Res 286, 124277. https://doi.org/10.1016/j.watres.2025.124277.

El Omar, A.K., Schmidhammer, U., Rousseau, B., LaVerne, J., Mostafavi, M., 2012. Competition reactions of $H_2O^{\bullet+}$ radical in concentrated Cl^- aqueous solutions: Picosecond pulse radiolysis study. J Phys Chem A 116(47), 11509-11518. https://pubs.acs.org/doi/10.1021/jp309381z.

Ge, L.K., Cao, S.K., Halsall, C., Niu, J.F., Bai, D.X., He, G.K., Zhang, P., Ma, H.R., 2023. Photodegradation of hydroxyfluorenes in ice and water: A comparison of kinetics, effects of water constituents, and phototransformation by-products. J Environ Sci 124, 139-145. https://doi.org/10.1016/j.jes.2021.11.002.

Ge, L.K., Hou, Z.M., Niu, J.F., Wang, S.Y., Zhang, P., Zhu, Y.Q., 2025. New insights into the environmental photochemistry of hydroxynaphthalene congeners in water and in ice: A distinct comparative study. J Hazard Mater 493, 138310. https://doi.org/10.1016/j.jhazmat.2025.138310.

Ge, L.K., Li, J., Na, G.S., Chen, C.-E., Huo, C., Zhang, P., Yao, Z.W., 2016a. Photochemical degradation of hydroxy PAHs in ice: Implications for the polar areas. Chemosphere 155, 375-379. https://doi.org/10.1016/j.chemosphere.2016.04.087.

Ge, L.K., Na, G.S., Chen, C.E., Li, J., Ju, M.W., Wang, Y., Li, K., Zhang, P., Yao, Z.W., 2016b. Aqueous photochemical degradation of hydroxylated PAHs: Kinetics, pathways, and multivariate effects of main water constituents. Sci Total Environ 547, 166-172. https://doi.org/10.1016/j.scitotenv.2015.12.143.

Liu, Q.Z., Xu, X., Lin, L.H., Yang, G., Wang, D.H., 2021. Occurrence, health risk assessment and regional impact of parent, halogenated and oxygenated polycyclic aromatic hydrocarbons in tap water. J Hazard Mater 413, 125360. https://doi.org/10.1016/j.jhazmat.2021.125360.

Mason, D.P., Elwood Madden, M.E., 2022. Raman spectroscopy of high salinity brines and ices. Icarus 372, 114759. https://doi.org/10.1016/j.icarus.2021.114759.

Ram, K., Anastasio, C., 2009. Photochemistry of phenanthrene, pyrene, and fluoranthene in ice and snow. Atmos Environ 43(14), 2252-2259. https://doi.org/10.1016/j.atmosenv.2009.01.044.

Sarmiento, D.J., Majestic, B.J., 2023. Formation of environmentally persistent free radicals from the

irradiation of polycyclic aromatic hydrocarbons. J Phys Chem A 127(25), 5390-5401. https://doi.org/10.1021/acs.jpca.3c01405.

Tillner, J., Hollard, C., Bach, C., Rosin, C., Munoz, J.-F., Dauchy, X., 2013. Simultaneous determination of polycyclic aromatic hydrocarbons and their chlorination by-products in drinking water and the coatings of water pipes by automated solid-phase microextraction followed by gas chromatography–mass spectrometry. J Chromatogr A 1315, 36-46. https://doi.org/10.1016/j.chroma.2013.09.047.

Wang, J.J., Liu, X.C., Beusen, A.H.W., Middelburg, J.J., 2023. Surface-water nitrate exposure to world populations has expanded and intensified during 1970–2010. Environ Sci Technol 57(48), 19395-19406. https://pubs.acs.org/doi/10.1021/acs.est.3c06150.

Wu, D., Hu, Y.L., Liu, Y., Zhang, R.Y., 2021. Review of chloride ion detection technology in water. Appl Sci 11(23), 11137. https://doi.org/10.3390/app112311137.

Yang, X., Rosario-Ortiz, F.L., Lei, Y., Pan, Y.H., Lei, X., Westerhoff, P., 2022. Multiple roles of dissolved organic matter in advanced oxidation processes. Environ Sci Technol 56(16), 11111-11131. https://doi.org/10.1021/acs.est.2c01017.

Zhao, X., Yang, P., Lu, J., Chen, J., 2024. Comparative study of the degradation of meta-chloronitrobenzene by UV/hydrogen peroxide and UV/persulfate oxidation: Degradation pathways and toxicity. Chem Eng J 490, 151502. https://doi.org/10.1016/j.cej.2024.151502.

Ice and aqueous photochemistry of high-ring chlorinated polycyclic aromatic hydrocarbons: A systematic assessment of persistence and risk in cold regions

Linke Ge[a,b], Rongyan Xu[a], Jack Garnett[b], Peng Zhang[a,*], Dongxiao Bai[a], Siyuan Wang[a,*]

[a]Shaanxi University Key Laboratory of Industrial Pollution Control and Environmental Health, School of Environmental Science and Engineering, Shaanxi University of Science & Technology, Xi'an 710021, China

[b]Lancaster Environment Centre, Lancaster University, Lancaster LA1 4YQ, United Kingdom

Abstract:

Chlorinated polycyclic aromatic hydrocarbons (Cl-PAHs) are toxic contaminants that are widely detected in cold aquatic environments, highlighting a need to understand their aqueous and glacial fate. We systematically investigated the photochemistry of three high-ring Cl-PAHs (≥ 3 rings), 2-chlorofluorene (2-ClFL), 9-chlorophenanthrene (9-ClPHE) and 1-chloropyrene (1-ClPY) in ice and aqueous matrices. Under simulated solar irradiation (λ > 290 nm), all three compounds underwent photodegradation that followed first-order kinetics, but with different rate constants and quantum yields. Overall, photodegradation in ice was up to 6-fold faster than in water, a difference attributed primarily to physical enrichment processes during freezing. HPLC-MS/MS analysis of intermediates indicated that photo-induced hydroxylation and dechlorination were the dominant primary reactions for these Cl-PAHs, and several secondary pathways differed between the two phases. The generation and participation of ·OH in the apparent photolysis were confirmed by EPR and quenching radical experiments. Furthermore, 9-ClPHE photodegraded more rapidly in seawater ice than in freshwater or pure-water ice,

* Corresponding author.

E-mail addresses: zhangpeng4477@sust.edu.cn (P. Zhang), wangsiyuan@sust.edu.cn (S. Wang).

whereas its aqueous photodegradation was fastest in pure water. This pattern likely reflects that Cl^- enhances photodegradation more in ice than in water, and that the inhibition effects of other major constituents (Fe(III), HASS and NO_3^-) are more pronounced in ice. Environmentally relevant photolytic half-lives ($t_{1/2,E}$) extrapolated from laboratory data for the three Cl-PAHs ranged from several hours to tens of days in selected cold regions. Although ECOSAR predictions indicated that many individual transformation products had comparable or lower toxicity, bioluminescence assays with *Vibrio fischeri* revealed substantial photo-enhanced combined toxicities of the parent Cl-PAHs and their intermediates. These results clarify both the similarities and key differences between the ice and aqueous photochemistry, improving evaluation of the environmental fate and risks posed by PAH analogues and derivatives in seasonally ice-covered regions.

Environmental Implication

Chlorinated PAHs are widely detected in aquatic systems, urging novel insights into their glacial and aqueous environmental fate, especially for high-ring Cl-PAHs (≥ 3 rings). In this study, not only photolysis kinetics, pathways and photo-induced toxicity of three high-ring Cl-PAHs varied between the reaction media (ice/water), but the main dissolved substances displayed more significant promotion or inhibition effects in ice than in water. These findings elucidate the nuanced similarities and divergences between ice and aqueous photochemistry, thereby enabling more accurate evaluation of the environmental fate and risks posed by PAH analogues and derivatives in seasonally ice-covered regions.

Keywords: Chlorinated PAHs; Ice photochemistry; Aqueous photochemistry; Photodegradation kinetics; Transformation mechanisms; Toxicity evolution

1. Introduction

Chlorinated PAHs (Cl-PAHs) are a significant category of substituted polycyclic aromatic hydrocarbons (SPAHs) generated by substituting hydrogen atoms with chlorine atoms in PAHs

(Ali et al. 2024, Jin et al. 2020, Xie et al. 2021). Cl-PAHs have emerged as environmental contaminants of concern due to their higher toxicity than parent PAHs, demonstrating multiple teratogenic, carcinogenic, and mutagenic effects (Peng et al. 2023). Importantly, Cl-PAHs in the atmosphere have been found to originate from diverse sources, including atmospheric transformation of industrial PAH emissions and incomplete combustion of fossil fuels plus others (Klimczak et al. 2023, Liu et al. 2023, Zhang et al. 2024). Furthermore, photo-chlorination of PAHs can also produce Cl-PAHs in waters during industrial and environmental processes. For example, chlorination disinfection of tap water (Liu et al. 2021), solar chlorination of seawater (Cai et al. 2024a, Tu et al. 2023), and phototransformation in saline ice under simulated sunlight (Li et al. 2024a). Consequently, Cl-PAHs are widely detected in the atmosphere (Oda et al. 2024), surface waters (Qi et al. 2023, Qiao et al. 2018, Wang et al. 2016), as well as sediments and soils (Table S1 and associated refs.). Concentrations of Cl-PAHs in environmental water samples collected throughout China were reported from 3.1 ng L^{-1} to 29.6 ng L^{-1} in Beijing urban rivers, and from 7.8 ng L^{-1} to 25.7 ng L^{-1} in Shaoping Lake of Henan (Qiao et al. 2018, Wang et al. 2016). Also, the mean concentration of Cl-PAHs detected in the surface water of Qingdao was 0.91 ng L^{-1} (Qi et al. 2023). Cl-PAHs have also been frequently detected in tap water (Liu et al. 2021, Tillner et al. 2013). Thus, given their hazardous nature, wide sources and environmental ubiquity of Cl-PAHs, it is essential to investigate different environmental transformation pathways and ecological toxicity to adequately assess their environmental risk.

Photochemical transformation has been demonstrated to play a key elimination mechanism of many organic pollutants in surface waters, atmosphere and surface soil (Guo et al. 2023, Hu et al. 2021, Tu et al. 2023). The photochemical behavior of certain Cl-PAHs has been examined (Ohura et al. 2008, Zhao et al. 2022), however, these focused on different media (i.e., cyclohexane, atmospheric particulates and surface soil) and included only limited Cl-PAHs (2

rings). In aqueous solutions, monochlorinated naphthalenes and 2,3-dichlornaphthalene underwent photochemical degradation under UV/simulated sunlight, which followed first-order kinetics, with the degradation pathways involving hydroxylation, dechlorination and other reactions (Kang et al. 2018, Yu et al. 2024). Furthermore, Ge et al. (2025a) found that 4-chloro-1-hydroxynaphthalene (4-Cl-1-OHN) displayed faster degradation under ice and water photolysis compared to other 3 hydroxyl naphthalenes without chlorine substitution, showing distinct pathways for ice and water phases. As for high-ring Cl-PAHs (≥ 3 rings), their aqueous photochemical transformation remains unknown. Therefore, not only photolytic kinetics and mechanisms need to be investigated for these high-ring Cl-PAHs, but their glacial and aqueous photochemical behavior requires comparative studies so as to provide a useful rationale to further assess their environmental persistence and risk in aquatic systems.

Ice and snow represent a crucial environmental medium, covering approximately 11%−40% of the Earth surface. In remote cold areas, especially in polar regions, ice/snow has been proved to serve as an important reactive repository for the deposited atmospheric persistent contaminants, such as PAHs (Azcune et al. 2022, Hung et al. 2022, Xie et al. 2022). Despite the lack of reported detection of Cl-PAHs in natural ice/snow, their presence in cold regions is most possible because the local abundant PAHs can be feasibly transformed into Cl-PAHs (Cai et al. 2024a, Liu et al. 2021, Tu et al. 2023). Previous studies have indicated that ice plays a dominant role in the photochemical attenuation of organic pollutants in cold areas, where microbial activity is negligible (Ge et al. 2023, Ge et al. 2025a). Especially, long-period sunlight prevails in summers of the Arctic and Antarctic, which promotes the phototransformation of pollutants. As for high-ring Cl-PAHs (≥ 3 rings), their photochemistry in ice remains unknown. In comparison with PAHs in ice, OH-PAHs and nitrated-PAHs exhibited the different ice photochemical behavior due to the hydroxylated and nitrated substitution, respectively (Ge et al. 2023, Ge et al. 2025a, Ge et al. 2016a, Xue et al. 2019a). Although Cl-PAHs exhibit similar

structures to their parent PAHs, the substituted chlorine as the auxochromic group is hypothesized to induce certain distinctions between their photochemical behavior (Cai et al. 2024b, Manfrin et al. 2020). Consequently, exploring the photodegradation of Cl-PAHs in ice would be of necessity to test the hypothesis.

Furthermore, the comparative studies on the ice and aqueous photochemistry have aroused considerable concerns for organic pollutants, such as PAHs and several derivatives, pesticides, and pharmaceuticals (Li et al. 2024b, Liu et al. 2023, Wang et al. 2023b). For instance, 4-nitro-1-hydroxynaphthalene (4-NO_2-1-OHN) and 4-Cl-1-OHN only in ice phase suffered from multiple hydroxylation, and 4-NO_2-1-OHN in ice underwent photo-isomerization as well, leading to their higher photo-modified toxicity in ice compared to aqueous solutions (Ge et al. 2025a). Moreover, the photolysis rates of 2- and 9-hydroxyfluorenes (OHFL) in ice were found to be significantly higher than in water, with co-existing dissolved components (e.g., Cl^-, Fe(III)) showing different effects on the photolysis in the two phases (Ge et al. 2023). These findings are interesting, accounting for the similarities and differences between the ice and aqueous photochemistry. However, new insights into environmental ice and aqueous photochemistry of high-ring Cl-PAHs (≥ 3 rings) are urged so as to seek a new systematic comparison between the two disciplines.

This study presents a systematic comparison of the ice and aqueous phase photolytic behavior of three Cl-PAHs, including 2-chlorofluorene (2-ClFL, 3-ring), 9-chlorophenanthrene (9-ClPHE, 3-ring) and 1-chloropyrene (1-ClPY, 4-ring) (Fig. S1), compounds detected in multiple environments, especially in natural waters (Table S1). We determined photolysis kinetics, identified reaction pathways, and assessed photo-induced changes in toxicity for each compound in both ice and liquid water. In addition, 9-ClPHE was also examined in greater detail and used as a representative high-ring congener to further elucidate mechanistic and kinetic differences in the presence of dissolved components in ice and aqueous solutions. To

our best knowledge, this is the first study to comprehensively investigate the ice and aqueous phase photochemistry of high-ring Cl-PAH congeners (≥ 3 rings), and to link their transformation pathways with resulting changes in toxicity in cold aquatic systems. This study provides new insights into the distinct phototransformation mechanisms of high-ring Cl-PAHs in ice and aqueous systems, which are currently under-represented in the literature and yet enable more accurate evaluation of the environmental persistence and risks posed by similar PAH analogues in seasonally ice-covered regions.

2. Materials and methods

2.1. Chemicals and prepared water solutions

2-ClFL (purity 98%)/1-ClPY (95%) and 9-ClPHE (98%) were purchased from Shanghai Yubo Biotechnology Co., LTD. and Acros Organics (Belgium), respectively (see Table S2 for further information). High-purity water (18.2 MΩ cm) was produced with a Millipore-Milli Q system. Natural freshwater was sampled from Xi'an Weihe River (34.37°N, 108.97°E), and the seawater was taken from Dalian coastal area (38.88°N, 121.57°E).

The environmental water samples were filtered by the membranes (pore size 0.22 μm) to remove particles and then stored at 4 °C until further analysis. Their properties and the major ions are shown in Table S3. Pure water, natural-freshwater and seawater samples were spiked with individual Cl-PAHs and 2% acetonitrile as co-solvent to give concentrations characteristically measured in the environment (C_0 = 0.2 μM) ready for use in photolytic experiments.

2.2. Photolytic kinetic experiments

As illustrated in Fig. S2, a rotating photochemical reactor was employed to perform the photolytic experiments, using a Pyrex well-jacketed and cooled mercury lamp (500 W) to simulate solar radiation (λ > 290 nm). The light intensities at the reaction sites were measured

with a UV-A radiometer at 420 nm (8.03 mW cm^{-2}) and 365 nm (8.09 mW cm^{-2}), respectively. Firstly, Cl-PAH solutions (V = 80 mL) were divided into two aliquots and retained in separate Pyrex tubes ready for aqueous and ice experiments. For the aqueous research, the aliquot was transferred directly into the apparatus at room temperature (25 ± 1 °C). For the ice study, the aliquot was frozen into ice and then placed into the experimental apparatus, which was kept in a freezer (−5 ± 1 °C). To test whether hydroxyl radicals (·OH) participated in the apparent photolysis, quenching radical experiments were performed using isopropanol as the quencher of ·OH (Text S1). The apparent quantum yields (Φ_s) for the ice and aqueous photodegradation were quantified based on methods used previously (Text S2) (Cui et al. 2025b, Ge et al. 2025a).

To explore the effects of some typical water constituents (e.g., Cl^-, Fe(III), humic acid and NO_3^-) on photodegradation kinetics of 9-ClPHE, a series of artificial solutions were prepared. Pure reagents (NaCl, $Fe_2(SO_4)_3$, humic acid sodium salt (HASS) and $NaNO_3$) were added to Milli Q water to give concentrations matching those observed in natural surface waters (Table S3). Furthermore, a four-factor central composite experiment was designed to examine the multivariate effects of coexisting water constituents (Table S4). The concentrations of target factors were selected based on their environmentally relevant ranges (Ge et al. 2016b, Wang et al. 2023a, Yang et al. 2022). Details can be found in the supplementary material (Text S3). Notably, all the photo-irradiating experiments and dark controls were conducted in triplicate.

2.3. Analytical methods

An Agilent 1260 Infinity II HPLC was employed to determine concentrations of three Cl-PAHs with the analytical parameters listed in Table S5. An Agilent 6470B triple quadrupole LC/MS system coupled with an electro spray ionization source operating in negative mode was used to identify key degradation products. The generated ·OH was identified by electron paramagnetic resonance (EPR) spectra with 5,5'-dimethyl-1-pirroline-N-oxide (DMPO) as a spin-trap reagent. Relevant details are provided in Text S4. The total organic carbon (TOC) of

natural waters and HASS solutions were determined by a liquid TOC–II Analyzer. In addition, the electrostatic potential (ESP), the highest occupied molecular orbital (HOMO), the lowest unoccupied molecular orbital (LUMO) and Fukui indices of the three Cl-PAHs were calculated by density functional theory (DFT).

2.4. Toxicity assessment

To determine the acute toxicity of Cl-PAHs during photolytic degradation, a bioassay using *Vibrio fischeri* was conducted with a HACH Eclox^{TM} Rapid Response Test working in the 'Luminescent Bacteria Toxicity Testing' mode. The luminescence inhibition rate (I%) was used to make a toxicity assessment as performed previously (Ge et al. 2025a, Ge et al. 2025b). Furthermore, an Ecological Structure-Activity Relationships (ECOSAR) predictive model (version 2.2) was used to estimate the acute toxicity of the parent compounds and individual degradation products to fish, daphnia and green algae (Ge et al. 2025b).

3. Results and discussion

3.1. Photolytic kinetics of three Cl-PAHs in ice and water

Slight pH fluctuations (less than 0.3 units, $p > 0.05$) were recorded in the individual photolytic experiments (Table S6). And negligible changes in solution concentration (< 2%) of the three Cl-PAHs were observed over the experimental period under dark conditions. This suggested that both physical losses (e.g., volatilisation) and chemical losses (e.g., hydrolysis and pyrolysis) played minor roles throughout the controlled experiments. As such, any reduction in the concentration of the three compounds in both ice and aqueous phase studies can be attributed to photodegradation caused by exposure to simulated sunlight. Photodegradation of the three Cl-PAHs in this study appeared to follow first-order kinetics, as evidenced by good linear fit of $\ln(C/C_0)$ versus time (t) ($r^2 > 0.97$) (Fig. 1). The corresponding photolytic rate constants (k), half-lives ($t_{1/2}$), and Φ_s are listed in Table S7.

As indicated in Fig. 1 and Table S7, photolytic rates of the individual Cl-PAHs were up to 6-

fold higher in ice than in water. Elevated photodegradation rates in ice compared to water were also found previously for other SPAHs, including 2-OHFL, 1-nitropyrene (1-NPY) and phenanthrene (Ge et al. 2016a, Ge et al. 2025b, Xue et al. 2019b). Given the lower temperatures in ice compared to water that would typically be associated with slower rates of reaction, this observation may, in part, be attributed to physical processes occurring during ice formation. During water freezing into ice, pollutant molecules are preferentially partitioned into liquid-like regions (LLRs), accompanied by both concentration-enhancement and ice-cage effects (Ge et al. 2023). The dual effects may respectively enhance solute concentrations at the grain boundaries of ice crystals and create micro-fields around them via solvent molecules. The synergistic mechanisms ultimately modulate the photolytic kinetics of the solute compounds through interfacial microenvironment. In instances where ice is formed from seawater, a network of microscopic liquid brine (highly saline) channels is formed which can contain increased levels of pollutants (Garnett et al. 2021, Garnett et al. 2019). In either case, enrichment of pollutants at ice grain boundaries can lead to enhanced photodegradation through a reduction in light pathway distance and possibly lowering the amount of light scatter (Ge et al. 2023, Ge et al. 2025b, Klanova et al. 2003, Weber et al. 2009).

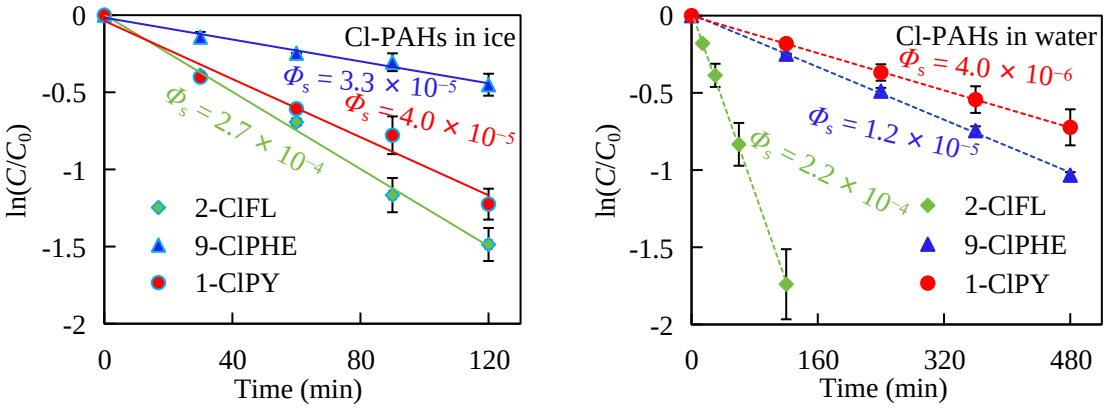

Fig. 1. Simulated solar photolytic kinetics of the three chlorinated PAHs (Cl-PAHs, 2-chlorofluorene (2-ClFL), 9-chlorophenanthrene (9-ClPHE) and 1-chloropyrene (1-ClPY)) in ice and in water.

Comparison of measured data also revealed differences in photochemical degradation rates,

which indicated that photolysis is also likely to be chemical specific. For example, 2-ClFL (3-ring) displayed the greatest decline rate under both ice and aqueous phases, while 9-ClPHE (3-ring) and 1-ClPY (4-ring) degradation occurred more slowly. Given the low light absorption of 2-ClFL compared to the other Cl-PAHs (Fig. S3), the higher degradation rate for this chemical is clearly related to its higher photolytic reactivity, as indicated by the higher Φ_s values, compared to 9-ClPHE and 1-ClPY (Table S7). Analysis of data (Table S7) also showed a much greater increase in degradation rates between ice and water conditions for 1-ClPY (6.10 ± 0.01 fold, $p < 0.01$) than 9-ClPHE (1.67 ± 0.03 fold, $p < 0.01$) and 2-ClFL (1.17 ± 0.21 fold). As discussed earlier, physical processes during ice formation may be partly attributable for this increase, however, physical ice processes are likely to act evenly across chemicals regardless of their properties and therefore the higher photodegradation rate of some chemicals is most likely related to differences in chemical properties such as chemical transformation pathways (See Section 3.3).

A comparison of Φ_s values was undertaken for Cl-PAHs (this study) and related PAHs to assess differences in photolytic kinetics of these environmental pollutants (Table S8 and associated refs.). Interestingly, not only in ice but also in water, photodegradation Φ_s values of Cl-PAHs (10^{-5}–10^{-4}) were shown to be 1−2 orders of magnitude lower compared to those of PAHs (10^{-3} in most cases), nitro-PAHs (10^{-4} in most cases) and hydroxy-PAHs (10^{-3}–10^{-1}). For instance, glacial 9-ClPHE and 1-ClPY displayed the lower Φ_s values of 3.3×10^{-5} and 4.0×10^{-5}, respectively, than their parent phenanthrene (3.8×10^{-3}) and pyrene (4.3×10^{-4}). PAHs and their derivatives such as Cl-PAHs exhibit a wide variety of structural isomers which can govern their photodegradation kinetics and chemical transformation efficiency (Table S8). The key determinants are differences in Φ_s values and the spectral overlap between compound absorption and light source irradiance (Ofrydopoulou et al. 2021).

3.2. Photolytic pathways of Cl-PAHs in ice and in water

The photolytic intermediates and transformation pathways of the three Cl-PAHs were investigated in ice and water by examining the total ion chromatograms in the negative monitoring mode (Fig. S4). Using relevant MS (Scan) and MS^2 (SIM-Scan) spectra (Fig. S5), significant intermediates were identified. Their molecular weights (*Mw*), retention times (t_R) and fragment ions (*m*/*z*) are shown in Table S9. Furthermore, the DFT calculations (Figs. S6-S8) indicated the most possible reaction sites of each compound susceptible to radical attack (e.g., ·OH). By integrating the HPLC-MS/MS data, the chemical structures of key products are tentatively proposed, along with the phototransformation pathways of the three Cl-PAHs both in ice and in water (Fig. 2).

As shown in Fig. 2, four 2-ClFL degradation products (P166, P182, P198 and P232) were formed in both ice and water via the same reactions, namely dechlorination and hydroxylation. However, ketonic P196 was formed exclusively in the aqueous phase through photo-oxidation. As for 9-ClPHE, the compound underwent hydroxylation to produce P228 in ice. Whereas, the aqueous 9-ClPHE underwent hydroxylation to produce P228, followed by dechlorination and hydroxylation to P210. Similar reactions occurred for 1-ClPY, transforming into identical degradation products (i.e., P252, P268 and P218) in both phases, and generating P202 only in the aqueous phase through dechlorination.

Regardless of the different intermediates observed in the two phases, photo-induced hydroxylation and dechlorination were determined to be the key reactions involved in the phototransformation of the three Cl-PAHs (Fig. 2). This finding aligns with previous studies, which showed OH-PAHs and nitro-PAHs underwent hydroxylation to form multiple hydroxyl intermediates in the two phases (Ge et al. 2023, Ge et al. 2025a, Ge et al. 2025b). The prevalence of hydroxylation reaction can be ascribed to the generation of ·OH radicals from the photo-sensitization of the parent compounds in the two phases. As shown in Fig. 3, EPR spectra showed four sets of peaks with 1:2:2:1 under irradiation, corresponding to the characteristic of

the DMPO-·OH, which verified the generation of ·OH from photo-sensitization of Cl-PAHs. Combined with radical quenching experiments (Text S1), the participation of ·OH in the apparent photolysis was confirmed, and the contribution ratios ($R_{\cdot OH}$) of self-sensitized photo-oxidation via ·OH to the apparent photolysis were illustrated in Fig. 3. The ·OH was speculated during the photolysis of several PAHs and SPAHs (Ge et al. 2025a, Sarmiento et al. 2023). However, the formation and participation of ·OH were proved in the present study. Furthermore, additional dechlorination is prevalent for chlorinated PAHs and analogue (Kang et al. 2021, Teng et al. 2025, Xu et al. 2025). For instance, certain low-ring Cl-PAHs (2 rings) displayed dechlorination in both ice and aqueous conditions (Ge et al. 2025a, Huang et al. 2021).

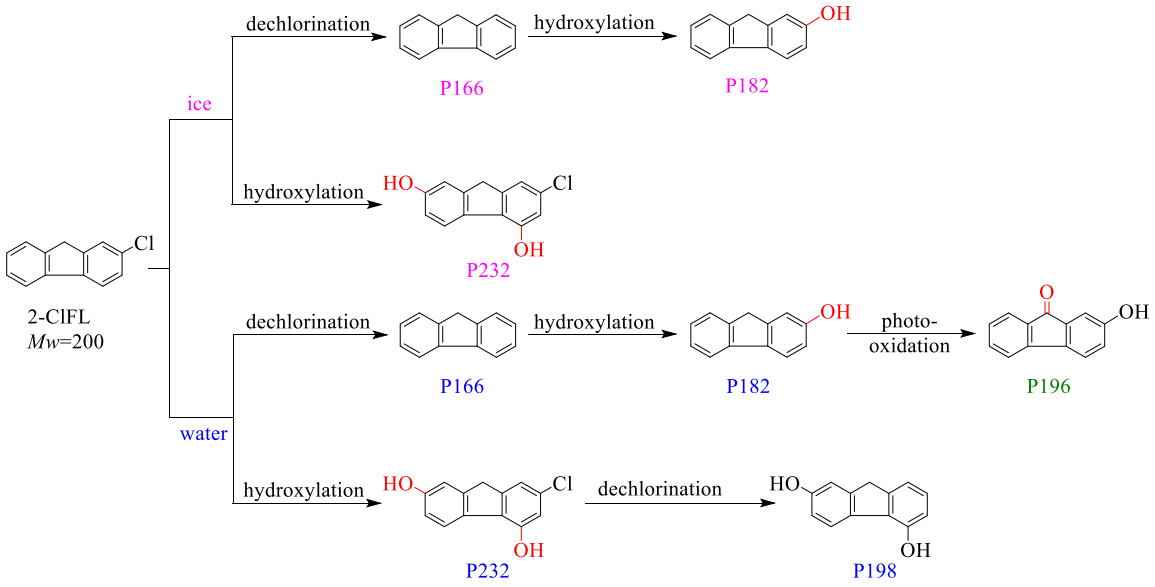

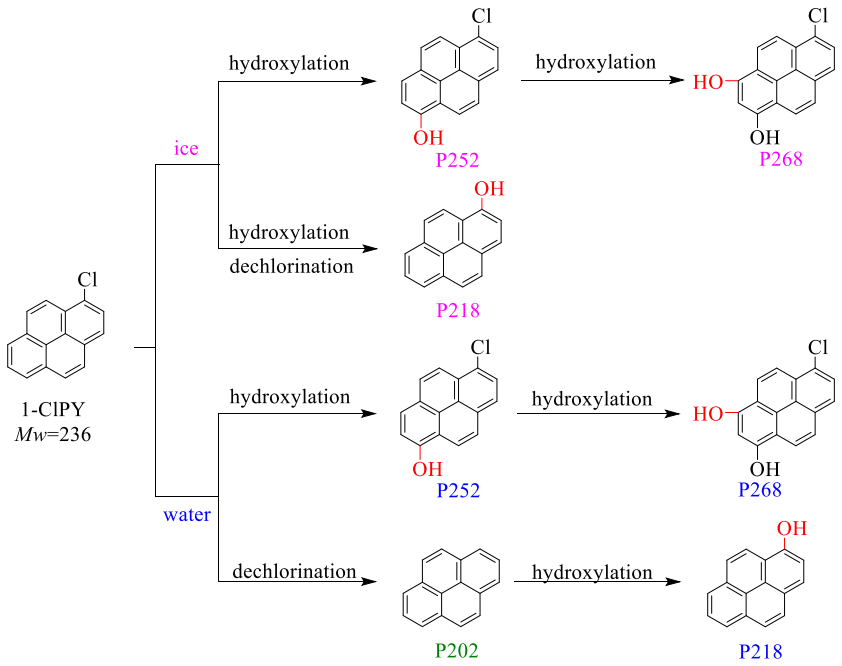

Fig. 2. Photolytic products and transformation pathways associated with the three Cl-PAHs. The photogenerated intermediates are designated as P_{Mw}, where *Mw* denotes molecular weights calculated from the most abundant isotopes. P_{Mw} is marked with different colors to distinguish the products generated in different phases. Among them, 'magenta' indicates products formed in ice, 'blue' indicates products in water, and 'green' represents products that were only formed in the aqueous phase.

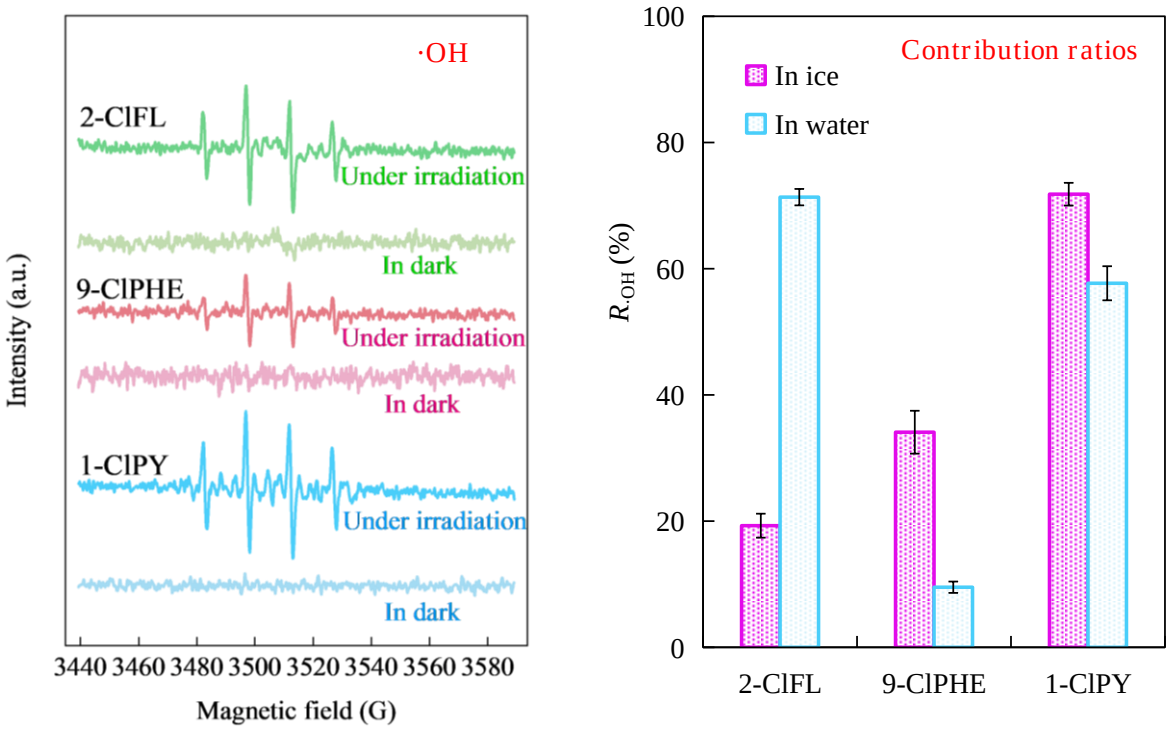

Fig. 3. The electron paramagnetic resonance (EPR) spectra (left) and the contribution ratios ($R_{\cdot OH}$) of self-sensitized photo-oxidation via ·OH to the apparent photolysis (right) for the three Cl-PAHs.

3.3. Effects of aqueous dissolved substances on the photodegradation of 9-ClPHE

The chemical 9-ClPHE (3-ring) was selected as a model Cl-PAH compound to further examine photodegradation kinetics in ice and water containing varying levels of other naturally occurring chemical substances (Table S10). Like previous experimental results (pure-water ice/pure water), it was found that 9-ClPHE photolyzed significantly faster in ice than in water (freshwater and seawater), as shown in Fig. 4. This finding supports the assertion that ice generally acts to enhance photodegradation of chemicals even in the presence of other matrix constituents, probably through a combination of physical (i.e., concentration processes involved during ice formation) and chemical (i.e., generation/promotion of reactive ions) mechanisms.

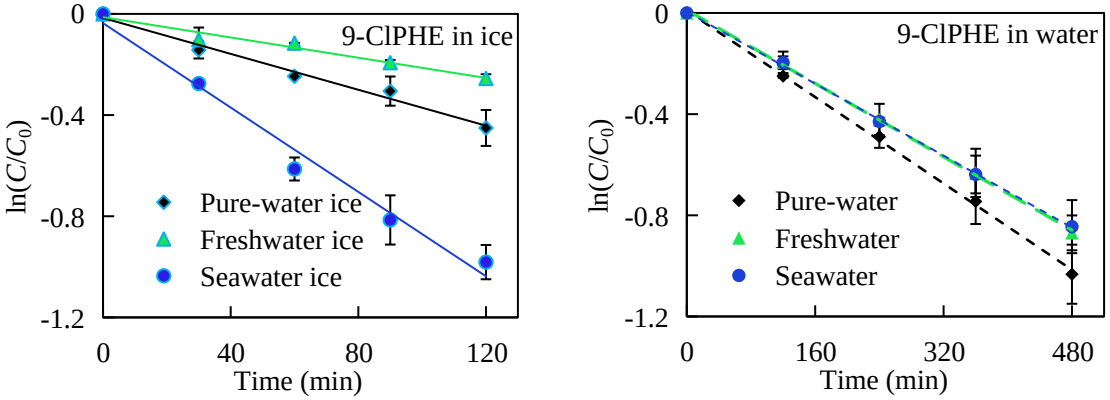

Fig. 4. Photodegradation kinetic curves of 9-ClPHE in varying ices and aqueous solutions under the same irradiating conditions ($\lambda > 290$ nm).

The photolytic rates of 9-ClPHE varied depending on the solution matrix (i.e., pure water, freshwater and seawater) and condition (e.g., ice/water). In seawater ice, 9-ClPHE underwent faster photolysis than in pure-water ice and freshwater ice. In contrast, 9-ClPHE photodegraded fastest in pure water compared to seawater and freshwater. These observations aligned with the prior study, which showed the photolytic rates of OH-PAHs (e.g., 2-OHFL and 9-OHFL) also varied markedly in different types of ice and waters, often with the highest rates appearing in seawater ice (Ge et al. 2023).

Further analysis of photodegradation rate data (rate constant, *k* values) with concentration

data for different matrix components (Cl^-, Fe(III), HASS and NO_3^-) showed significant differences ($p < 0.05$) between concentrations for different constituents. This strongly suggested that different chemicals played varying roles phototransformation of 9-ClPHE in both the ice and aqueous (Fig. 5). Specifically, in the presence of Cl^-, the photolysis of 9-ClPHE was promoted in the two phases ($p < 0.05$). Although the values of k were in the same order of magnitude (10^{-3} min^{-1}), Cl^- appeared to promote photodegradation significantly more in ice compared to water, with maximal degradation rates appearing around 0.50 M and 0.68 M, respectively. The enhanced rate of photolysis of 9-ClPHE in the presence of Cl^- can be ascribed to the formation of more reactive chlorine species (e.g., $ClOH^{\cdot-}$) via scavenging ·OH by Cl^- in neutral solution (El Omar et al. 2012), understood as follows:

$$9\text{-ClPHE} + h\nu \longrightarrow 9\text{-ClPHE}^* \quad (1)$$

$$9\text{-ClPHE}^* \xrightarrow{+H_2O} \cdot OH \text{ (proved by EPR spectra in Fig. 3)} \quad (2)$$

$$\cdot OH + Cl^- \underset{k_2}{\overset{k_1}{\rightleftharpoons}} ClOH^{\cdot-} \quad (k_1 = 4.3 \times 10^9\ M^{-1}s^{-1},\ k_2 = 6.1 \times 10^9\ M^{-1}s^{-1}) \quad (3)$$

At high concentrations of Cl^-, generation of reactive $ClOH^{\cdot-}$ species is likely to reach a point whereby further promotion effects are weakened through the transformation of $ClOH^{\cdot-}$ into $Cl\cdot$ and $Cl_2^{\cdot-}$ (El Omar et al. 2012). Meanwhile, changes in the microstructure of ice under high salinity conditions also influence the photodegradation rate of coexisting organic solutes (Chen et al. 2019, Mason et al. 2022).

Other dissolved components (HASS, NO_3^- and Fe(III)) present in the seawater and freshwater (Table S3) were also investigated to examine their effect on the photochemistry of 9-ClPHE in ice and water (Table S10). In general, these components were demonstrated to inhibit photodegradation in both ice and water, though inhibition effects were more prominent in ice than in water. Increased inhibition of photolysis in ice can be rationalized using the same physical mechanisms described earlier, which highlighted enrichment of dissolved solutes at ice grain interfaces. Hence, the inhibition effects of some dissolved species (e.g., HASS, NO_3^- and Fe(III)) are also likely to be enhanced.

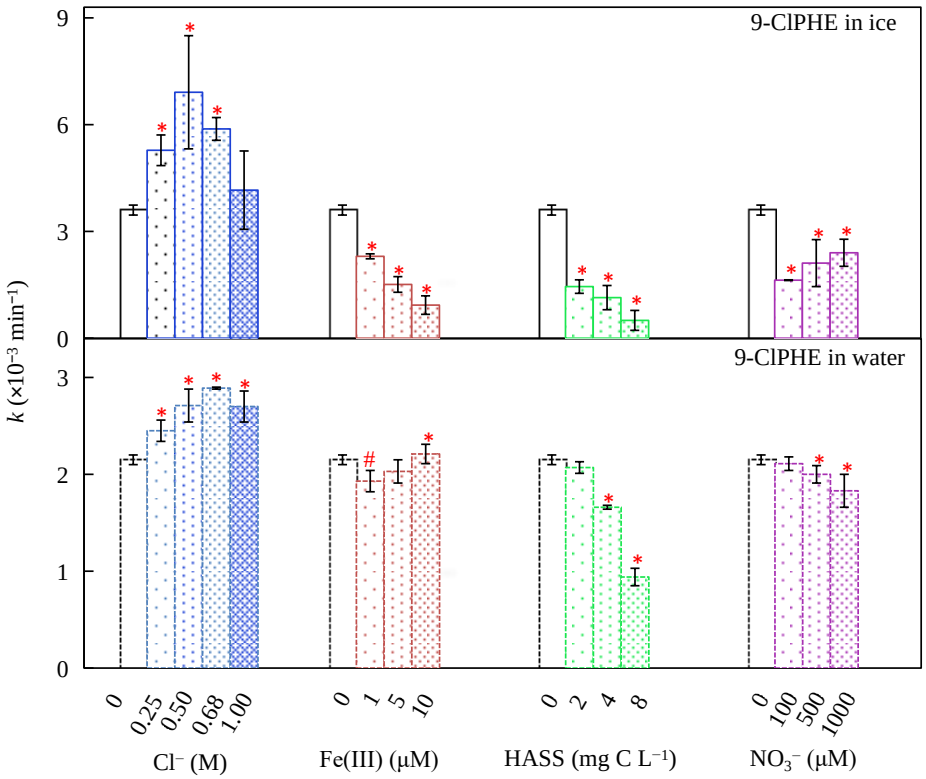

Fig. 5. Impacts of the soluble substances on the photolytic *k* values of 9-ClPHE in the two phases (ice/water). The symbols * and # indicate remarkable differences at the 0.05 and 0.1 significance levels (*p*), respectively, when comparing *k* to that without added dissolved substances.

Inhibition of 9-ClPHE photodegradation was particularly evident in the presence of HASS, which showed an approximately 3-fold reduction in rates. For NO_3^- and Fe(III), this effect was less prevalent at about 2-fold reduction. Though these species have been reported to promote the photodegradation of pollutants by the sensitization effect (Ge et al. 2016b, Huang et al. 2024), it was apparent in this study that their net affect led to inhibition. This observation can be ascribed to the absorption of a similar light spectrum by 9-ClPHE and dissolved species, which can act in a competitive manner (Ge et al. 2016b). An assessment of the absorption spectra (Fig. S9) strongly supports this assertion by displaying a large overlap in the region spectrum around 290 nm. In comparison, DOM exerted distinct inhibition or promotion effects on photodegradation depending on the hydrophobicity and hydrophilicity of antibiotics (Cui et al. 2025a). Together, these results confirm that photodegradation is highly dependent on the

chemical structure and optical properties of these coexisting dissolved substances.

A multivariate analysis was performed on the central composite experiments to explore the effect of coexisting water constituents on photodegradation kinetic properties of 9-ClPHE (Table S11). The corresponding regression coefficients (β_x) and their significance levels (p) are presented in Table S12. If the p value is less than 0.05, the corresponding β_x is a significant factor. Thus, Cl^-, HASS, NO_3^- and Cl^--Cl^- interaction were significant factors contributing to the photodegradation of 9-ClPHE. The fitting equation can be expressed more simply as follows:

$$k = \beta_0 + \beta_1 x_1 + \beta_3 x_3 + \beta_4 x_4 + \beta_{11} x_1^2 \quad (1)$$

where x_1, x_3 and x_4 respectively denote the levels of Cl^-, HASS and NO_3^- (Table S4). Negative values of β_3 and β_4 were observed (Table S12), indicating that NO_3^- and HASS inhibited the photodegradation of 9-ClPHE. In contrast, the values of β_1 and β_{11} were positive, thus Cl^- and Cl^--Cl^- interaction promoted the photodegradation. Based on the sum of squares, the contributions of Cl^-, HASS, NO_3^- and Cl^--Cl^- interaction were assessed to be 16.22%, 60.47%, 3.12% and 3.87%, respectively. As for Fe(III), the inhibition effect on the photodegradation was considered to be significant at $p < 0.1$ (Table S12). The above experimental results were consistent with the single-factor experiment findings.

3.4. Environmental photochemical persistence and risk in cold regions

Laboratory-derived data were extrapolated to estimate apparent environmental photolytic half-lives ($t_{1/2,E}$) of Cl-PAHs in cold regions (Text S5). As reported in Table 1, estimated $t_{1/2,E}$ values for surface ice and snow ranged from 0.54 days (1-ClPY in the Arctic) to 65 days (2-ClFL in Xi'an, China), while surface waters generally showed longer life times. This wide range reflects dependence of chemical identity, environmental media, latitude, and season. Compared to the parent PAHs and OH-PAHs (Table S13), Cl-PAHs generally displayed much longer $t_{1/2,E}$. For instance, the $t_{1/2,E}$ values for 2-ClFL ranged from 17.17 days (Arctic; 78.91°N, 11.93°E; Ice/Snow) to 77.37 days (Antarctic; 62.21°S, 58.96°W; Water), which were larger than those

for 2-OHFL from 0.012 days (Arctic; 78.91°N, 11.93°E; Ice/Snow) to 0.027 days (Antarctic; 62.21°S, 58.96°W; Snow), and for fluorene (FL) from 0.79 days (Summit, Greenland; 72.58°N, 38.49°W; Snow) to 7.88 days (Alert, Nunavut; 82.5°N, 62.3°W; Snow) (Table S13 and associated refs.). The other two Cl-PAHs were also more persistent than their respective parent PAHs and OH-PAHs. Notably, all parent PAHs and their derivatives exhibit wide variability in the photolytic $t_{1/2,E}$ values, depending on their molecular structures and environmental conditions. Given the greater persistence of Cl-PAHs, the pollutants are likely to persist longer and pose higher ecological risk in cold regions.

Table 1. Environmental photolytic half-lives ($t_{1/2,E}$) of the apparent photodegradation for the three Cl-PAHs in surface ice/snow and water of the Antarctica, Arctic, and Xi'an, China.

Area, season (latitude, longitude)	Medium	($t_{1/2,E}$ / day)		
		2-ClFL	9-ClPHE	1-ClPY
Antarctica, Summer (62.21°S, 58.96°W)	Ice/Snow	64.14	24.93	0.90
	Water	77.37	68.56	8.99
Arctic, Summer (78.91°N, 11.93°E)	Ice/Snow	17.17	15.35	0.54
	Water	20.71	42.22	5.41
Xi'an, Winter (34.37°N, 108.97°E)	Ice/Snow	65.20	32.47	1.14
	Water	78.65	89.28	11.38
Xi'an, Summer	Water	15.14	33.60	4.37

The toxicity evolution during photodegradation of the three Cl-PAHs was assessed using *Vibrio fischeri* (Fig. 6). Reaction solutions typically exhibited higher luminescence inhibition rate (I%) values following the initial sampling time point ($p < 0.01$), I% values appeared to fluctuate and display high variability throughout irradiation time (Fig. 6). This feature indicated changing toxicity throughout the decomposition of Cl-PAH, most likely through the generation of different toxic intermediates. Compared with other SPAHs (Ge et al. 2025a, Ge et al. 2025b), parent Cl-PAHs showed higher I% values, which may be attributed to higher toxicities of chlorine-containing organic contaminants (Zhao et al. 2019). The ECOSAR assessment agreed

broadly with the bioassay but estimated lower toxicities for the transformation products than for the parent compounds (Table S14). Nevertheless, residual parent compounds and transformation intermediates still produced significant combined toxicity in the biotest (Fig. 6). This might be attributed to the formation of hydroxylated products, which would more easily pass through the lipid cell membrane of *Vibrio fischeri* and exert a stronger inhibition effect (An et al. 2021, Ge et al. 2025a, Zhao et al. 2024). PAHs, OH-PAHs and nitrated-PAHs have also been reported to exhibit notable photo-modified toxicity to *Vibrio fischeri* (El-Alawi et al. 2002, Ge et al. 2016b, Ge et al. 2025b). Together, these results indicate that photo-modified toxicities of chlorinated PAHs and related analogues should be accounted for in risk assessments for cold-region environment.

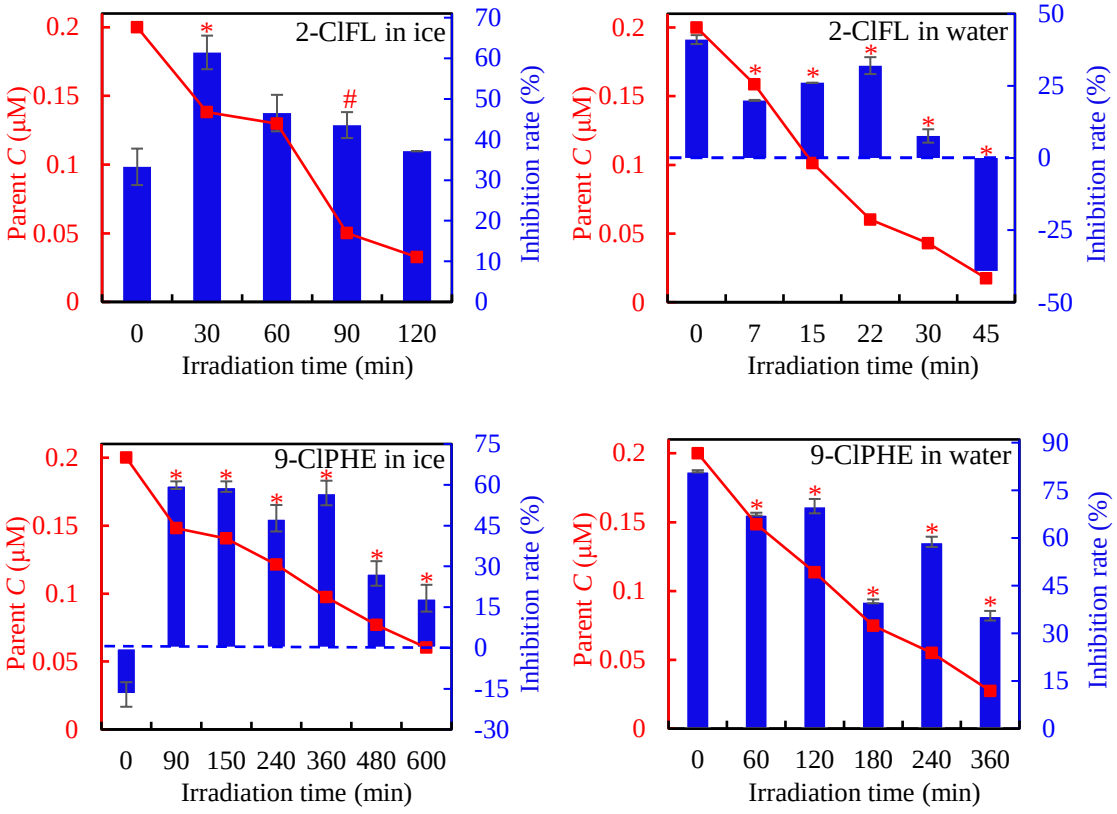

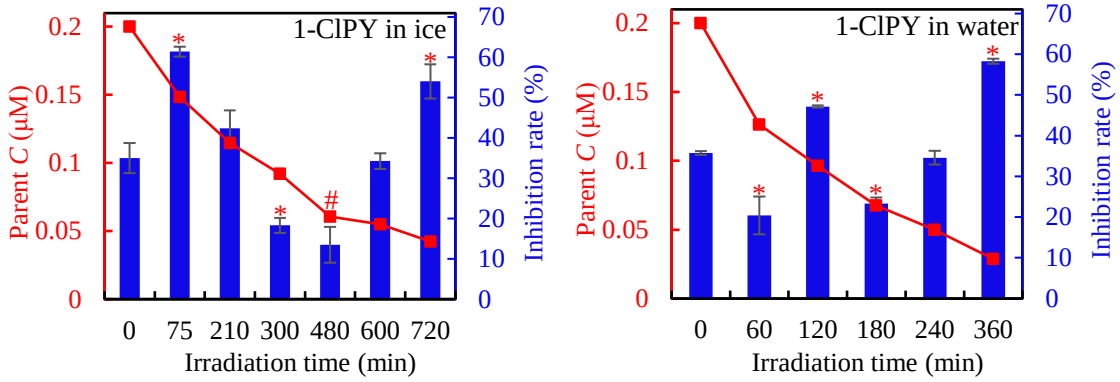

Fig. 6. The evolution of parent concentrations (C, ■) of the three Cl-PAHs, as well as the changes of luminescence inhibition rates (I%, ■) to *Vibrio fischeri* with the irradiation time in ice and in water. * and # indicate significant difference at $p < 0.01$ and 0.05, respectively, between the corresponding I% value at t and the initial value at t_0.

4. Conclusion

This study provides a systematic comparison of the ice versus aqueous photochemistry for three high-ring chlorinated PAHs (≥ 3 rings). This topic is underrepresented but important for their environmental persistence and risk assessment in cold regions. Under identical simulated solar irradiation, differences in the rates of photodegradation of Cl-PAHs were established and attributed to both physical processes occurring during formation of ice, and also chemical processes induced by the presence of other dissolved species in freshwater and seawater. In the apparent photolysis of the three Cl-PAHs, the photo-sensitized generation and participation of ·OH were proved. And photo-induced hydroxylation and dechlorination were the primary reactions, but several secondary pathways and intermediates were identified depending on the phase. Estimated half-lives of Cl-PAHs ranged from several hours to dozens of days in surface ice/snow, which were found to be consistently shorter than in surface waters under comparable regional and seasonal conditions.

The bioassay using *Vibrio fischeri* demonstrated significant photo-enhanced joint toxicities of the parent Cl-PAHs and photogenerated intermediates, though ECOSAR assessment showed the comparable or lower toxicities of the individual transformation products. The findings

reported here fill a critical gap in understanding the environmental phototransformation mechanisms of high-ring Cl-PAHs (≥ 3 rings) in seasonally frozen water of cold regions, such as high-latitude and high-altitude areas. The results provide a useful framework to better assess the environmental persistence and risks of chlorinated PAHs, analogues and other derivatives in cold regions.

CRediT authorship contribution statement

Linke Ge: Writing – review & editing, Supervision, Methodology, Investigation, Funding acquisition, Conceptualization. **Rongyan Xu:** Writing – review & editing, Writing – original draft, Investigation. **Jack Garnett:** Writing – review & editing, Formal analysis. **Peng Zhang:** Writing–review & editing, Formal analysis. **Dongxiao Bai:** Writing – review & editing, Validation. **Siyuan Wang:** Writing – review & editing, Conceptualization.

Acknowledgements

This work was supported by the National Natural Science Foundation of China (Nos. 21976045 and 22076112), the Key Research and Development Program of Shaanxi Province (No. 2024SF-YBXM-567), and the China Scholarship Council (CSC) Scholarship (No. 202308610123).

Appendix A. Supplementary data

Supplementary data to this article can be found online at doi.org/10.1016/j.########.

Data availability

Data will be made available on request.

References

Ali, L., Alam, A., Ali, A.M., Teoh, W.Y., Altarawneh, M., 2024. A comprehensive review into emission sources, formation mechanisms, ecological effects, and biotransformation routes of halogenated polycyclic aromatic hydrocarbons (HPAHs). Ecotoxicol Environ Saf 286, 117196. https://doi.org/10.1016/j.ecoenv.2024.117196.

An, Z., Han, D., Sun, J., Mei, Q., Wei, B., Li, M., Qiu, Z., Bo, X., Wang, X., Xie, J., Zhan, J., He, M., 2021.

Full insights into the roles of pH on hydroxylation of aromatic acids/bases and toxicity evaluation. Water Res 190, 116689. https://doi.org/10.1016/j.watres.2020.116689.

Azcune, G., Griffero, L., Pareja, L., Ríos, J.M., Galbán-Malagón, C., Pérez-Parada, A., 2022. Trends in the monitoring of legacy and emerging organic pollutants in protected areas. Trends Environ Anal Chem 34, e00165. https://doi.org/10.1016/j.teac.2022.e00165.

Cai, B.C., Hu, X.F., Li, Y.J., Bai, Y.X., Xie, H., 2024a. Cation radical induced photochlorination of naphthalene in saline water under UV light irradiation. ACS ES&T Water 4(4), 1925-1936. https://doi.org/10.1021/acsestwater.4c00056.

Cai, Y., Li, X.C., Feng, M.B., Chovelon, J.-M., Lu, J.H., Chen, J., Ji, Y.F., 2024b. Photochemical degradation of bisphenol S and its tetrahalogenated derivatives in water. Water Res 262, 122131. https://doi.org/10.1016/j.watres.2024.122131.

Chen, C., Chen, L., Yao, Y., Artigas, F., Huang, Q., Zhang, W., 2019. Organotin release from polyvinyl chloride microplastics and concurrent photodegradation in water: Impacts from salinity, dissolved organic matter, and light exposure. Environ Sci Technol 53(18), 10741-10752. https://pubs.acs.org/doi/10.1021/acs.est.9b03428.

Cui, J.S., Chen, Y., Cheng, F.Y., Yang, H., Qu, J., Zhang, Y.N., Peijnenburg, W.J.G.M., 2025a. Hydrophilicity-dependent photodegradation of antibiotics in ice: Freeze-concentration effects and dissolved organic matter interactions drive divergent kinetics, pathways and toxicity. Water Res 286, 124277. https://doi.org/10.1016/j.watres.2025.124277.

Cui, N.N., Ge, L.K., Halsall, C., Niu, J.F., Zheng, J.S., Zhang, P., 2025b. Dissociation-dependent kinetics and distinct pathways for direct photolysis and •OH/$SO_4^{\bullet-}$ radical dominated photodegradation of ionizable antiviral drugs in aquatic systems. Water Res 279, 123452. https://doi.org/10.1016/j.watres.2025.123452.

El-Alawi, Y.S., McConkey, B.J., George Dixon, D., Greenberg, B.M., 2002. Measurement of short- and long-term toxicity of polycyclic aromatic hydrocarbons using luminescent bacteria. Ecotoxicol Environ Saf 51(1), 12-21. https://doi.org/10.1006/eesa.2001.2108.

El Omar, A.K., Schmidhammer, U., Rousseau, B., LaVerne, J., Mostafavi, M., 2012. Competition reactions of $H_2O^{\bullet+}$ radical in concentrated Cl^- aqueous solutions: Picosecond pulse radiolysis study. J Phys Chem A 116(47), 11509-11518. https://pubs.acs.org/doi/10.1021/jp309381z.

Garnett, J., Halsall, C., Thomas, M., Crabeck, O., France, J., Joerss, H., Ebinghaus, R., Kaiser, J., Leeson, A., Wynn, P.M., 2021. Investigating the uptake and fate of poly- and perfluoroalkylated substances (PFAS) in sea ice using an experimental sea ice chamber. Environ Sci Technol 55(14), 9601-9608. https://doi.org/10.1021/acs.est.1c01645.

Garnett, J., Halsall, C., Thomas, M., France, J., Kaiser, J., Graf, C., Leeson, A., Wynn, P., 2019. Mechanistic insight into the uptake and fate of persistent organic pollutants in sea ice. Environ Sci Technol 53(12), 6757-6764. https://doi.org/10.1021/acs.est.9b00967.

Ge, L.K., Cao, S.K., Halsall, C., Niu, J.F., Bai, D.X., He, G.K., Zhang, P., Ma, H.R., 2023. Photodegradation of hydroxyfluorenes in ice and water: A comparison of kinetics, effects of water constituents, and phototransformation by-products. J Environ Sci 124, 139-145. https://doi.org/10.1016/j.jes.2021.11.002.

Ge, L.K., Hou, Z.M., Niu, J.F., Wang, S.Y., Zhang, P., Zhu, Y.Q., 2025a. New insights into the environmental photochemistry of hydroxynaphthalene congeners in water and in ice: A distinct comparative study. J Hazard Mater 493, 138310. https://doi.org/10.1016/j.jhazmat.2025.138310.

Ge, L.K., Li, J., Na, G.S., Chen, C.E., Huo, C., Zhang, P., Yao, Z.W., 2016a. Photochemical degradation of hydroxy PAHs in ice: Implications for the polar areas. Chemosphere 155, 375-379. https://doi.org/10.1016/j.chemosphere.2016.04.087.

Ge, L.K., Na, G.S., Chen, C.E., Li, J., Ju, M.W., Wang, Y., Li, K., Zhang, P., Yao, Z.W., 2016b. Aqueous photochemical degradation of hydroxylated PAHs: Kinetics, pathways, and multivariate effects of main water constituents. Sci Total Environ 547, 166-172. https://doi.org/10.1016/j.scitotenv.2015.12.143.

Ge, L.K., Wang, S.Y., Cui, N.N., Wang, Z.Y., Zhang, P., 2025b. Insight into the environmental photochemistry of nitrated polycyclic aromatic hydrocarbons in water and in ice: Kinetics, pathways and photo-modified toxicity. Environ Res 279, 121749. https://doi.org/10.1016/j.envres.2025.121749.

Guo, Z.Y., Kodikara, D., Albi, L.S., Hatano, Y., Chen, G., Yoshimura, C., Wang, J.Q., 2023. Photodegradation of organic micropollutants in aquatic environment: Importance, factors and processes. Water Res 231, 118236. https://doi.org/10.1016/j.watres.2022.118236.

Hu, W., Liu, D.D., Su, S.H., Ren, L.J., Ren, H., Wei, L., Yue, S.Y., Xie, Q.R., Zhang, Z.M., Wang, Z.H., Yang, N., Wu, L.B., Deng, J.J., Qi, Y.L., Fu, P.Q., 2021. Photochemical degradation of organic matter in the atmosphere. Adv Sustainable Syst 5(11), 2100027. https://doi.org/10.1002/adsu.202100027.

Huang, C.C., Zeng, Y.H., Luo, X.J., Ren, Z.H., Tian, Y.K., Mai, B.X., 2021. Comprehensive exploration of the ultraviolet degradation of polychlorinated biphenyls in different media. Sci Total Environ 755, 142590. https://doi.org/10.1016/j.scitotenv.2020.142590.

Huang, S.N., Zhang, Z.B., Lin, C.Y., Cheng, H.F., 2024. Solar photodegradation of a novel des-F(6)-fluoroquinolone, garenoxacin, and ecotoxicity of its phototransformation products. Environ Sci Technol 58(31), 13918-13928. https://doi.org/10.1021/acs.est.4c03206.

Hung, H., Halsall, C., Ball, H., Bidleman, T., Dachs, J., De Silva, A., Hermanson, M., Kallenborn, R., Muir, D., Sühring, R., Wang, X.P., Wilson, S., 2022. Climate change influence on the levels and trends of persistent organic pollutants (POPs) and chemicals of emerging Arctic concern (CEACs) in the Arctic physical environment – a review. Environ Sci Proc Imp 24(10), 1577-1615. https://doi.org/10.1039/D1EM00485A.

Jin, R., Zheng, M.H., Lammel, G., Bandowe, B.A.M., Liu, G.R., 2020. Chlorinated and brominated polycyclic aromatic hydrocarbons: Sources, formation mechanisms, and occurrence in the environment. Prog Energy Combust Sci 76, 100803. https://doi.org/10.1016/j.pecs.2019.100803.

Kang, C.L., Bao, S.Q., Wang, Y.H., Xiao, K.K., Zhu, L., Liu, F., Tian, T., 2018. Comparison of the photoconversion of 1-chloronaphthalene and 2,3-dichlornaphthalene in water. Water Sci Technol 78(9), 1946-1955. https://doi.org/10.2166/wst.2018.469.

Kang, Q., Bao, S.Q., Chen, B., 2021. Phototransformation of three polychlorinated naphthalenes on surface of atmospheric particulate matter. J Hazard Mater 409, 124895. https://doi.org/10.1016/j.jhazmat.2020.124895.

Klanova, J., Klan, P., Nosek, J., Holoubek, I., 2003. Environmental ice photochemistry: Monochlorophenols. Environ Sci Technol 37(8), 1568 -1574. https://doi.org/10.1021/es025875n.

Klimczak, M., Liu, G.R., Fernandes, A.R., Kilanowicz, A., Falandysz, J., 2023. An updated global overview of the manufacture and unintentional formation of polychlorinated naphthalenes (PCNs). J Hazard Mater 457, 131786. https://doi.org/10.1016/j.jhazmat.2023.131786.

Li, Y.J., Hu, X.F., Xie, H., Cai, B.C., Bai, Y.X., 2024a. Photochlorination of anthracene in saline ice under simulated solar light. Water 16(9), 1237. https://doi.org/10.3390/w16091237.

Li, Z.J., Zhang, J., Dong, D.M., Zhang, L.W., Sun, H.Y., Wang, Y.K., Sun, Z.J., He, S.N., Guo, Z.Y., 2024b. Photodegradation for different dissociated species of norfloxacin and ofloxacin in water ice under solar irradiation. J Hazard Mater 461, 132595. https://doi.org/10.1016/j.jhazmat.2023.132595.

Liu, J.Y., Xue, S., Jiang, C.H., Zhang, Z.H., Lin, Y.Z., 2023. Effect of dissolved organic matter on sulfachloropyridazine photolysis in liquid water and ice. Water Res 246, 120714. https://doi.org/10.1016/j.watres.2023.120714.

Liu, Q.Z., Xu, X., Lin, L.H., Yang, G., Wang, D.H., 2021. Occurrence, health risk assessment and regional impact of parent, halogenated and oxygenated polycyclic aromatic hydrocarbons in tap water. J Hazard Mater 413, 125360. https://doi.org/10.1016/j.jhazmat.2021.125360.

Manfrin, A., Hänggli, A., Wildenberg, J., McNeill, K., 2020. Substituent effects on the direct photolysis of benzotrifluoride derivatives. Environ Sci Technol 54(18), 11109-11117. https://doi.org/10.1021/acs.est.9b07429.

Mason, D.P., Elwood Madden, M.E., 2022. Raman spectroscopy of high salinity brines and ices. Icarus 372, 114759. https://doi.org/10.1016/j.icarus.2021.114759.

Oda, M., Ikemori, F., Ohura, T., 2024. Contiguous hourly variations and relativeness of polycyclic aromatic hydrocarbons and their chlorinated derivatives in urban PM2.5. Atmos Environ 334, 120710. https://doi.org/10.1016/j.atmosenv.2024.120710.

Ofrydopoulou, A., Evgenidou, E., Nannou, C., Vasquez, M.I., Lambropoulou, D., 2021. Exploring the phototransformation and assessing the in vitro and in silico toxicity of a mixture of pharmaceuticals susceptible to photolysis. Sci Total Environ 756, 144079. https://doi.org/10.1016/j.scitotenv.2020.144079.

Ohura, T., Amagai, T., Makino, M., 2008. Behavior and prediction of photochemical degradation of chlorinated polycyclic aromatic hydrocarbons in cyclohexane. Chemosphere 70(11), 2110-2117. https://doi.org/10.1016/j.chemosphere.2007.08.064.

Peng, B., Dong, Q.L., Li, F.Z., Wang, T., Qiu, X.H., Zhu, T., 2023. A systematic review of polycyclic aromatic hydrocarbon derivatives: Occurrences, levels, biotransformation, exposure biomarkers, and toxicity. Environ Sci Technol 57(41), 15314-15335. https://doi.org/10.1021/acs.est.3c03170.

Qi, A.A., Wang, P.C., Lv, J.H., Zhao, T., Huang, Q., Wang, Y.M., Zhang, X.F., Wang, M., Xiao, Y., Yang, L.X., Ji, Y.Q., Wang, W.X., 2023. Distributions of PAHs, NPAHs, OPAHs, BrPAHs, and ClPAHs in air, bulk deposition, soil, and water in the Shandong Peninsula, China: Urban-rural gradient, interface exchange, and long-range transport. Ecotoxicol Environ Saf 265. https://doi.org/10.1016/j.ecoenv.2023.115494.

Qiao, M., Bai, Y.H., Cao, W., Huo, Y., Zhao, X., Liu, D.Q., Li, Z.R., 2018. Impact of secondary effluent from wastewater treatment plants on urban rivers: Polycyclic aromatic hydrocarbons and derivatives. Chemosphere 211, 185-191. https://doi.org/10.1016/j.chemosphere.2018.07.167.

Sarmiento, D.J., Majestic, B.J., 2023. Formation of environmentally persistent free radicals from the irradiation of polycyclic aromatic hydrocarbons. J Phys Chem A 127(25), 5390-5401. https://doi.org/10.1021/acs.jpca.3c01405.

Teng, X.L., Xu, J.Q., Wang, Z.Y., Qu, R.J., 2025. Photodegradation of chlorinated persistent organic oollutants (Cl-POPs) in oearl river suspended particulate matter–water systems: Kinetics, quantitative structure–activity relationship (QSAR) development, and mechanism. Environ Sci Technol 59(8), 4059-4067. https://doi.org/10.1021/acs.est.4c07246.

Tillner, J., Hollard, C., Bach, C., Rosin, C., Munoz, J.-F., Dauchy, X., 2013. Simultaneous determination of polycyclic aromatic hydrocarbons and their chlorination by-products in drinking water and the coatings of water pipes by automated solid-phase microextraction followed by gas chromatography–mass spectrometry. J Chromatogr A 1315, 36-46. https://doi.org/10.1016/j.chroma.2013.09.047.

Tu, Z.N., Qi, Y.M., Tang, X.S., Wang, Z.Y., Qu, R.J., 2023. Photochemical transformation of anthracene (ANT) in surface soil: Chlorination and hydroxylation. J Hazard Mater 452, 131252. https://doi.org/10.1016/j.jhazmat.2023.131252.

Wang, J.J., Liu, X.C., Beusen, A.H.W., Middelburg, J.J., 2023a. Surface-water nitrate exposure to world populations has expanded and intensified during 1970–2010. Environ Sci Technol 57(48), 19395-19406. https://pubs.acs.org/doi/10.1021/acs.est.3c06150.

Wang, X.L., Kang, H.Y., Wu, J.F., 2016. Determination of chlorinated polycyclic aromatic hydrocarbons in water by solid-phase extraction coupled with gas chromatography and mass spectrometry. J Sep Sci 39(9), 1742-1748. https://doi.org/10.1002/jssc.201501286.

Wang, Y.K., Song, Z.W., Zhang, L.W., Dong, D.M., Li, Z.J., Sun, H.Y., Wang, L.T., Guo, Z.Y., 2023b. Distribution and photodegradation of typical nonsteroidal anti-inflammatory drugs in an ice-water system: Simulation of surface waters with an ice cover. J Cleaner Prod 402, 136823. https://doi.org/10.1016/j.jclepro.2023.136823.

Weber, J., Kurková, R., Klánová, J., Klán, P., Halsall, C.J., 2009. Photolytic degradation of methyl-parathion and fenitrothion in ice and water: Implications for cold environments. Environ Pollut 157(12), 3308-3313. https://doi.org/10.1016/j.envpol.2009.05.045.

Xie, J.Q., Tao, L., Wu, Q., Lei, S.M., Lin, T., 2021. Environmental profile, distributions and potential sources of halogenated polycyclic aromatic hydrocarbons. J Hazard Mater 419, 126164. https://doi.org/10.1016/j.jhazmat.2021.126164.

Xie, Z.Y., Zhang, P., Wu, Z.L., Zhang, S., Wei, L.J., Mi, L.J., Kuester, A., Gandrass, J., Ebinghaus, R., Yang, R.Q., Wang, Z., Mi, W.Y., 2022. Legacy and emerging organic contaminants in the polar regions. Sci Total Environ 835, 155376. https://doi.org/10.1016/j.scitotenv.2022.155376.

Xu, J.Q., Wei, X.Y., Wei, J.Y., He, M.Q., Teng, X.L., Wang, Z.Y., Qu, R.J., 2025. Photodegradation of PCB-209 on suspended particles: Discrepancy in mechanism of direct dechlorination and active species-

mediated indirect dechlorination reactions. Water Res 283, 123797. https://doi.org/10.1016/j.watres.2025.123797.

Xue, H.H., Zheng, N., Kang, C.L., Wang, Y., Wang, Y.W., 2019a. Photochemical degradation of nitrated PAHs in snow. Atmos Environ 199, 260-264. https://doi.org/10.1016/j.atmosenv.2018.11.026.

Xue, S., Sun, J.J., Liu, Y., Zhang, Z.H., Lin, Y.Z., Liu, Q., 2019b. Effect of dissolved organic matter fractions on photodegradation of phenanthrene in ice. J Hazard Mater 361, 30-36. https://doi.org/10.1016/j.jhazmat.2018.08.072.

Yang, X., Rosario-Ortiz, F.L., Lei, Y., Pan, Y.H., Lei, X., Westerhoff, P., 2022. Multiple roles of dissolved organic matter in advanced oxidation processes. Environ Sci Technol 56(16), 11111-11131. https://doi.org/10.1021/acs.est.2c01017.

Yu, Y.T., Liu, M.D., Wang, S.M., Zhang, C.X., Zhang, X., Liu, L., Xue, S., 2024. Unveiling the photodegradation mechanism of monochlorinated naphthalenes under UV-C irradiation: Affecting factors analysis, the roles of hydroxyl radicals, and DFT calculation. Molecules 29(19), 4535. https://doi.org/10.3390/molecules29194535.

Zhang, Z.W., Chen, Q., Bai, C.F., Zhu, Y.H., She, J., Ge, X., Li, M.B., Li, L.Z., Yu, Y.X., 2024. Identification and seasonal variation of specific particulate bound (halogenated) polycyclic aromatic hydrocarbons in air from different metal industrial parks in Northwest China. Environ Sci Pollut Res 31(29), 41914-41925. https://doi.org/10.1007/s11356-024-33883-w.

Zhao, Q., Fang, Q., Liu, H.Y., Li, Y.J., Cui, H.S., Zhang, B.J., Tian, S.L., 2019. Halide-specific enhancement of photodegradation for sulfadiazine in estuarine waters: Roles of halogen radicals and main water constituents. Water Res 160, 209-216. https://doi.org/10.1016/j.watres.2019.05.061.

Zhao, X., Yang, P., Lu, J., Chen, J., 2024. Comparative study of the degradation of meta-chloronitrobenzene by UV/hydrogen peroxide and UV/persulfate oxidation: Degradation pathways and toxicity. Chem Eng J 490, 151502. https://doi.org/10.1016/j.cej.2024.151502.

Zhao, X.Q., Cheng, P.F., Borch, T., Waigi, M.G., Peng, F., Gao, Y.Z., 2022. Humidity induces the formation of radicals and enhances photodegradation of chlorinated-PAHs on Fe(III)-montmorillonite. J Hazard Mater 423, 127210. https://doi.org/10.1016/j.jhazmat.2021.127210.

Ice and aqueous photochemistry of high-ring chlorinated polycyclic aromatic hydrocarbons: A systematic assessment of persistence and risk in cold regions

Linke Ge[a,b], Rongyan Xu[a], Jack Garnett[b], Peng Zhang[a,*], Dongxiao Bai[a], Siyuan Wang[a,*]

[a]Shaanxi University Key Laboratory of Industrial Pollution Control and Environmental Health, School of Environmental Science and Engineering, Shaanxi University of Science & Technology, Xi'an 710021, China

[b]Lancaster Environment Centre, Lancaster University, Lancaster LA1 4YQ, United Kingdom

Abstract:

Chlorinated polycyclic aromatic hydrocarbons (Cl-PAHs) are toxic contaminants that are widely detected in cold aquatic environments, highlighting a need to understand their aqueous and glacial fate. We systematically investigated the photochemistry of three high-ring Cl-PAHs (≥ 3 rings), 2-chlorofluorene (2-ClFL), 9-chlorophenanthrene (9-ClPHE) and 1-chloropyrene (1-ClPY) in ice and aqueous matrices. Under simulated solar irradiation (λ > 290 nm), all three compounds underwent photodegradation that followed first-order kinetics, but with different rate constants and quantum yields. Overall, photodegradation in ice was up to 6-fold faster than in water, a difference attributed primarily to physical enrichment processes during freezing. HPLC-MS/MS analysis of intermediates indicated that photo-induced hydroxylation and dechlorination were the dominant primary reactions for these Cl-PAHs, and several secondary pathways differed between the two phases. The generation and participation of ·OH in the apparent photolysis were confirmed by EPR and quenching radical experiments. Furthermore, 9-ClPHE photodegraded more rapidly in seawater ice than in freshwater or pure-water ice,

* Corresponding author.

E-mail addresses: zhangpeng4477@sust.edu.cn (P. Zhang), wangsiyuan@sust.edu.cn (S. Wang).

whereas its aqueous photodegradation was fastest in pure water. This pattern likely reflects that Cl^- enhances photodegradation more in ice than in water, and that the inhibition effects of other major constituents (Fe(III), HASS and NO_3^-) are more pronounced in ice. Environmentally relevant photolytic half-lives ($t_{1/2,E}$) extrapolated from laboratory data for the three Cl-PAHs ranged from several hours to tens of days in selected cold regions. Although ECOSAR predictions indicated that many individual transformation products had comparable or lower toxicity, bioluminescence assays with *Vibrio fischeri* revealed substantial photo-enhanced combined toxicities of the parent Cl-PAHs and their intermediates. These results clarify both the similarities and key differences between the ice and aqueous photochemistry, improving evaluation of the environmental fate and risks posed by PAH analogues and derivatives in seasonally ice-covered regions.

Environmental Implication

Chlorinated PAHs are widely detected in aquatic systems, urging novel insights into their glacial and aqueous environmental fate, especially for high-ring Cl-PAHs (≥ 3 rings). In this study, not only photolysis kinetics, pathways and photo-induced toxicity of three high-ring Cl-PAHs varied between the reaction media (ice/water), but the main dissolved substances displayed more significant promotion or inhibition effects in ice than in water. These findings elucidate the nuanced similarities and divergences between ice and aqueous photochemistry, thereby enabling more accurate evaluation of the environmental fate and risks posed by PAH analogues and derivatives in seasonally ice-covered regions.

Keywords: Chlorinated PAHs; Ice photochemistry; Aqueous photochemistry; Photodegradation kinetics; Transformation mechanisms; Toxicity evolution

1. Introduction

Chlorinated PAHs (Cl-PAHs) are a significant category of substituted polycyclic aromatic hydrocarbons (SPAHs) generated by substituting hydrogen atoms with chlorine atoms in PAHs

(Ali et al. 2024, Jin et al. 2020, Xie et al. 2021). Cl-PAHs have emerged as environmental contaminants of concern due to their higher toxicity than parent PAHs, demonstrating multiple teratogenic, carcinogenic, and mutagenic effects (Peng et al. 2023). Importantly, Cl-PAHs in the atmosphere have been found to originate from diverse sources, including atmospheric transformation of industrial PAH emissions and incomplete combustion of fossil fuels plus others (Klimczak et al. 2023, Liu et al. 2023, Zhang et al. 2024). Furthermore, photo-chlorination of PAHs can also produce Cl-PAHs in waters during industrial and environmental processes. For example, chlorination disinfection of tap water (Liu et al. 2021), solar chlorination of seawater (Cai et al. 2024a, Tu et al. 2023), and phototransformation in saline ice under simulated sunlight (Li et al. 2024a). Consequently, Cl-PAHs are widely detected in the atmosphere (Oda et al. 2024), surface waters (Qi et al. 2023, Qiao et al. 2018, Wang et al. 2016), as well as sediments and soils (Table S1 and associated refs.). Concentrations of Cl-PAHs in environmental water samples collected throughout China were reported from 3.1 ng L^{-1} to 29.6 ng L^{-1} in Beijing urban rivers, and from 7.8 ng L^{-1} to 25.7 ng L^{-1} in Shaoping Lake of Henan (Qiao et al. 2018, Wang et al. 2016). Also, the mean concentration of Cl-PAHs detected in the surface water of Qingdao was 0.91 ng L^{-1} (Qi et al. 2023). Cl-PAHs have also been frequently detected in tap water (Liu et al. 2021, Tillner et al. 2013). Thus, given their hazardous nature, wide sources and environmental ubiquity of Cl-PAHs, it is essential to investigate different environmental transformation pathways and ecological toxicity to adequately assess their environmental risk.

Photochemical transformation has been demonstrated to play a key elimination mechanism of many organic pollutants in surface waters, atmosphere and surface soil (Guo et al. 2023, Hu et al. 2021, Tu et al. 2023). The photochemical behavior of certain Cl-PAHs has been examined (Ohura et al. 2008, Zhao et al. 2022), however, these focused on different media (i.e., cyclohexane, atmospheric particulates and surface soil) and included only limited Cl-PAHs (2

rings). In aqueous solutions, monochlorinated naphthalenes and 2,3-dichlornaphthalene underwent photochemical degradation under UV/simulated sunlight, which followed first-order kinetics, with the degradation pathways involving hydroxylation, dechlorination and other reactions (Kang et al. 2018, Yu et al. 2024). Furthermore, Ge et al. (2025a) found that 4-chloro-1-hydroxynaphthalene (4-Cl-1-OHN) displayed faster degradation under ice and water photolysis compared to other 3 hydroxyl naphthalenes without chlorine substitution, showing distinct pathways for ice and water phases. As for high-ring Cl-PAHs (≥ 3 rings), their aqueous photochemical transformation remains unknown. Therefore, not only photolytic kinetics and mechanisms need to be investigated for these high-ring Cl-PAHs, but their glacial and aqueous photochemical behavior requires comparative studies so as to provide a useful rationale to further assess their environmental persistence and risk in aquatic systems.

Ice and snow represent a crucial environmental medium, covering approximately 11%−40% of the Earth surface. In remote cold areas, especially in polar regions, ice/snow has been proved to serve as an important reactive repository for the deposited atmospheric persistent contaminants, such as PAHs (Azcune et al. 2022, Hung et al. 2022, Xie et al. 2022). Despite the lack of reported detection of Cl-PAHs in natural ice/snow, their presence in cold regions is most possible because the local abundant PAHs can be feasibly transformed into Cl-PAHs (Cai et al. 2024a, Liu et al. 2021, Tu et al. 2023). Previous studies have indicated that ice plays a dominant role in the photochemical attenuation of organic pollutants in cold areas, where microbial activity is negligible (Ge et al. 2023, Ge et al. 2025a). Especially, long-period sunlight prevails in summers of the Arctic and Antarctic, which promotes the phototransformation of pollutants. As for high-ring Cl-PAHs (≥ 3 rings), their photochemistry in ice remains unknown. In comparison with PAHs in ice, OH-PAHs and nitrated-PAHs exhibited the different ice photochemical behavior due to the hydroxylated and nitrated substitution, respectively (Ge et al. 2023, Ge et al. 2025a, Ge et al. 2016a, Xue et al. 2019a). Although Cl-PAHs exhibit similar

structures to their parent PAHs, the substituted chlorine as the auxochromic group is hypothesized to induce certain distinctions between their photochemical behavior (Cai et al. 2024b, Manfrin et al. 2020). Consequently, exploring the photodegradation of Cl-PAHs in ice would be of necessity to test the hypothesis.

Furthermore, the comparative studies on the ice and aqueous photochemistry have aroused considerable concerns for organic pollutants, such as PAHs and several derivatives, pesticides, and pharmaceuticals (Li et al. 2024b, Liu et al. 2023, Wang et al. 2023b). For instance, 4-nitro-1-hydroxynaphthalene (4-NO_2-1-OHN) and 4-Cl-1-OHN only in ice phase suffered from multiple hydroxylation, and 4-NO_2-1-OHN in ice underwent photo-isomerization as well, leading to their higher photo-modified toxicity in ice compared to aqueous solutions (Ge et al. 2025a). Moreover, the photolysis rates of 2- and 9-hydroxyfluorenes (OHFL) in ice were found to be significantly higher than in water, with co-existing dissolved components (e.g., Cl^-, Fe(III)) showing different effects on the photolysis in the two phases (Ge et al. 2023). These findings are interesting, accounting for the similarities and differences between the ice and aqueous photochemistry. However, new insights into environmental ice and aqueous photochemistry of high-ring Cl-PAHs (≥ 3 rings) are urged so as to seek a new systematic comparison between the two disciplines.

This study presents a systematic comparison of the ice and aqueous phase photolytic behavior of three Cl-PAHs, including 2-chlorofluorene (2-ClFL, 3-ring), 9-chlorophenanthrene (9-ClPHE, 3-ring) and 1-chloropyrene (1-ClPY, 4-ring) (Fig. S1), compounds detected in multiple environments, especially in natural waters (Table S1). We determined photolysis kinetics, identified reaction pathways, and assessed photo-induced changes in toxicity for each compound in both ice and liquid water. In addition, 9-ClPHE was also examined in greater detail and used as a representative high-ring congener to further elucidate mechanistic and kinetic differences in the presence of dissolved components in ice and aqueous solutions. To

our best knowledge, this is the first study to comprehensively investigate the ice and aqueous phase photochemistry of high-ring Cl-PAH congeners (≥ 3 rings), and to link their transformation pathways with resulting changes in toxicity in cold aquatic systems. This study provides new insights into the distinct phototransformation mechanisms of high-ring Cl-PAHs in ice and aqueous systems, which are currently under-represented in the literature and yet enable more accurate evaluation of the environmental persistence and risks posed by similar PAH analogues in seasonally ice-covered regions.

2. Materials and methods

2.1. Chemicals and prepared water solutions

2-ClFL (purity 98%)/1-ClPY (95%) and 9-ClPHE (98%) were purchased from Shanghai Yubo Biotechnology Co., LTD. and Acros Organics (Belgium), respectively (see Table S2 for further information). High-purity water (18.2 MΩ cm) was produced with a Millipore-Milli Q system. Natural freshwater was sampled from Xi'an Weihe River (34.37°N, 108.97°E), and the seawater was taken from Dalian coastal area (38.88°N, 121.57°E).

The environmental water samples were filtered by the membranes (pore size 0.22 μm) to remove particles and then stored at 4 °C until further analysis. Their properties and the major ions are shown in Table S3. Pure water, natural-freshwater and seawater samples were spiked with individual Cl-PAHs and 2% acetonitrile as co-solvent to give concentrations characteristically measured in the environment (C_0 = 0.2 μM) ready for use in photolytic experiments.

2.2. Photolytic kinetic experiments

As illustrated in Fig. S2, a rotating photochemical reactor was employed to perform the photolytic experiments, using a Pyrex well-jacketed and cooled mercury lamp (500 W) to simulate solar radiation (λ > 290 nm). The light intensities at the reaction sites were measured

with a UV-A radiometer at 420 nm (8.03 mW cm^{-2}) and 365 nm (8.09 mW cm^{-2}), respectively. Firstly, Cl-PAH solutions (V = 80 mL) were divided into two aliquots and retained in separate Pyrex tubes ready for aqueous and ice experiments. For the aqueous research, the aliquot was transferred directly into the apparatus at room temperature (25 ± 1 °C). For the ice study, the aliquot was frozen into ice and then placed into the experimental apparatus, which was kept in a freezer (−5 ± 1 °C). To test whether hydroxyl radicals (·OH) participated in the apparent photolysis, quenching radical experiments were performed using isopropanol as the quencher of ·OH (Text S1). The apparent quantum yields (Φ_s) for the ice and aqueous photodegradation were quantified based on methods used previously (Text S2) (Cui et al. 2025b, Ge et al. 2025a).

To explore the effects of some typical water constituents (e.g., Cl^-, Fe(III), humic acid and NO_3^-) on photodegradation kinetics of 9-ClPHE, a series of artificial solutions were prepared. Pure reagents (NaCl, $Fe_2(SO_4)_3$, humic acid sodium salt (HASS) and $NaNO_3$) were added to Milli Q water to give concentrations matching those observed in natural surface waters (Table S3). Furthermore, a four-factor central composite experiment was designed to examine the multivariate effects of coexisting water constituents (Table S4). The concentrations of target factors were selected based on their environmentally relevant ranges (Ge et al. 2016b, Wang et al. 2023a, Yang et al. 2022). Details can be found in the supplementary material (Text S3). Notably, all the photo-irradiating experiments and dark controls were conducted in triplicate.

2.3. Analytical methods

An Agilent 1260 Infinity II HPLC was employed to determine concentrations of three Cl-PAHs with the analytical parameters listed in Table S5. An Agilent 6470B triple quadrupole LC/MS system coupled with an electro spray ionization source operating in negative mode was used to identify key degradation products. The generated ·OH was identified by electron paramagnetic resonance (EPR) spectra with 5,5'-dimethyl-1-pirroline-N-oxide (DMPO) as a spin-trap reagent. Relevant details are provided in Text S4. The total organic carbon (TOC) of

natural waters and HASS solutions were determined by a liquid TOC–II Analyzer. In addition, the electrostatic potential (ESP), the highest occupied molecular orbital (HOMO), the lowest unoccupied molecular orbital (LUMO) and Fukui indices of the three Cl-PAHs were calculated by density functional theory (DFT).

2.4. Toxicity assessment

To determine the acute toxicity of Cl-PAHs during photolytic degradation, a bioassay using *Vibrio fischeri* was conducted with a HACH Eclox^{TM} Rapid Response Test working in the 'Luminescent Bacteria Toxicity Testing' mode. The luminescence inhibition rate (I%) was used to make a toxicity assessment as performed previously (Ge et al. 2025a, Ge et al. 2025b). Furthermore, an Ecological Structure-Activity Relationships (ECOSAR) predictive model (version 2.2) was used to estimate the acute toxicity of the parent compounds and individual degradation products to fish, daphnia and green algae (Ge et al. 2025b).

3. Results and discussion

3.1. Photolytic kinetics of three Cl-PAHs in ice and water

Slight pH fluctuations (less than 0.3 units, $p > 0.05$) were recorded in the individual photolytic experiments (Table S6). And negligible changes in solution concentration (< 2%) of the three Cl-PAHs were observed over the experimental period under dark conditions. This suggested that both physical losses (e.g., volatilisation) and chemical losses (e.g., hydrolysis and pyrolysis) played minor roles throughout the controlled experiments. As such, any reduction in the concentration of the three compounds in both ice and aqueous phase studies can be attributed to photodegradation caused by exposure to simulated sunlight. Photodegradation of the three Cl-PAHs in this study appeared to follow first-order kinetics, as evidenced by good linear fit of $\ln(C/C_0)$ versus time (t) ($r^2 > 0.97$) (Fig. 1). The corresponding photolytic rate constants (k), half-lives ($t_{1/2}$), and Φ_s are listed in Table S7.

As indicated in Fig. 1 and Table S7, photolytic rates of the individual Cl-PAHs were up to 6-

fold higher in ice than in water. Elevated photodegradation rates in ice compared to water were also found previously for other SPAHs, including 2-OHFL, 1-nitropyrene (1-NPY) and phenanthrene (Ge et al. 2016a, Ge et al. 2025b, Xue et al. 2019b). Given the lower temperatures in ice compared to water that would typically be associated with slower rates of reaction, this observation may, in part, be attributed to physical processes occurring during ice formation. During water freezing into ice, pollutant molecules are preferentially partitioned into liquid-like regions (LLRs), accompanied by both concentration-enhancement and ice-cage effects (Ge et al. 2023). The dual effects may respectively enhance solute concentrations at the grain boundaries of ice crystals and create micro-fields around them via solvent molecules. The synergistic mechanisms ultimately modulate the photolytic kinetics of the solute compounds through interfacial microenvironment. In instances where ice is formed from seawater, a network of microscopic liquid brine (highly saline) channels is formed which can contain increased levels of pollutants (Garnett et al. 2021, Garnett et al. 2019). In either case, enrichment of pollutants at ice grain boundaries can lead to enhanced photodegradation through a reduction in light pathway distance and possibly lowering the amount of light scatter (Ge et al. 2023, Ge et al. 2025b, Klanova et al. 2003, Weber et al. 2009).

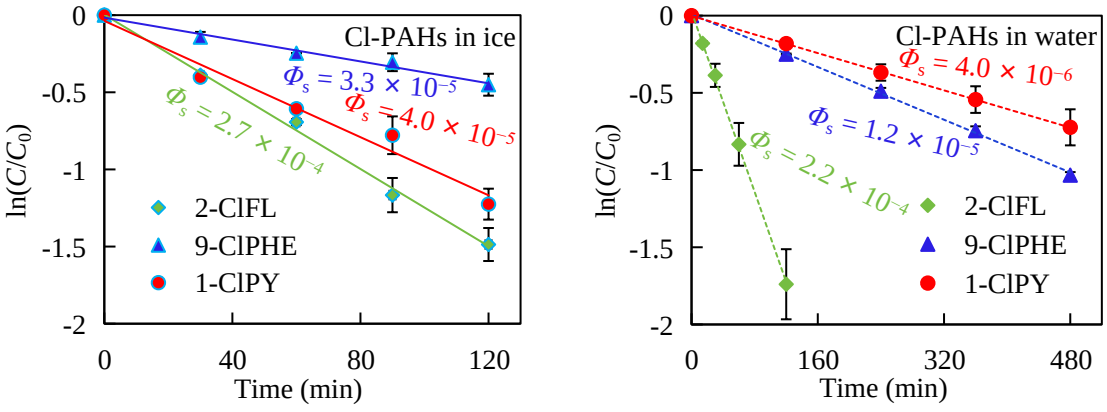

Fig. 1. Simulated solar photolytic kinetics of the three chlorinated PAHs (Cl-PAHs, 2-chlorofluorene (2-ClFL), 9-chlorophenanthrene (9-ClPHE) and 1-chloropyrene (1-ClPY)) in ice and in water.

Comparison of measured data also revealed differences in photochemical degradation rates,

which indicated that photolysis is also likely to be chemical specific. For example, 2-ClFL (3-ring) displayed the greatest decline rate under both ice and aqueous phases, while 9-ClPHE (3-ring) and 1-ClPY (4-ring) degradation occurred more slowly. Given the low light absorption of 2-ClFL compared to the other Cl-PAHs (Fig. S3), the higher degradation rate for this chemical is clearly related to its higher photolytic reactivity, as indicated by the higher Φ_s values, compared to 9-ClPHE and 1-ClPY (Table S7). Analysis of data (Table S7) also showed a much greater increase in degradation rates between ice and water conditions for 1-ClPY (6.10 ± 0.01 fold, $p < 0.01$) than 9-ClPHE (1.67 ± 0.03 fold, $p < 0.01$) and 2-ClFL (1.17 ± 0.21 fold). As discussed earlier, physical processes during ice formation may be partly attributable for this increase, however, physical ice processes are likely to act evenly across chemicals regardless of their properties and therefore the higher photodegradation rate of some chemicals is most likely related to differences in chemical properties such as chemical transformation pathways (See Section 3.3).

A comparison of Φ_s values was undertaken for Cl-PAHs (this study) and related PAHs to assess differences in photolytic kinetics of these environmental pollutants (Table S8 and associated refs.). Interestingly, not only in ice but also in water, photodegradation Φ_s values of Cl-PAHs (10^{-5}–10^{-4}) were shown to be 1−2 orders of magnitude lower compared to those of PAHs (10^{-3} in most cases), nitro-PAHs (10^{-4} in most cases) and hydroxy-PAHs (10^{-3}–10^{-1}). For instance, glacial 9-ClPHE and 1-ClPY displayed the lower Φ_s values of 3.3×10^{-5} and 4.0×10^{-5}, respectively, than their parent phenanthrene (3.8×10^{-3}) and pyrene (4.3×10^{-4}). PAHs and their derivatives such as Cl-PAHs exhibit a wide variety of structural isomers which can govern their photodegradation kinetics and chemical transformation efficiency (Table S8). The key determinants are differences in Φ_s values and the spectral overlap between compound absorption and light source irradiance (Ofrydopoulou et al. 2021).

3.2. Photolytic pathways of Cl-PAHs in ice and in water

The photolytic intermediates and transformation pathways of the three Cl-PAHs were investigated in ice and water by examining the total ion chromatograms in the negative monitoring mode (Fig. S4). Using relevant MS (Scan) and MS^2 (SIM-Scan) spectra (Fig. S5), significant intermediates were identified. Their molecular weights (*Mw*), retention times (t_R) and fragment ions (*m*/*z*) are shown in Table S9. Furthermore, the DFT calculations (Figs. S6-S8) indicated the most possible reaction sites of each compound susceptible to radical attack (e.g., ·OH). By integrating the HPLC-MS/MS data, the chemical structures of key products are tentatively proposed, along with the phototransformation pathways of the three Cl-PAHs both in ice and in water (Fig. 2).

As shown in Fig. 2, four 2-ClFL degradation products (P166, P182, P198 and P232) were formed in both ice and water via the same reactions, namely dechlorination and hydroxylation. However, ketonic P196 was formed exclusively in the aqueous phase through photo-oxidation. As for 9-ClPHE, the compound underwent hydroxylation to produce P228 in ice. Whereas, the aqueous 9-ClPHE underwent hydroxylation to produce P228, followed by dechlorination and hydroxylation to P210. Similar reactions occurred for 1-ClPY, transforming into identical degradation products (i.e., P252, P268 and P218) in both phases, and generating P202 only in the aqueous phase through dechlorination.

Regardless of the different intermediates observed in the two phases, photo-induced hydroxylation and dechlorination were determined to be the key reactions involved in the phototransformation of the three Cl-PAHs (Fig. 2). This finding aligns with previous studies, which showed OH-PAHs and nitro-PAHs underwent hydroxylation to form multiple hydroxyl intermediates in the two phases (Ge et al. 2023, Ge et al. 2025a, Ge et al. 2025b). The prevalence of hydroxylation reaction can be ascribed to the generation of ·OH radicals from the photo-sensitization of the parent compounds in the two phases. As shown in Fig. 3, EPR spectra showed four sets of peaks with 1:2:2:1 under irradiation, corresponding to the characteristic of

the DMPO-·OH, which verified the generation of ·OH from photo-sensitization of Cl-PAHs. Combined with radical quenching experiments (Text S1), the participation of ·OH in the apparent photolysis was confirmed, and the contribution ratios ($R_{\cdot OH}$) of self-sensitized photo-oxidation via ·OH to the apparent photolysis were illustrated in Fig. 3. The ·OH was speculated during the photolysis of several PAHs and SPAHs (Ge et al. 2025a, Sarmiento et al. 2023). However, the formation and participation of ·OH were proved in the present study. Furthermore, additional dechlorination is prevalent for chlorinated PAHs and analogue (Kang et al. 2021, Teng et al. 2025, Xu et al. 2025). For instance, certain low-ring Cl-PAHs (2 rings) displayed dechlorination in both ice and aqueous conditions (Ge et al. 2025a, Huang et al. 2021).

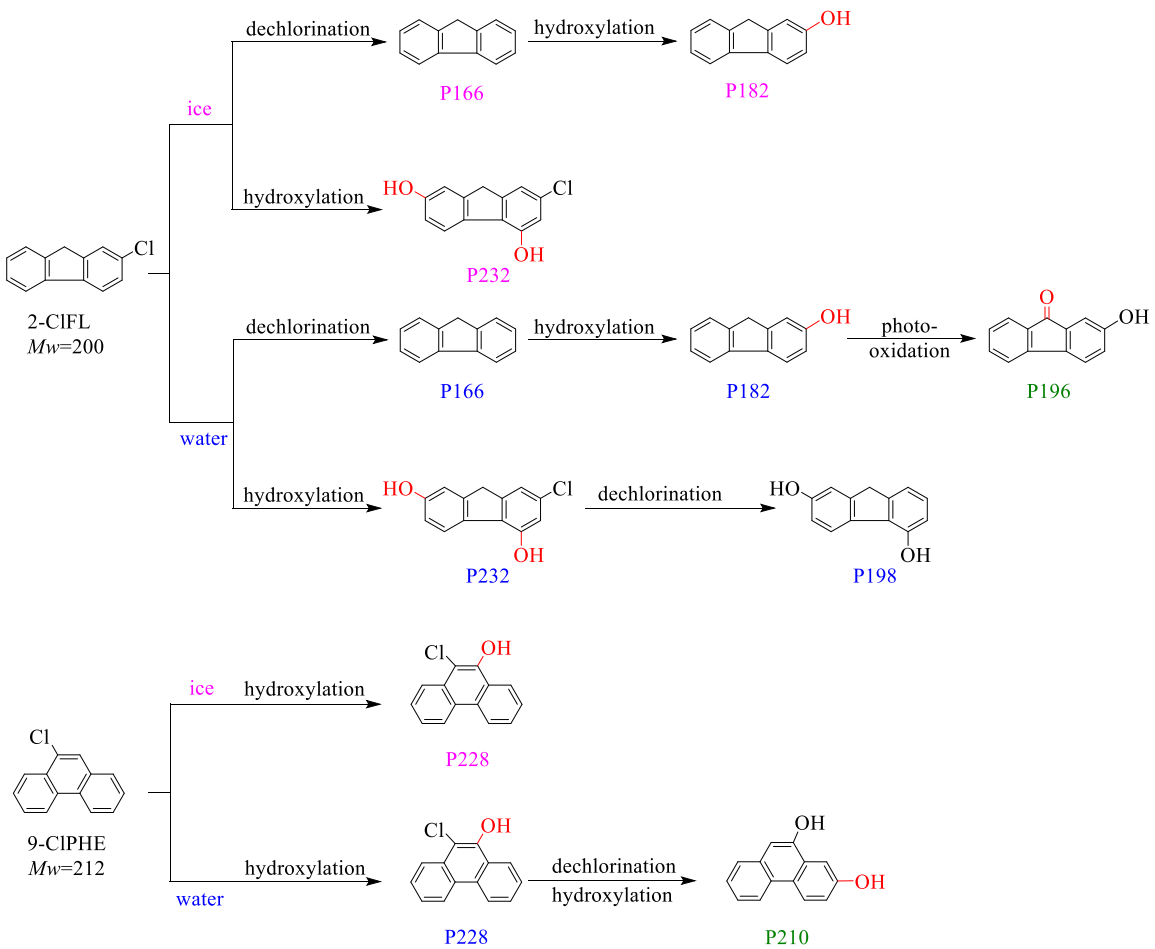

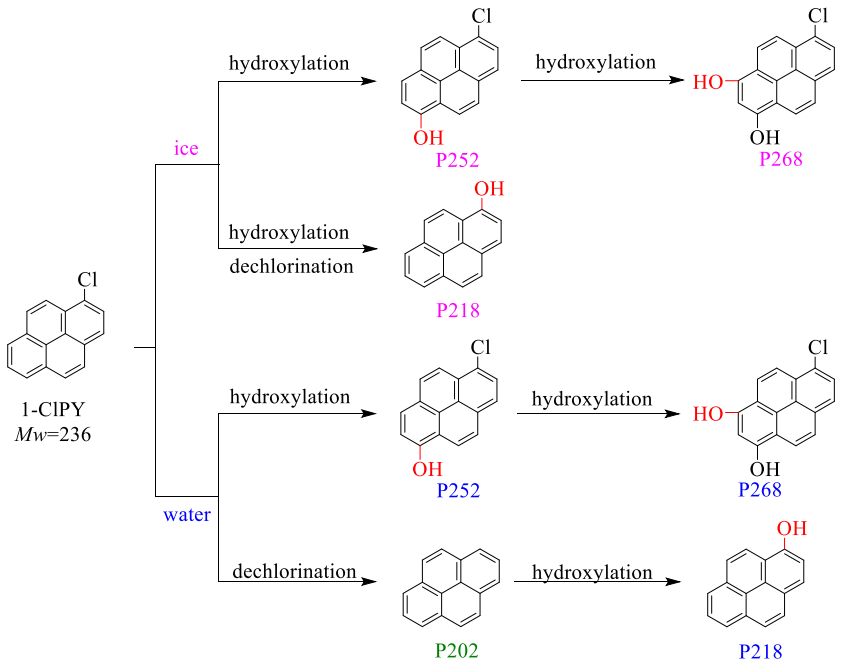

Fig. 2. Photolytic products and transformation pathways associated with the three Cl-PAHs. The photogenerated intermediates are designated as P_{Mw}, where *Mw* denotes molecular weights calculated from the most abundant isotopes. P_{Mw} is marked with different colors to distinguish the products generated in different phases. Among them, 'magenta' indicates products formed in ice, 'blue' indicates products in water, and 'green' represents products that were only formed in the aqueous phase.

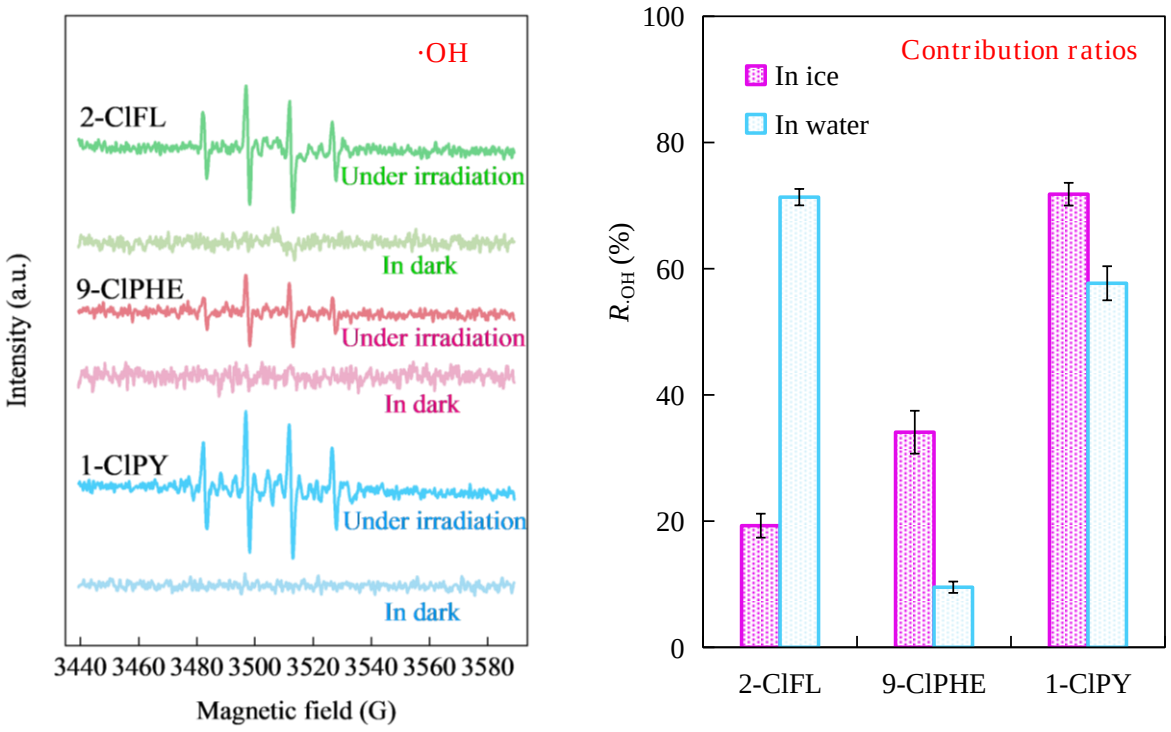

Fig. 3. The electron paramagnetic resonance (EPR) spectra (left) and the contribution ratios ($R_{\cdot OH}$) of self-sensitized photo-oxidation via ·OH to the apparent photolysis (right) for the three Cl-PAHs.

3.3. Effects of aqueous dissolved substances on the photodegradation of 9-ClPHE

The chemical 9-ClPHE (3-ring) was selected as a model Cl-PAH compound to further examine photodegradation kinetics in ice and water containing varying levels of other naturally occurring chemical substances (Table S10). Like previous experimental results (pure-water ice/pure water), it was found that 9-ClPHE photolyzed significantly faster in ice than in water (freshwater and seawater), as shown in Fig. 4. This finding supports the assertion that ice generally acts to enhance photodegradation of chemicals even in the presence of other matrix constituents, probably through a combination of physical (i.e., concentration processes involved during ice formation) and chemical (i.e., generation/promotion of reactive ions) mechanisms.

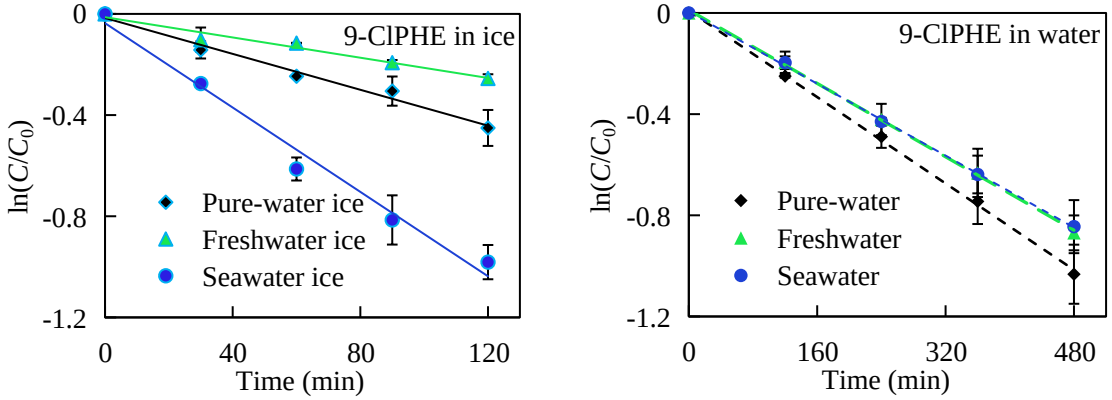

Fig. 4. Photodegradation kinetic curves of 9-ClPHE in varying ices and aqueous solutions under the same irradiating conditions ($\lambda > 290$ nm).

The photolytic rates of 9-ClPHE varied depending on the solution matrix (i.e., pure water, freshwater and seawater) and condition (e.g., ice/water). In seawater ice, 9-ClPHE underwent faster photolysis than in pure-water ice and freshwater ice. In contrast, 9-ClPHE photodegraded fastest in pure water compared to seawater and freshwater. These observations aligned with the prior study, which showed the photolytic rates of OH-PAHs (e.g., 2-OHFL and 9-OHFL) also varied markedly in different types of ice and waters, often with the highest rates appearing in seawater ice (Ge et al. 2023).

Further analysis of photodegradation rate data (rate constant, *k* values) with concentration

data for different matrix components (Cl^-, Fe(III), HASS and NO_3^-) showed significant differences ($p < 0.05$) between concentrations for different constituents. This strongly suggested that different chemicals played varying roles phototransformation of 9-ClPHE in both the ice and aqueous (Fig. 5). Specifically, in the presence of Cl^-, the photolysis of 9-ClPHE was promoted in the two phases ($p < 0.05$). Although the values of k were in the same order of magnitude (10^{-3} min^{-1}), Cl^- appeared to promote photodegradation significantly more in ice compared to water, with maximal degradation rates appearing around 0.50 M and 0.68 M, respectively. The enhanced rate of photolysis of 9-ClPHE in the presence of Cl^- can be ascribed to the formation of more reactive chlorine species (e.g., $ClOH^{\cdot -}$) via scavenging ·OH by Cl^- in neutral solution (El Omar et al. 2012), understood as follows:

$$9\text{-ClPHE} + h\nu \longrightarrow 9\text{-ClPHE}^* \quad (1)$$

$$9\text{-ClPHE}^* \xrightarrow{+H_2O} \cdot OH \text{ (proved by EPR spectra in Fig. 3)} \quad (2)$$

$$\cdot OH + Cl^- \underset{k_2}{\overset{k_1}{\rightleftharpoons}} ClOH^{\cdot -} \quad (k_1 = 4.3 \times 10^9\ M^{-1}s^{-1},\ k_2 = 6.1 \times 10^9\ M^{-1}s^{-1}) \quad (3)$$

At high concentrations of Cl^-, generation of reactive $ClOH^{\cdot -}$ species is likely to reach a point whereby further promotion effects are weakened through the transformation of $ClOH^{\cdot -}$ into $Cl\cdot$ and $Cl_2^{\cdot -}$ (El Omar et al. 2012). Meanwhile, changes in the microstructure of ice under high salinity conditions also influence the photodegradation rate of coexisting organic solutes (Chen et al. 2019, Mason et al. 2022).

Other dissolved components (HASS, NO_3^- and Fe(III)) present in the seawater and freshwater (Table S3) were also investigated to examine their effect on the photochemistry of 9-ClPHE in ice and water (Table S10). In general, these components were demonstrated to inhibit photodegradation in both ice and water, though inhibition effects were more prominent in ice than in water. Increased inhibition of photolysis in ice can be rationalized using the same physical mechanisms described earlier, which highlighted enrichment of dissolved solutes at ice grain interfaces. Hence, the inhibition effects of some dissolved species (e.g., HASS, NO_3^-

and Fe(III)) are also likely to be enhanced.

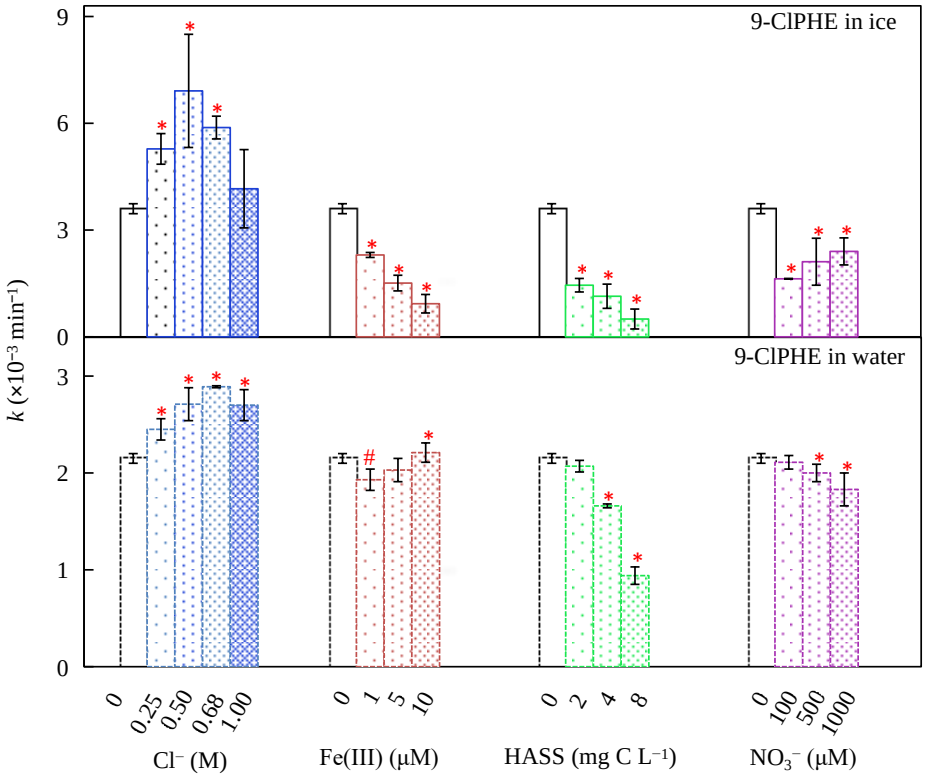

Fig. 5. Impacts of the soluble substances on the photolytic *k* values of 9-ClPHE in the two phases (ice/water). The symbols * and # indicate remarkable differences at the 0.05 and 0.1 significance levels (*p*), respectively, when comparing *k* to that without added dissolved substances.

Inhibition of 9-ClPHE photodegradation was particularly evident in the presence of HASS, which showed an approximately 3-fold reduction in rates. For NO_3^- and Fe(III), this effect was less prevalent at about 2-fold reduction. Though these species have been reported to promote the photodegradation of pollutants by the sensitization effect (Ge et al. 2016b, Huang et al. 2024), it was apparent in this study that their net affect led to inhibition. This observation can be ascribed to the absorption of a similar light spectrum by 9-ClPHE and dissolved species, which can act in a competitive manner (Ge et al. 2016b). An assessment of the absorption spectra (Fig. S9) strongly supports this assertion by displaying a large overlap in the region spectrum around 290 nm. In comparison, DOM exerted distinct inhibition or promotion effects on photodegradation depending on the hydrophobicity and hydrophilicity of antibiotics (Cui et

al. 2025a). Together, these results confirm that photodegradation is highly dependent on the chemical structure and optical properties of these coexisting dissolved substances.

A multivariate analysis was performed on the central composite experiments to explore the effect of coexisting water constituents on photodegradation kinetic properties of 9-ClPHE (Table S11). The corresponding regression coefficients (β_x) and their significance levels (p) are presented in Table S12. If the p value is less than 0.05, the corresponding β_x is a significant factor. Thus, Cl^-, HASS, NO_3^- and Cl^--Cl^- interaction were significant factors contributing to the photodegradation of 9-ClPHE. The fitting equation can be expressed more simply as follows:

$$k = \beta_0 + \beta_1 x_1 + \beta_3 x_3 + \beta_4 x_4 + \beta_{11} x_1^2 \quad (1)$$

where x_1, x_3 and x_4 respectively denote the levels of Cl^-, HASS and NO_3^- (Table S4). Negative values of β_3 and β_4 were observed (Table S12), indicating that NO_3^- and HASS inhibited the photodegradation of 9-ClPHE. In contrast, the values of β_1 and β_{11} were positive, thus Cl^- and Cl^--Cl^- interaction promoted the photodegradation. Based on the sum of squares, the contributions of Cl^-, HASS, NO_3^- and Cl^--Cl^- interaction were assessed to be 16.22%, 60.47%, 3.12% and 3.87%, respectively. As for Fe(III), the inhibition effect on the photodegradation was considered to be significant at $p < 0.1$ (Table S12). The above experimental results were consistent with the single-factor experiment findings.

3.4. Environmental photochemical persistence and risk in cold regions

Laboratory-derived data were extrapolated to estimate apparent environmental photolytic half-lives ($t_{1/2,E}$) of Cl-PAHs in cold regions (Text S5). As reported in Table 1, estimated $t_{1/2,E}$ values for surface ice and snow ranged from 0.54 days (1-ClPY in the Arctic) to 65 days (2-ClFL in Xi'an, China), while surface waters generally showed longer life times. This wide range reflects dependence of chemical identity, environmental media, latitude, and season. Compared to the parent PAHs and OH-PAHs (Table S13), Cl-PAHs generally displayed much longer $t_{1/2,E}$. For instance, the $t_{1/2,E}$ values for 2-ClFL ranged from 17.17 days (Arctic; 78.91°N, 11.93°E;

Ice/Snow) to 77.37 days (Antarctic; 62.21°S, 58.96°W; Water), which were larger than those for 2-OHFL from 0.012 days (Arctic; 78.91°N, 11.93°E; Ice/Snow) to 0.027 days (Antarctic; 62.21°S, 58.96°W; Snow), and for fluorene (FL) from 0.79 days (Summit, Greenland; 72.58°N, 38.49°W; Snow) to 7.88 days (Alert, Nunavut; 82.5°N, 62.3°W; Snow) (Table S13 and associated refs.). The other two Cl-PAHs were also more persistent than their respective parent PAHs and OH-PAHs. Notably, all parent PAHs and their derivatives exhibit wide variability in the photolytic $t_{1/2,E}$ values, depending on their molecular structures and environmental conditions. Given the greater persistence of Cl-PAHs, the pollutants are likely to persist longer and pose higher ecological risk in cold regions.

Table 1. Environmental photolytic half-lives ($t_{1/2,E}$) of the apparent photodegradation for the three Cl-PAHs in surface ice/snow and water of the Antarctica, Arctic, and Xi'an, China.

Area, season (latitude, longitude)	Medium	($t_{1/2,E}$ / day)		
		2-ClFL	9-ClPHE	1-ClPY
Antarctica, Summer	Ice/Snow	64.14	24.93	0.90
(62.21°S, 58.96°W)	Water	77.37	68.56	8.99
Arctic, Summer	Ice/Snow	17.17	15.35	0.54
(78.91°N, 11.93°E)	Water	20.71	42.22	5.41
Xi'an, Winter	Ice/Snow	65.20	32.47	1.14
(34.37°N, 108.97°E)	Water	78.65	89.28	11.38
Xi'an, Summer	Water	15.14	33.60	4.37

The toxicity evolution during photodegradation of the three Cl-PAHs was assessed using *Vibrio fischeri* (Fig. 6). Reaction solutions typically exhibited higher luminescence inhibition rate (I%) values following the initial sampling time point ($p < 0.01$), I% values appeared to fluctuate and display high variability throughout irradiation time (Fig. 6). This feature indicated changing toxicity throughout the decomposition of Cl-PAH, most likely through the generation of different toxic intermediates. Compared with other SPAHs (Ge et al. 2025a, Ge et al. 2025b), parent Cl-PAHs showed higher I% values, which may be attributed to higher toxicities of

chlorine-containing organic contaminants (Zhao et al. 2019). The ECOSAR assessment agreed broadly with the bioassay but estimated lower toxicities for the transformation products than for the parent compounds (Table S14). Nevertheless, residual parent compounds and transformation intermediates still produced significant combined toxicity in the biotest (Fig. 6). This might be attributed to the formation of hydroxylated products, which would more easily pass through the lipid cell membrane of *Vibrio fischeri* and exert a stronger inhibition effect (An et al. 2021, Ge et al. 2025a, Zhao et al. 2024). PAHs, OH-PAHs and nitrated-PAHs have also been reported to exhibit notable photo-modified toxicity to *Vibrio fischeri* (El-Alawi et al. 2002, Ge et al. 2016b, Ge et al. 2025b). Together, these results indicate that photo-modified toxicities of chlorinated PAHs and related analogues should be accounted for in risk assessments for cold-region environment.

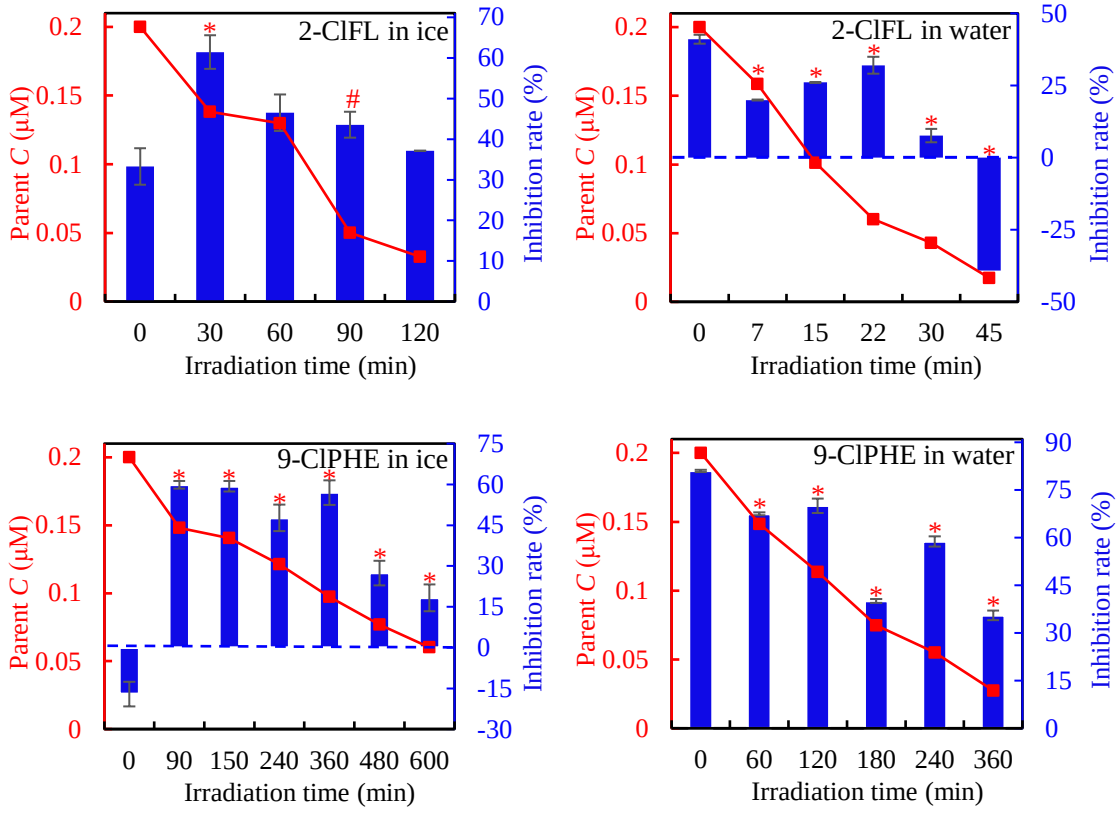

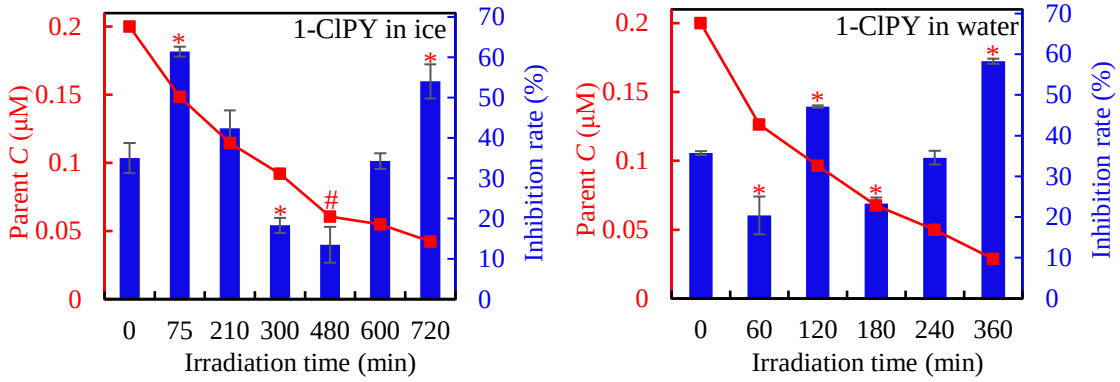

Fig. 6. The evolution of parent concentrations (C, ■) of the three Cl-PAHs, as well as the changes of luminescence inhibition rates (I%, ■) to *Vibrio fischeri* with the irradiation time in ice and in water. * and # indicate significant difference at $p < 0.01$ and 0.05, respectively, between the corresponding I% value at t and the initial value at t_0.

4. Conclusion

This study provides a systematic comparison of the ice versus aqueous photochemistry for three high-ring chlorinated PAHs (≥ 3 rings). This topic is underrepresented but important for their environmental persistence and risk assessment in cold regions. Under identical simulated solar irradiation, differences in the rates of photodegradation of Cl-PAHs were established and attributed to both physical processes occurring during formation of ice, and also chemical processes induced by the presence of other dissolved species in freshwater and seawater. In the apparent photolysis of the three Cl-PAHs, the photo-sensitized generation and participation of ·OH were proved. And photo-induced hydroxylation and dechlorination were the primary reactions, but several secondary pathways and intermediates were identified depending on the phase. Estimated half-lives of Cl-PAHs ranged from several hours to dozens of days in surface ice/snow, which were found to be consistently shorter than in surface waters under comparable regional and seasonal conditions.

The bioassay using *Vibrio fischeri* demonstrated significant photo-enhanced joint toxicities of the parent Cl-PAHs and photogenerated intermediates, though ECOSAR assessment showed the comparable or lower toxicities of the individual transformation products. The findings

reported here fill a critical gap in understanding the environmental phototransformation mechanisms of high-ring Cl-PAHs (≥ 3 rings) in seasonally frozen water of cold regions, such as high-latitude and high-altitude areas. The results provide a useful framework to better assess the environmental persistence and risks of chlorinated PAHs, analogues and other derivatives in cold regions.

CRediT authorship contribution statement

Linke Ge: Writing – review & editing, Supervision, Methodology, Investigation, Funding acquisition, Conceptualization. **Rongyan Xu:** Writing – review & editing, Writing – original draft, Investigation. **Jack Garnett:** Writing – review & editing, Formal analysis. **Peng Zhang:** Writing–review & editing, Formal analysis. **Dongxiao Bai:** Writing – review & editing, Validation. **Siyuan Wang:** Writing – review & editing, Conceptualization.

Acknowledgements

This work was supported by the National Natural Science Foundation of China (Nos. 21976045 and 22076112), the Key Research and Development Program of Shaanxi Province (No. 2024SF-YBXM-567), and the China Scholarship Council (CSC) Scholarship (No. 202308610123).

Appendix A. Supplementary data

Supplementary data to this article can be found online at doi.org/10.1016/j.########.

Data availability

Data will be made available on request.

References

Ali, L., Alam, A., Ali, A.M., Teoh, W.Y., Altarawneh, M., 2024. A comprehensive review into emission sources, formation mechanisms, ecological effects, and biotransformation routes of halogenated polycyclic aromatic hydrocarbons (HPAHs). Ecotoxicol Environ Saf 286, 117196. https://doi.org/10.1016/j.ecoenv.2024.117196.

An, Z., Han, D., Sun, J., Mei, Q., Wei, B., Li, M., Qiu, Z., Bo, X., Wang, X., Xie, J., Zhan, J., He, M., 2021.

Full insights into the roles of pH on hydroxylation of aromatic acids/bases and toxicity evaluation. Water Res 190, 116689. https://doi.org/10.1016/j.watres.2020.116689.

Azcune, G., Griffero, L., Pareja, L., Ríos, J.M., Galbán-Malagón, C., Pérez-Parada, A., 2022. Trends in the monitoring of legacy and emerging organic pollutants in protected areas. Trends Environ Anal Chem 34, e00165. https://doi.org/10.1016/j.teac.2022.e00165.

Cai, B.C., Hu, X.F., Li, Y.J., Bai, Y.X., Xie, H., 2024a. Cation radical induced photochlorination of naphthalene in saline water under UV light irradiation. ACS ES&T Water 4(4), 1925-1936. https://doi.org/10.1021/acsestwater.4c00056.

Cai, Y., Li, X.C., Feng, M.B., Chovelon, J.-M., Lu, J.H., Chen, J., Ji, Y.F., 2024b. Photochemical degradation of bisphenol S and its tetrahalogenated derivatives in water. Water Res 262, 122131. https://doi.org/10.1016/j.watres.2024.122131.

Chen, C., Chen, L., Yao, Y., Artigas, F., Huang, Q., Zhang, W., 2019. Organotin release from polyvinyl chloride microplastics and concurrent photodegradation in water: Impacts from salinity, dissolved organic matter, and light exposure. Environ Sci Technol 53(18), 10741-10752. https://pubs.acs.org/doi/10.1021/acs.est.9b03428.

Cui, J.S., Chen, Y., Cheng, F.Y., Yang, H., Qu, J., Zhang, Y.N., Peijnenburg, W.J.G.M., 2025a. Hydrophilicity-dependent photodegradation of antibiotics in ice: Freeze-concentration effects and dissolved organic matter interactions drive divergent kinetics, pathways and toxicity. Water Res 286, 124277. https://doi.org/10.1016/j.watres.2025.124277.

Cui, N.N., Ge, L.K., Halsall, C., Niu, J.F., Zheng, J.S., Zhang, P., 2025b. Dissociation-dependent kinetics and distinct pathways for direct photolysis and •OH/$SO_4^{\bullet-}$ radical dominated photodegradation of ionizable antiviral drugs in aquatic systems. Water Res 279, 123452. https://doi.org/10.1016/j.watres.2025.123452.

El-Alawi, Y.S., McConkey, B.J., George Dixon, D., Greenberg, B.M., 2002. Measurement of short- and long-term toxicity of polycyclic aromatic hydrocarbons using luminescent bacteria. Ecotoxicol Environ Saf 51(1), 12-21. https://doi.org/10.1006/eesa.2001.2108.

El Omar, A.K., Schmidhammer, U., Rousseau, B., LaVerne, J., Mostafavi, M., 2012. Competition reactions of $H_2O^{\bullet+}$ radical in concentrated Cl^- aqueous solutions: Picosecond pulse radiolysis study. J Phys Chem A 116(47), 11509-11518. https://pubs.acs.org/doi/10.1021/jp309381z.

Garnett, J., Halsall, C., Thomas, M., Crabeck, O., France, J., Joerss, H., Ebinghaus, R., Kaiser, J., Leeson, A., Wynn, P.M., 2021. Investigating the uptake and fate of poly- and perfluoroalkylated substances (PFAS) in sea ice using an experimental sea ice chamber. Environ Sci Technol 55(14), 9601-9608. https://doi.org/10.1021/acs.est.1c01645.

Garnett, J., Halsall, C., Thomas, M., France, J., Kaiser, J., Graf, C., Leeson, A., Wynn, P., 2019. Mechanistic insight into the uptake and fate of persistent organic pollutants in sea ice. Environ Sci Technol 53(12), 6757-6764. https://doi.org/10.1021/acs.est.9b00967.

Ge, L.K., Cao, S.K., Halsall, C., Niu, J.F., Bai, D.X., He, G.K., Zhang, P., Ma, H.R., 2023. Photodegradation of hydroxyfluorenes in ice and water: A comparison of kinetics, effects of water constituents, and phototransformation by-products. J Environ Sci 124, 139-145. https://doi.org/10.1016/j.jes.2021.11.002.

Ge, L.K., Hou, Z.M., Niu, J.F., Wang, S.Y., Zhang, P., Zhu, Y.Q., 2025a. New insights into the environmental photochemistry of hydroxynaphthalene congeners in water and in ice: A distinct comparative study. J Hazard Mater 493, 138310. https://doi.org/10.1016/j.jhazmat.2025.138310.

Ge, L.K., Li, J., Na, G.S., Chen, C.E., Huo, C., Zhang, P., Yao, Z.W., 2016a. Photochemical degradation of hydroxy PAHs in ice: Implications for the polar areas. Chemosphere 155, 375-379. https://doi.org/10.1016/j.chemosphere.2016.04.087.

Ge, L.K., Na, G.S., Chen, C.E., Li, J., Ju, M.W., Wang, Y., Li, K., Zhang, P., Yao, Z.W., 2016b. Aqueous photochemical degradation of hydroxylated PAHs: Kinetics, pathways, and multivariate effects of main water constituents. Sci Total Environ 547, 166-172. https://doi.org/10.1016/j.scitotenv.2015.12.143.

Ge, L.K., Wang, S.Y., Cui, N.N., Wang, Z.Y., Zhang, P., 2025b. Insight into the environmental photochemistry of nitrated polycyclic aromatic hydrocarbons in water and in ice: Kinetics, pathways and photo-modified toxicity. Environ Res 279, 121749. https://doi.org/10.1016/j.envres.2025.121749.

Guo, Z.Y., Kodikara, D., Albi, L.S., Hatano, Y., Chen, G., Yoshimura, C., Wang, J.Q., 2023. Photodegradation of organic micropollutants in aquatic environment: Importance, factors and processes. Water Res 231, 118236. https://doi.org/10.1016/j.watres.2022.118236.

Hu, W., Liu, D.D., Su, S.H., Ren, L.J., Ren, H., Wei, L., Yue, S.Y., Xie, Q.R., Zhang, Z.M., Wang, Z.H., Yang, N., Wu, L.B., Deng, J.J., Qi, Y.L., Fu, P.Q., 2021. Photochemical degradation of organic matter in the atmosphere. Adv Sustainable Syst 5(11), 2100027. https://doi.org/10.1002/adsu.202100027.

Huang, C.C., Zeng, Y.H., Luo, X.J., Ren, Z.H., Tian, Y.K., Mai, B.X., 2021. Comprehensive exploration of the ultraviolet degradation of polychlorinated biphenyls in different media. Sci Total Environ 755, 142590. https://doi.org/10.1016/j.scitotenv.2020.142590.

Huang, S.N., Zhang, Z.B., Lin, C.Y., Cheng, H.F., 2024. Solar photodegradation of a novel des-F(6)-fluoroquinolone, garenoxacin, and ecotoxicity of its phototransformation products. Environ Sci Technol 58(31), 13918-13928. https://doi.org/10.1021/acs.est.4c03206.

Hung, H., Halsall, C., Ball, H., Bidleman, T., Dachs, J., De Silva, A., Hermanson, M., Kallenborn, R., Muir, D., Sühring, R., Wang, X.P., Wilson, S., 2022. Climate change influence on the levels and trends of persistent organic pollutants (POPs) and chemicals of emerging Arctic concern (CEACs) in the Arctic physical environment – a review. Environ Sci Proc Imp 24(10), 1577-1615. https://doi.org/10.1039/D1EM00485A.

Jin, R., Zheng, M.H., Lammel, G., Bandowe, B.A.M., Liu, G.R., 2020. Chlorinated and brominated polycyclic aromatic hydrocarbons: Sources, formation mechanisms, and occurrence in the environment. Prog Energy Combust Sci 76, 100803. https://doi.org/10.1016/j.pecs.2019.100803.

Kang, C.L., Bao, S.Q., Wang, Y.H., Xiao, K.K., Zhu, L., Liu, F., Tian, T., 2018. Comparison of the photoconversion of 1-chloronaphthalene and 2,3-dichlornaphthalene in water. Water Sci Technol 78(9), 1946-1955. https://doi.org/10.2166/wst.2018.469.

Kang, Q., Bao, S.Q., Chen, B., 2021. Phototransformation of three polychlorinated naphthalenes on surface of atmospheric particulate matter. J Hazard Mater 409, 124895. https://doi.org/10.1016/j.jhazmat.2020.124895.

Klanova, J., Klan, P., Nosek, J., Holoubek, I., 2003. Environmental ice photochemistry: Monochlorophenols. Environ Sci Technol 37(8), 1568 -1574. https://doi.org/10.1021/es025875n.

Klimczak, M., Liu, G.R., Fernandes, A.R., Kilanowicz, A., Falandysz, J., 2023. An updated global overview of the manufacture and unintentional formation of polychlorinated naphthalenes (PCNs). J Hazard Mater 457, 131786. https://doi.org/10.1016/j.jhazmat.2023.131786.

Li, Y.J., Hu, X.F., Xie, H., Cai, B.C., Bai, Y.X., 2024a. Photochlorination of anthracene in saline ice under simulated solar light. Water 16(9), 1237. https://doi.org/10.3390/w16091237.

Li, Z.J., Zhang, J., Dong, D.M., Zhang, L.W., Sun, H.Y., Wang, Y.K., Sun, Z.J., He, S.N., Guo, Z.Y., 2024b. Photodegradation for different dissociated species of norfloxacin and ofloxacin in water ice under solar irradiation. J Hazard Mater 461, 132595. https://doi.org/10.1016/j.jhazmat.2023.132595.

Liu, J.Y., Xue, S., Jiang, C.H., Zhang, Z.H., Lin, Y.Z., 2023. Effect of dissolved organic matter on sulfachloropyridazine photolysis in liquid water and ice. Water Res 246, 120714. https://doi.org/10.1016/j.watres.2023.120714.

Liu, Q.Z., Xu, X., Lin, L.H., Yang, G., Wang, D.H., 2021. Occurrence, health risk assessment and regional impact of parent, halogenated and oxygenated polycyclic aromatic hydrocarbons in tap water. J Hazard Mater 413, 125360. https://doi.org/10.1016/j.jhazmat.2021.125360.

Manfrin, A., Hänggli, A., Wildenberg, J., McNeill, K., 2020. Substituent effects on the direct photolysis of benzotrifluoride derivatives. Environ Sci Technol 54(18), 11109-11117. https://doi.org/10.1021/acs.est.9b07429.

Mason, D.P., Elwood Madden, M.E., 2022. Raman spectroscopy of high salinity brines and ices. Icarus 372, 114759. https://doi.org/10.1016/j.icarus.2021.114759.

Oda, M., Ikemori, F., Ohura, T., 2024. Contiguous hourly variations and relativeness of polycyclic aromatic hydrocarbons and their chlorinated derivatives in urban PM2.5. Atmos Environ 334, 120710. https://doi.org/10.1016/j.atmosenv.2024.120710.

Ofrydopoulou, A., Evgenidou, E., Nannou, C., Vasquez, M.I., Lambropoulou, D., 2021. Exploring the phototransformation and assessing the in vitro and in silico toxicity of a mixture of pharmaceuticals susceptible to photolysis. Sci Total Environ 756, 144079. https://doi.org/10.1016/j.scitotenv.2020.144079.

Ohura, T., Amagai, T., Makino, M., 2008. Behavior and prediction of photochemical degradation of chlorinated polycyclic aromatic hydrocarbons in cyclohexane. Chemosphere 70(11), 2110-2117. https://doi.org/10.1016/j.chemosphere.2007.08.064.

Peng, B., Dong, Q.L., Li, F.Z., Wang, T., Qiu, X.H., Zhu, T., 2023. A systematic review of polycyclic aromatic hydrocarbon derivatives: Occurrences, levels, biotransformation, exposure biomarkers, and toxicity. Environ Sci Technol 57(41), 15314-15335. https://doi.org/10.1021/acs.est.3c03170.

Qi, A.A., Wang, P.C., Lv, J.H., Zhao, T., Huang, Q., Wang, Y.M., Zhang, X.F., Wang, M., Xiao, Y., Yang, L.X., Ji, Y.Q., Wang, W.X., 2023. Distributions of PAHs, NPAHs, OPAHs, BrPAHs, and ClPAHs in air, bulk deposition, soil, and water in the Shandong Peninsula, China: Urban-rural gradient, interface exchange, and long-range transport. Ecotoxicol Environ Saf 265. https://doi.org/10.1016/j.ecoenv.2023.115494.

Qiao, M., Bai, Y.H., Cao, W., Huo, Y., Zhao, X., Liu, D.Q., Li, Z.R., 2018. Impact of secondary effluent from wastewater treatment plants on urban rivers: Polycyclic aromatic hydrocarbons and derivatives. Chemosphere 211, 185-191. https://doi.org/10.1016/j.chemosphere.2018.07.167.

Sarmiento, D.J., Majestic, B.J., 2023. Formation of environmentally persistent free radicals from the irradiation of polycyclic aromatic hydrocarbons. J Phys Chem A 127(25), 5390-5401. https://doi.org/10.1021/acs.jpca.3c01405.

Teng, X.L., Xu, J.Q., Wang, Z.Y., Qu, R.J., 2025. Photodegradation of chlorinated persistent organic oollutants (Cl-POPs) in oearl river suspended particulate matter–water systems: Kinetics, quantitative structure–activity relationship (QSAR) development, and mechanism. Environ Sci Technol 59(8), 4059-4067. https://doi.org/10.1021/acs.est.4c07246.

Tillner, J., Hollard, C., Bach, C., Rosin, C., Munoz, J.-F., Dauchy, X., 2013. Simultaneous determination of polycyclic aromatic hydrocarbons and their chlorination by-products in drinking water and the coatings of water pipes by automated solid-phase microextraction followed by gas chromatography–mass spectrometry. J Chromatogr A 1315, 36-46. https://doi.org/10.1016/j.chroma.2013.09.047.

Tu, Z.N., Qi, Y.M., Tang, X.S., Wang, Z.Y., Qu, R.J., 2023. Photochemical transformation of anthracene (ANT) in surface soil: Chlorination and hydroxylation. J Hazard Mater 452, 131252. https://doi.org/10.1016/j.jhazmat.2023.131252.

Wang, J.J., Liu, X.C., Beusen, A.H.W., Middelburg, J.J., 2023a. Surface-water nitrate exposure to world populations has expanded and intensified during 1970–2010. Environ Sci Technol 57(48), 19395-19406. https://pubs.acs.org/doi/10.1021/acs.est.3c06150.

Wang, X.L., Kang, H.Y., Wu, J.F., 2016. Determination of chlorinated polycyclic aromatic hydrocarbons in water by solid-phase extraction coupled with gas chromatography and mass spectrometry. J Sep Sci 39(9), 1742-1748. https://doi.org/10.1002/jssc.201501286.

Wang, Y.K., Song, Z.W., Zhang, L.W., Dong, D.M., Li, Z.J., Sun, H.Y., Wang, L.T., Guo, Z.Y., 2023b. Distribution and photodegradation of typical nonsteroidal anti-inflammatory drugs in an ice-water system: Simulation of surface waters with an ice cover. J Cleaner Prod 402, 136823. https://doi.org/10.1016/j.jclepro.2023.136823.

Weber, J., Kurková, R., Klánová, J., Klán, P., Halsall, C.J., 2009. Photolytic degradation of methyl-parathion and fenitrothion in ice and water: Implications for cold environments. Environ Pollut 157(12), 3308-3313. https://doi.org/10.1016/j.envpol.2009.05.045.

Xie, J.Q., Tao, L., Wu, Q., Lei, S.M., Lin, T., 2021. Environmental profile, distributions and potential sources of halogenated polycyclic aromatic hydrocarbons. J Hazard Mater 419, 126164. https://doi.org/10.1016/j.jhazmat.2021.126164.

Xie, Z.Y., Zhang, P., Wu, Z.L., Zhang, S., Wei, L.J., Mi, L.J., Kuester, A., Gandrass, J., Ebinghaus, R., Yang, R.Q., Wang, Z., Mi, W.Y., 2022. Legacy and emerging organic contaminants in the polar regions. Sci Total Environ 835, 155376. https://doi.org/10.1016/j.scitotenv.2022.155376.

Xu, J.Q., Wei, X.Y., Wei, J.Y., He, M.Q., Teng, X.L., Wang, Z.Y., Qu, R.J., 2025. Photodegradation of PCB-209 on suspended particles: Discrepancy in mechanism of direct dechlorination and active species-

mediated indirect dechlorination reactions. Water Res 283, 123797. https://doi.org/10.1016/j.watres.2025.123797.

Xue, H.H., Zheng, N., Kang, C.L., Wang, Y., Wang, Y.W., 2019a. Photochemical degradation of nitrated PAHs in snow. Atmos Environ 199, 260-264. https://doi.org/10.1016/j.atmosenv.2018.11.026.

Xue, S., Sun, J.J., Liu, Y., Zhang, Z.H., Lin, Y.Z., Liu, Q., 2019b. Effect of dissolved organic matter fractions on photodegradation of phenanthrene in ice. J Hazard Mater 361, 30-36. https://doi.org/10.1016/j.jhazmat.2018.08.072.

Yang, X., Rosario-Ortiz, F.L., Lei, Y., Pan, Y.H., Lei, X., Westerhoff, P., 2022. Multiple roles of dissolved organic matter in advanced oxidation processes. Environ Sci Technol 56(16), 11111-11131. https://doi.org/10.1021/acs.est.2c01017.

Yu, Y.T., Liu, M.D., Wang, S.M., Zhang, C.X., Zhang, X., Liu, L., Xue, S., 2024. Unveiling the photodegradation mechanism of monochlorinated naphthalenes under UV-C irradiation: Affecting factors analysis, the roles of hydroxyl radicals, and DFT calculation. Molecules 29(19), 4535. https://doi.org/10.3390/molecules29194535.

Zhang, Z.W., Chen, Q., Bai, C.F., Zhu, Y.H., She, J., Ge, X., Li, M.B., Li, L.Z., Yu, Y.X., 2024. Identification and seasonal variation of specific particulate bound (halogenated) polycyclic aromatic hydrocarbons in air from different metal industrial parks in Northwest China. Environ Sci Pollut Res 31(29), 41914-41925. https://doi.org/10.1007/s11356-024-33883-w.

Zhao, Q., Fang, Q., Liu, H.Y., Li, Y.J., Cui, H.S., Zhang, B.J., Tian, S.L., 2019. Halide-specific enhancement of photodegradation for sulfadiazine in estuarine waters: Roles of halogen radicals and main water constituents. Water Res 160, 209-216. https://doi.org/10.1016/j.watres.2019.05.061.

Zhao, X., Yang, P., Lu, J., Chen, J., 2024. Comparative study of the degradation of meta-chloronitrobenzene by UV/hydrogen peroxide and UV/persulfate oxidation: Degradation pathways and toxicity. Chem Eng J 490, 151502. https://doi.org/10.1016/j.cej.2024.151502.

Zhao, X.Q., Cheng, P.F., Borch, T., Waigi, M.G., Peng, F., Gao, Y.Z., 2022. Humidity induces the formation of radicals and enhances photodegradation of chlorinated-PAHs on Fe(III)-montmorillonite. J Hazard Mater 423, 127210. https://doi.org/10.1016/j.jhazmat.2021.127210.

Declaration of interests

☒The authors declare that they have no known competing financial interests or personal relationships that could have appeared to influence the work reported in this paper.

☐The authors declare the following financial interests/personal relationships which may be considered as potential competing interests: